AD-A091 407 AIR FORCE INST OF TECH WRIGHT-PATTERSON AFB OH F/G 20/5
UNIDIRECTIONAL COMPOSITES AS ELECTRODES/PREIONIZATION SOURCES F--ETC(U)
DEC 79 S G WAX
UNCLASSIFIED AFIT-CI-79-249D NL

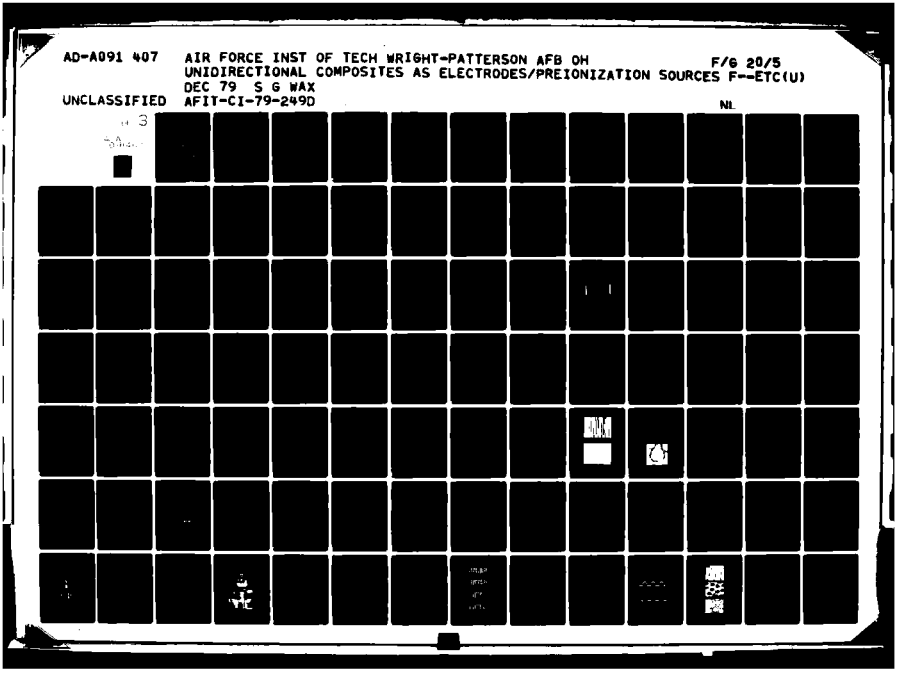

UNCLASS

SECURITY CLASSIFICATION OF THIS PAGE (When Data Entered)

REPORT DOCUMENTATION PAGE

READ INSTRUCTIONS BEFORE COMPLETING FORM

1. REPORT NUMBER: 79-249D
2. GOVT ACCESSION NO.: AD-A091407
3. RECIPIENT'S CATALOG NUMBER:
4. TITLE (and Subtitle): Unidirectional Composites as Electrodes/ Preionization Sources for CO_2 TEA Lasers
5. TYPE OF REPORT & PERIOD COVERED: THESIS/DISSERTATION
6. PERFORMING ORG. REPORT NUMBER:
7. AUTHOR(s): Capt Steven G. Wax
8. CONTRACT OR GRANT NUMBER(s): AFIT-[illegible]
9. PERFORMING ORGANIZATION NAME AND ADDRESS: AFIT STUDENT AT: Georgia Institute of Technology
10. PROGRAM ELEMENT, PROJECT, TASK AREA & WORK UNIT NUMBERS: Doctoral Thesis
11. CONTROLLING OFFICE NAME AND ADDRESS: AFIT/NR, WPAFB OH 45433
12. REPORT DATE: Dec 79
13. NUMBER OF PAGES: 205
14. MONITORING AGENCY NAME & ADDRESS (if different from Controlling Office)
15. SECURITY CLASS. (of this report): UNCLASS
15a. DECLASSIFICATION/DOWNGRADING SCHEDULE

LEVEL II

16. DISTRIBUTION STATEMENT (of this Report)

APPROVED FOR PUBLIC RELEASE; DISTRIBUTION UNLIMITED

DTIC ELECTE NOV 6 1980 S C

17. DISTRIBUTION STATEMENT (of the abstract entered in Block 20, if different from Report)

18. SUPPLEMENTARY NOTES

APPROVED FOR PUBLIC RELEASE: IAW AFR 190-17

25 SEP 1980

Fredric C. Lynch
FREDRIC C. LYNCH, Major, USAF
Director of Public Affairs
Air Force Institute of Technology (ATC)
Wright-Patterson AFB, OH 45433

19. KEY WORDS (Continue on reverse side if necessary and identify by block number)

20. ABSTRACT (Continue on reverse side if necessary and identify by block number)

ATTACHED

DD FORM 1 JAN 73 1473 EDITION OF 1 NOV 65 IS OBSOLETE

UNCLASS

80 10 14 202

AD A091407

DDC FILE COPY

Unidirectional Composites as Electrodes/Preionization Sources for CO_2 TEA Lasers (206 pages)

Steven G. Wax

Capt. USAF

Transverse Excited Atmospheric (TEA) CO_2 lasers offer improvements over low pressure CO_2 lasers, but efficient operation at atmospheric pressure is often difficult to achieve. The purpose of this research was to examine the feasibility of using unidirectional oxide metal composites grown at the Georgia Institute of Technology to obviate the problems of high pressure CO_2 laser operation.

The research was divided into two areas. In the first, Gd_2O_3-Ce_2O_3-Mo and UO_2-W composites were examined for use directly as electrodes in CO_2 lasers. Using discharge apparatus similar to that used for CO_2 lasers, the discharge characteristics from polished and exposed pin composite electrodes were examined. The results of the cathode fall tests indicated that cathode fall for every composite electrode tested was higher than for the aluminum standard. No significant advantage with the composite electrodes at high pressure was observed.

In the second phase of the research, low voltage field emitters (LVFE) were examined as a preionization source for

the discharge. These emitters were prepared using thin film techniques from the UO_2-W composites. In this phase, field emission at atmospheric pressure, the control of a dishcarge by field emission and the survivability of the LVFE structure at high pressure were all considered. Results indicated that field emission at up to 760 torr in helium was possible at conditions which posed minimal damage to the LVFE structure. Emission from the LVFE cathodes was also shown to be suitable for tailoring of gas discharge characteristics to those desired in laser operation. While true preionization was not accomplished, the LVFE structure has been shown to be a potentially viable technique for use in controlling atmospheric pressure gas discharges.

KEY WORDS: Laser
Preionization
Field Emission
Electrode

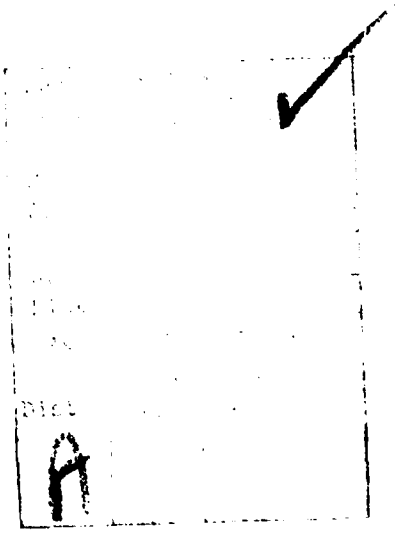

UNIDIRECTIONAL COMPOSITES AS ELECTRODES/PREIONIZATION SOURCES FOR CO_2 TEA LASERS

A THESIS

Presented to

The Faculty of the Division of Graduate Studies

by

Steven Gary Wax

In Partial Fulfillment

of the Requirements for the Degree

Doctor of Philosophy

in the School of Ceramic Engineering

Georgia Institute of Technology

December 1979

ACKNOWLEDGMENTS

I would first like to thank my advisor, Dr. J. K. Cochran, for his guidance throughout this effort. Without his assistance and encouragement, this research would not have been possible.

I would also like to thank Dr. R. K. Feeney for serving on my reading committee and providing invaluable electrical engineering assistance. Dr. Feeney and his group were always there whenever I required any electrical device, or help with its operation.

I am extremely grateful to Dr. A. T. Chapman for his constructive suggestions with the manuscript as well as his words of encouragement throughout the course of this research.

To Dr. D. N. Hill, I owe a special thanks. Dr. Hill was always willing to spend the time to explain or discuss any aspect of the work even when he was writing his own dissertation and had little time to spare. Without his understanding of the LVFE concept and his patience explaining it to me, I could not have accomplished this effort.

Mr. T. Mackrovitch certainly deserves thanks for his help in fabrication and assembly of the test equipment and deserves much of the credit for the timely completion of the research.

Finally, I owe a special debt of gratitude to my wife,

Kathy, who was always there with love, patience, and understanding when I needed it, and to Christopher Paul whose joyous arrival made the last few difficult months bearable.

TABLE OF CONTENTS

Page

ACKNOWLEDGMENTS. . . . . .

LIST OF TABLES . . . . . .

LIST OF ILLUSTRATIONS. . . . . .

SUMMARY. . . . . .

Chapter

I. INTRODUCTION. 1

II. BACKGROUND. 4

CO_2 Laser Operation
Electrical Discharges in Gases
Townsend Discharge
Glow Discharge
Arc Discharge
TEA Lasers
Conventional TEA Lasers
Preionized TEA Lasers
Field Emission from Oxide-Metal Composites
Field Emission
Oxide-Metal Composites

III. PROCEDURE 50

Unidirectional Composite Electrode
Discharge Test Apparatus
Composite Electrode Fabrication
Discharge Tests-CW
Discharge Tests-Pulsed
LVFE Preionization Source
Preionization Apparatus
LVFE Fabrication
Preionization Testing

IV. RESULTS AND DISCUSSION. 84

LVFE Cathodes as Preionization Sources
Field Emission at Laser Gas Pressures
LVFE Preionization of a Discharge
Survivability of LVFE Cathodes at Laser Gas Pressures

Page

Composite Electrode Tests

V. CONCLUSIONS AND RECOMMENDATIONS. 140

Conclusions
Recommendations

Appendix

A. GROWTH OF UNIDIRECTIONAL OXIDE-METAL COMPOSITES 143

UO_2-W
Gd_2O_3-Ce_2O_3-Mo

B. LVFE PREIONIZATION SOURCE TESTS. 145

Test HP-1
Test HP-2
Test HP-3
Test HP-4
Test HP-5
Test HP-6
Test HP-7
Test HP-9
Test HP-10
Test HP-11
Test HP-13
Test HP-14
Test HP-15
Test HP-16
Test HP-17
Test HP-18
Test HP-19
Test HP-20
Test HP-21
Test HP-22
Test HP-23
Test HP-24
Test HP-25

C. SPACE CHARGE AT HIGH PRESSURE. 183

D. RESULTS FOR COMPOSITE ELECTRODE TESTS. 186

CW Tests
Pulsed Discharge Tests

BIBLIOGRAPHY. 201

VITA. 205

LIST OF TABLES

Table		Page
1.	Stoletow Constants.	15
2.	Cathode Fall (Volts).	26
3.	Values for C for Pd_n = C (cm-torr).	27
4.	Glow Discharge Cathode Current Density (J/p^2) (microamp/cm^2/$torr^2$).	27
5.	Chemical Composition of UO_2-W Etches.	57
6.	Electrodes for CW Cathode Fall Tests.	62
7.	Test Configurations for LVFE Cathode Testing. .	85
8.	LVFE Cathode Emission Summary	87
9.	Field Emission Current vs Pressure for Cathode JP9-1, Test HP-15	89
10.	Field Emission Current vs Applied Voltage for Selected Pressure, Cathode JP9-2, Test HP-23. .	92
11.	Space Charge Estimate for Cathode Emission. . .	96
12.	Summary of Three Electrode Discharge Tests. . .	106
13.	Linear Regression Coefficients for Equation (23).	109
14.	E/p vs Pin Voltage for Test HP-25	112
15.	Summary of Post-Test Condition.	119
16.	Cathode Fall Summary for CW Discharge Tests . .	129
17.	Cathode Fall Summary for Pulsed Discharge Tests	132
B-1.	Preionization Source Test Summary	146
B-2.	LVFE Cathode Summary.	147
B-3.	Field Emission from Cathode E17-1, Test HP-4 (500 torr).	149

Table		Page
B-4.	Field Emission from Cathode E20-1, Test HP-7 (500 torr)	152
B-5.	Emission from Cathode E20-1, Test HP-9 (500 torr)	153
B-6.	Field Emission from Cathode E20-1 at Two Collector Spacings, Test HP-9 (500 torr)	155
B-7.	Field Emission from Cathode L19D-A, Test HP-13 (7.7 torr)	158
B-8.	Field Emission from Cathode E13-2, Test HP-14 (500 torr)	159
B-9.	Discharge Current from Cathode E13-2, Test HP-14 (500 torr)	161
B-10.	Field Emission Current vs Pressure for Cathode JP9-1, Test HP-15	163
B-11.	Field Emission from Cathode JP9-1, Test HP-15 (39 torr)	164
B-12.	Emission/Discharge Current vs Anode Voltage for Cathode JP9-1, Test HP-16 (350 torr)	165
B-13.	Discharge Current vs Anode Voltage for Cathode JP9-1, Test HP-17 (31 torr)	167
B-14.	Field Emission vs Time for Cathode JP9-3, Test HP-19 (500 torr)	169
B-15.	Discharge Current vs Anode Voltage for Cathode L19D-B, Test HP-21 (13 torr)	171
B-16.	Field Emission Current vs Time for Cathode JP9-2, Test HP-22 (10^{-6} torr)	173
B-17.	Field Emission Current vs Time for Cathode JP9-2, Test HP-23 (10^{-6} torr)	176
B-18.	Comparison of 760 torr and 0.030 torr Field Emission from Cathode JP9-2, Test HP-23	177
B-19.	Discharge Current from Cathode E1-2, Test HP-24 (760 torr)	179

Table		Page
B-20.	Discharge Current from Cathode E1-2, Test HP-24 (760 torr).	180
B-21.	Discharge Current from Cathode ER+E, Test HP-25 (760 torr).	182
C-1.	Space Charge Current Limit.	185
D-1	CW Discharge Data for Cathode G-1 (500 kΩ). . .	187
D-2.	CW Discharge Data for Cathode AL-1 (500 kΩ) . .	188
D-3.	CW Discharge Data for Cathode U-1E (250 kΩ) . .	189
D-4.	CW Discharge Data for Cathode U-1 (68 kΩ) . . .	190
D-5.	CW Discharge Data for Cathode G-1E (500 kΩ) . .	190
D-6.	Pulsed Discharge Data for Cathode U-2	191
D-7.	Pulsed Discharge Data for Cathode AL-1.	192
D-8.	Pulsed Discharge Data for Cathode G-2E.	194
D-9.	Pulsed Discharge Data for Cathode U-1E.	194
D-10.	Pulsed Discharge Data for Cathode U-3	196
D-11.	High Pressure Pulsed Data for Cathode AL-1. . .	197
D-12.	High Pressure Pulsed Data for Cathode U-2 . . .	197
D-13.	High Pressure Pulsed Data for Cathode U-1E. . .	198
D-14.	Minimum Sparking Voltage for Cathodes AL-1, U-2, U-1E	199

LIST OF ILLUSTRATIONS

Figure		Page
1.	Energy State Diagram for $He/CO_2/N_2$ Laser System.	7
2.	Fractional Power Transfer to N_2 Molecule.	9
3.	CO_2 Laser Discharge Configurations, (a) Longitudinal, (b) Transverse	11
4.	Typical Voltage-Current Relationship in a Gas Discharge	13
5.	Major Parts of the Glow Discharge	20
6.	Simple Gas Discharge Circuit.	22
7.	Paschen Law Curve for Sparking Voltage and Discharge Voltage	24
8.	Schematic of a Waveguide Laser.	32
9.	Electrode Configuration for a Double Discharge Laser	37
10.	Peak DC (18 μsec pulse) Current Versus Applied DC Voltage for Various AC (100 nsec) Voltages	39
11.	Typical Exposed Pin Cathodes.	48
12.	The Low Voltage Field Emitter (LVFE) Structure.	49
13.	Schematic of Composite Electrode Discharge Apparatus	51
14.	Schematic of Composite Electrode Waveguide Configuration	52
15.	Composite Electrode Fabrication	55
16.	Composite Electrode CW Discharge Circuit.	59
17.	Composite Electrode Pulsed Discharge Circuit.	64
18.	Photograph of Emission Test Fixture Mounted on Conflat Flange, Showing Electrical Connections.	67

Figure		Page
19.	Circuit for Two Electrode LVFE Preionization Configuration.	68
20.	Photograph of (a) Three Electrode Discharge Test Fixture Mounted on Conflat Flange, X0.5 and (b) View of Three Electrode Configuration X3	70
21.	Circuit for Three Electrode LVFE Preionization Configuration.	71
22.	Schematic Diagram Illustrating the Steps in the Formation of the Active Area	74
23.	Schematic Diagram of Vapor Deposition System .	76
24.	Schematic Diagram Showing the Steps in the Formation of the LVFE Structure.	77
25.	Examples of the LVFE Structure During Each of the Fabrication Steps Illustrated in Figure 24	78
26.	Oscilloscope Traces of Extractor Voltage and Emission Current	81
27.	Empirical Versus Experimental Field Intensified Ionization as a Function of Pressure. . .	90
28.	Fowler-Nordheim Plots for Selected Emission Tests.	93
29.	Current Flow in (a) Two Electrode and (b) Three Electrode Configurations	99
30.	Fowler-Nordheim Plot of Measured Current from Cathode E20-1 at Low and High Accelerating Fields	103
31.	Discharge Current Density Versus Anode-Mesh Voltage at Constant Pin Voltage for Selected Discharge Tests.	107
32.	Discharge Current Density Versus Anode-Mesh Voltage at Various Pin Voltages for Cathode ER+E, Test HP-25	111

Figure		Page
33.	Fowler-Nordheim Plot of Discharge Current at Various Anode-Mesh Voltages for Cathode ER+E Test HP-25.	114
34.	Example of Major Damage to LVFE Structure (Cathode L19D-B, Test HP-21) at 13 Torr, X7500, 45°.	121
35.	Example of Minor Damage to LVFE Structure (Cathode E17-2, (a) Pre-test and (b) Post-Test (HP-4), X7500, 45°.	122
36.	Comparison of Damage to LVFE Cathode E20-1 at (a) High Accelerating Field (Test HP-9) and (b) Low Accelerating Field (Test HP-7), X7500, 45°	123
37.	Deposit on Field Emission Tips Resulting from Discharge in Laser Gas, X5000, 45°.	125
38.	Discharge Voltage, V_D, Versus Pressure Times Distance pd, for CW Discharge Tests of Composite Electrodes (a) AL-1, (b) G-1, (c) G-1E, (d) U-1, (e) U-1E	128
39.	Discharge Voltage, V_D, Versus Pressure Times Distance PD, for Pulsed Discharge Tests of Composite Electrodes (a) AL-1 and U-2, (b) G-2, U-1E and U-3.	131
40.	Examples of Pre-Test Exposed Pin Composite Electrodes, (a) Gd_2O_3-Ce_2O_3-Mo, (b) UO_2-W, X5000, 45°.	134
41.	Minimum Sparking Voltage Versus Pressure for Composite Electrodes Al-1, U-3, U-1E.	136
42.	Examples of Damage at High Pressure to Composite Electrodes (a) Polished UO_2-W (b) Exposed Pin UO_2-W, X2500, 20°	138

SUMMARY

Transverse Excited Atmospheric (TEA) CO_2 lasers offer improvements over low pressure CO_2 lasers, but efficient operation at atmospheric pressure is often difficult to achieve. Poor uniformity, losses due to cathode fall and tendency to arc are all inherent problems with standard CO_2 discharge electrodes at high pressure. In addition, high pressure discharges are not inherently suitable for laser operation. Although preionization techniques can eliminate these problems, the most common schemes involve high power and cumbersome electronics. The purpose of this research was to examine the feasibility of using unidirectional oxide metal composites grown at the Georgia Institute of Technology to obviate the problems of high pressure CO_2 laser operation.

The research was divided into two areas. In the first, Gd_2O_3-Ce_2O_3-Mo and UO_2-W composites were examined for use directly as electrodes in CO_2 lasers. Using discharge apparatus similar to that used for CO_2 lasers, the discharge characteristics from polished and exposed pin composite electrodes were examined and compared to an aluminum electrode. Both CW and pulsed cathode fall tests were performed as well as high (100-600 torr) pressure pulsed stability tests. The results of the cathode fall tests indicated that cathode fall for every composite electrode tested was higher

than for the aluminum standard. In addition, no significant advantage with the composite electrodes at high pressure was observed.

In the second phase of the research, low voltage field emitters (LVFE) were examined as a preionization source for the discharge. These emitters were prepared using thin film techniques from the UO_2-W composites. In examining the feasibility of using the LVFE as a preionization source, field emission at atmospheric pressure, the control discharge by field emission and the survivability of the LVFE structure at high pressure were all considered. Results indicated that field emission at up to 760 torr in helium was possible at conditions which posed minimal damage to the LVFE structure. Emission from the LVFE cathodes was also shown to be suitable for tailoring of gas discharge characteristics to those desired in laser operation. While true preionization was not accomplished, the LVFE structure has been shown to be a potentially viable technique for use in controlling atmospheric pressure gas discharges.

CHAPTER I

INTRODUCTION

Transverse Excited Atmospheric (TEA) CO_2 lasers offer significant improvements over low pressure CO_2 lasers in gain, efficiency and tunability. However, with high pressure operation, it is often difficult to achieve the proper discharge characteristics. Poor uniformity, losses due to cathode fall and the tendency to arc are all inherent problems with standard electrodes. Although preionization can eliminate these problems, the most common schemes involve either short, high-voltage discharges or large high power electron sources making them too cumbersome for small compact laser designs. With these problems in mind, it is clear that improvements in state of the art in CO_2 TEA lasers must involve either improved electrode/discharge characteristics, or a simple, efficient preionization scheme. Based on a comprehensive review of the work in these areas, it appears that the unidirectional composites grown at Georgia Tech offer significant possibilites for improvement of both discharge characteristics and preionization.

The UO_2-W and Gd_2O_3-Ce_2O_3-Mo composites consist of single crystal metal fibers about 3000-4000 Å in diameter grown in an oxide matrix at densities of between 10^6 and 10^7 pins/cm^2. Extensive work has been done at Georgia Tech

using the UO_2-W composites as field emitters. Processing for shaping and lengthening the metal pins has been developed for UO_2-W and limited success was also achieved with the Gd_2O_3-Ce_2O_3-Mo composites. In initiating this effort, it was hoped that the high pin densities of these composites would provide the uniformity required of laser electrodes, while the shape of the pins might independently control the emission of electrons and thus change the discharge characteristics.

In recent work, the UO_2-W composites have been used as Low Voltage Field Emitters (LVFE). These devices operate by creating highly enhanced fields in the neighborhood of the tungsten pins permitting the emission of electrons at applied voltages as low as 40 V. It was hypothesized that the electrons from the LVFE devices could be used as a preionization source for the TEA lasers. If so, this would allow preionization at several hundred rather than several thousand volts.

The research presented in this dissertation was divided into two areas. In the first, the composites were examined for use directly as electrodes in high pressure CO_2 discharges. Polished and exposed pin composites were compared with an aluminum cathode for discharge uniformity and favorable discharge voltage-current characteristics. In the second area, the LVFE structure was examined as an electron source for control and/or preionization of a gas discharge. This

included evaluation of high pressure field emission, the use of emission to control gas discharges, and the survivability of the emitters in the high pressure discharge environment.

CHAPTER II

BACKGROUND

The major area of emphasis in this survey is the transverse excited atmospheric (TEA) CO_2 waveguide laser including both its design and operation. However, as a prerequisite to this subject, it is necessary to discuss the operation of CO_2 lasers and the phenomenon of electrical discharges in gases. While a complete discourse on these areas is beyond the scope of this literature search, the following sections should provide enough background to allow an understanding of the principles of TEA laser operation. In addition, a discussion of the oxide-metal composites and their possible use in CO_2 lasers is included.

CO_2 Laser Operation

Atoms can be raised from one energy state to a higher energy state by the absorption of light with a wavelength corresponding to the energy change of the transition. Atoms in the higher state can then decay spontaneously back to their original state or can be stimulated to decay by light of the appropriate wavelength. This latter process, stimulated emission, results in the radiation of a quantum of energy in phase (adding constructively) to the stimulating wave. This increases the amplitude of the wave [1]. The

acronym LASER stands for Light Amplification by Stimulated Emission of Radiation. Since the stimulated emission competes with the spontaneous emission (which results in quanta which are most likely not in phase with existing waves) only energy states which have long lifetimes (low spontaneous rates) can have significant amplification. Also, since the rates of stimulated emission and absorption are identical [1], net amplification can only occur when there are more atoms in the higher energy state. This condition, the opposite of the normal Boltzmann distribution, is termed a "population inversion." The method for obtaining this inversion, "pumping," clearly must be other than by direct simulation. Assuming a population inversion exists, the method for lasing becomes clear. The presence of the appropriate wavelength of light causes stimulated emission which adds constructively to the wave. Cavity design and highly reflective mirrors are used to preferentially select "in phase" waves and pass them through the medium as many as 100 times. The specific wavelength of the stimulated emission is enhanced while all other extraneous wavelengths are eliminated by destructive interference. The laser beam itself is composed of the small amount of light (≈5%) which passes through one of the mirrors.

While the above characteristics are inherent in all laser systems, the way in which the energy states are arranged and pumped varies greatly from system to system. In the

$CO_2/N_2/H_e$ system, the population inversion is accomplished by energy transfer from the non-lasing component, N_2. Figure 1 depicts the major energy states of this system. An electrical discharge is used to excite the N_2 molecules from state (0) → state (1). This state has almost the identical energy as a CO_2 energy state (2) and resonant energy transfer from the N_2 to the CO_2 raises the CO_2 molecules to this state. A population inversion is thus built up between CO_2 states (2) and (3) and the decay to state (3) results in the lasing. The CO_2 is then quenched from state (3) to the ground state by collisions with helium molecules [2].

The above description is actually an over simplification of the situation. The energy states of the CO_2 molecule are quantum states representing a combination of three fundamental vibration modes of the molecules. These modes are discussed extensively in several references including [1] and [3]. Also, state (3) is really two distinct energy levels each composed of several vibrational states. These become important in tuning the CO_2 laser to the desired frequency. For the purpose of this discussion, however, the state (2) → (3) transition can be considered characteristic of a CO_2 laser producing light at about 10.6 μm.

As mentioned previously, resonant transfer from the nitrogen molecule to the CO_2 molecule is the primary source of population inversion. The CO_2 molecule can also be

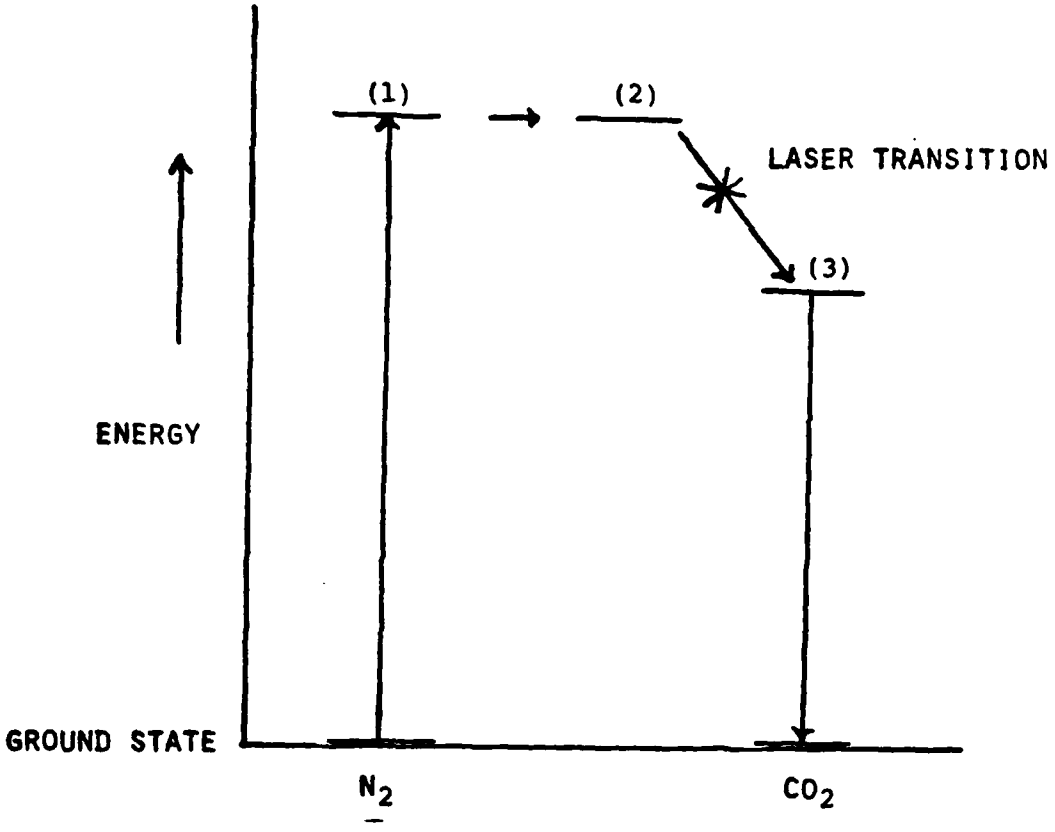

Figure 1. Energy State Diagram for $He/CO_2/N_2$ Laser System.

excited directly by inelastic collisions with low energy electrons. However, only when the electrical discharge involves time scales of less than one μsec is resonant transfer not important [2]. Thus, in producing an efficient CO_2 laser, it is important to expend as much of the energy as possible on the vibrational excitation of the nitrogen molecules.

In CO_2 lasers, the nitrogen molecule is excited by passing an electrical discharge through the gas mixture. Unfortunately, it is not possible to increase the excitement simply by increasing the energy of the discharge. Beyond a certain value, the energy of the discharge will cause electronic excitation and ionization of the nitrogen molecule as well as dissociation of the CO_2 molecule. Figure 2 taken from reference [3] shows that the fraction of the power transferred to the desired vibrational mode decreases dramatically past an E/N range of $4\text{-}6\text{x}10^{-16}$V-cm^2. The parameter E/N (field strength/gas number density) is proportional to the energy imparted initially to an electron divided by its mean free path and thus provides a measure of the energy an electron can impart to a molecule it strikes. Since number density is directly related to pressure, p, the parameter E/p has a similar proportionality. This parameter will be discussed at length in the next section. However, it is clear from Figure 2 that there is an optimum value of E/p that will produce the most effective N_2 excitation. This value for CO_2/N_2 lasers

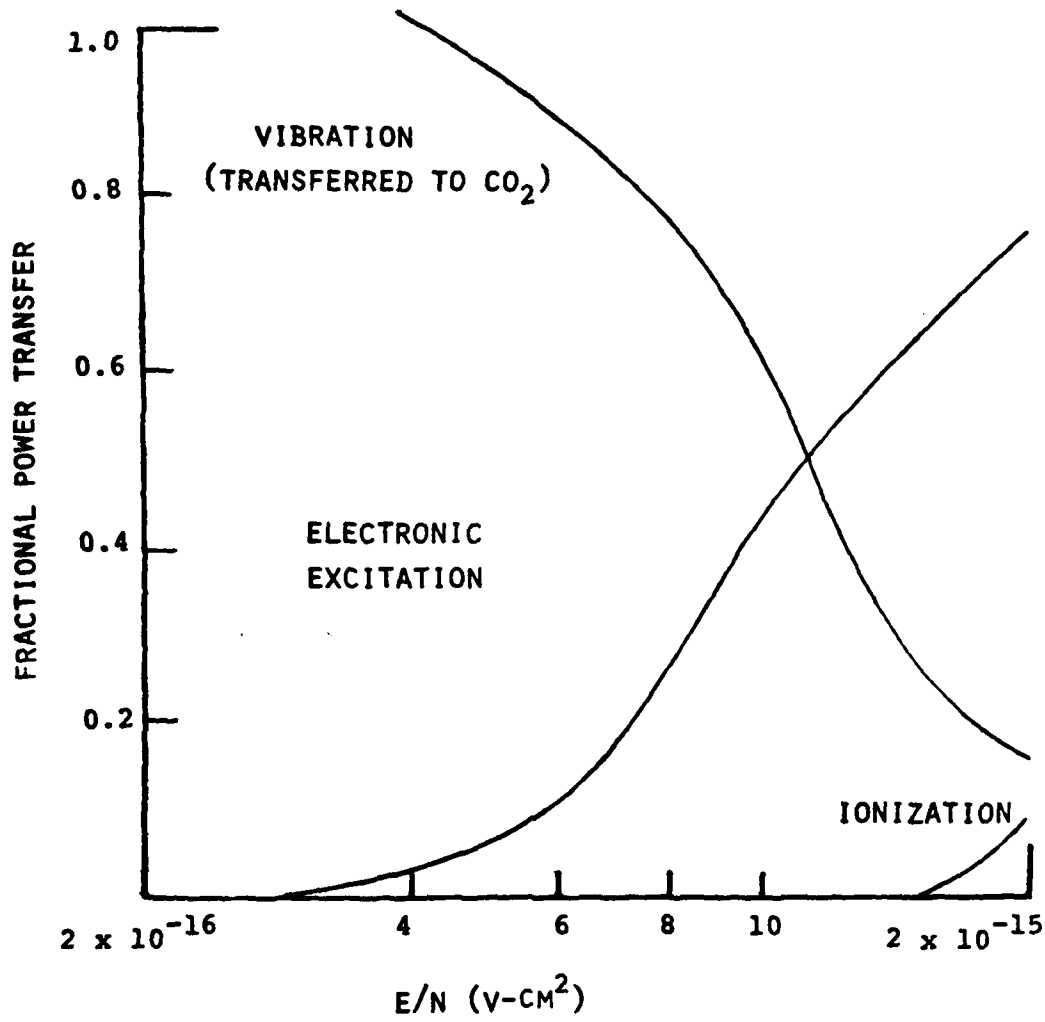

Figure 2. Fractional Power Transfer to N_2 Molecule.

has been derived theoretically [3], and experimentally for various conditions [2, 4, 5, 6], and is always between 4-20 V/cm-torr, with the most common values between 4-8 V/cm-torr. Operation within this optimum range must be considered in any new or modified CO_2 laser design.

CO_2 lasers are commonly designed using a longitudinal discharge depicted in Figure 3a. In the CO_2 system, the laser output can be increased simply by increasing the pressure of the CO_2 [1]. However, in the longitudinal discharge, the optimum value of E/p cannot be reached without extremely large voltages (as high as 40 kV). This is because the field strength is voltage/distance and the longitudinal distance is large. A solution to this dilemma can be achieved if a transverse discharge, Figure 3b, is used. Now the distance is on the order of 0.1-0.5 cm and at atmospheric pressure, the optimum E/p can be reached with as little as 1.5 kV.

It is clear that the nature of the electrical discharge must play an important role in the operation of a CO_2 TEA laser. The subsequent sections describe the properties of electrical discharges in general and how they relate to efficient laser operation.

Electrical Discharges in Gases

Townsend Discharge

When a potential difference is established between

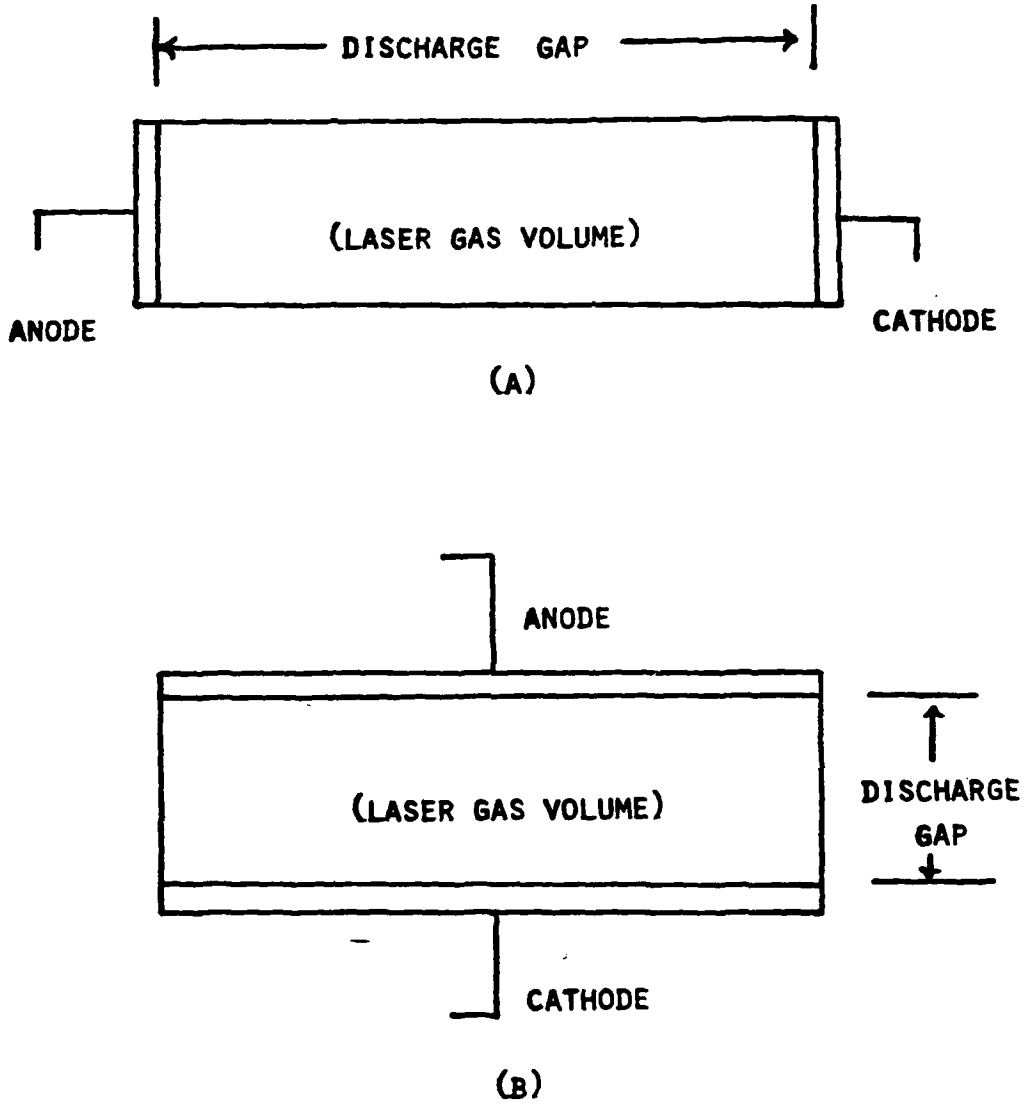

Figure 3. CO_2 Laser Discharge Configurations, (a) Longitudinal, (b) Transverse.

electrodes, the gas acts as an insulator unless the potential across the gas exceeds a specific value--the sparking or breakdown potential of the gas [7]. The type of discharge that results when the sparking voltage is exceeded depends on many factors including gas pressure, gap distance, and the constants of the external circuit [8]. Figure 4 depicts the typical discharge characteristics.

At voltages below the sparking potential, V_{sp}, the discharge is termed non-sustaining. Although lasers generally operate at conditions where the source voltage, V_s, exceeds the sparking voltage, V_{sp}. The theory in the $V_s < V_{sp}$ regime is well known and can provide insight into the desired regime (when $V_s > V_{sp}$).

During a non-sustaining discharge, current flows only when there is a small initial current, usually due to photo-electric emission from the cathode [7]. As the voltage is increased, the current to the anode increases as electrons move with their drift velocity [8]. As voltage increases further, eventually all electrons which are emitted by the cathode reach the anode. At this point, further ionization of the gas begins. This is known as the Townsend avalanche and results in a rapid amplification of the initial current. The growth in current in the Townsend avalanche is related to the rate at which electrons ionize the gas. Since the number of ionizations is related to the field, it is often called "field intensified ionization" [8]. If I_o is the current

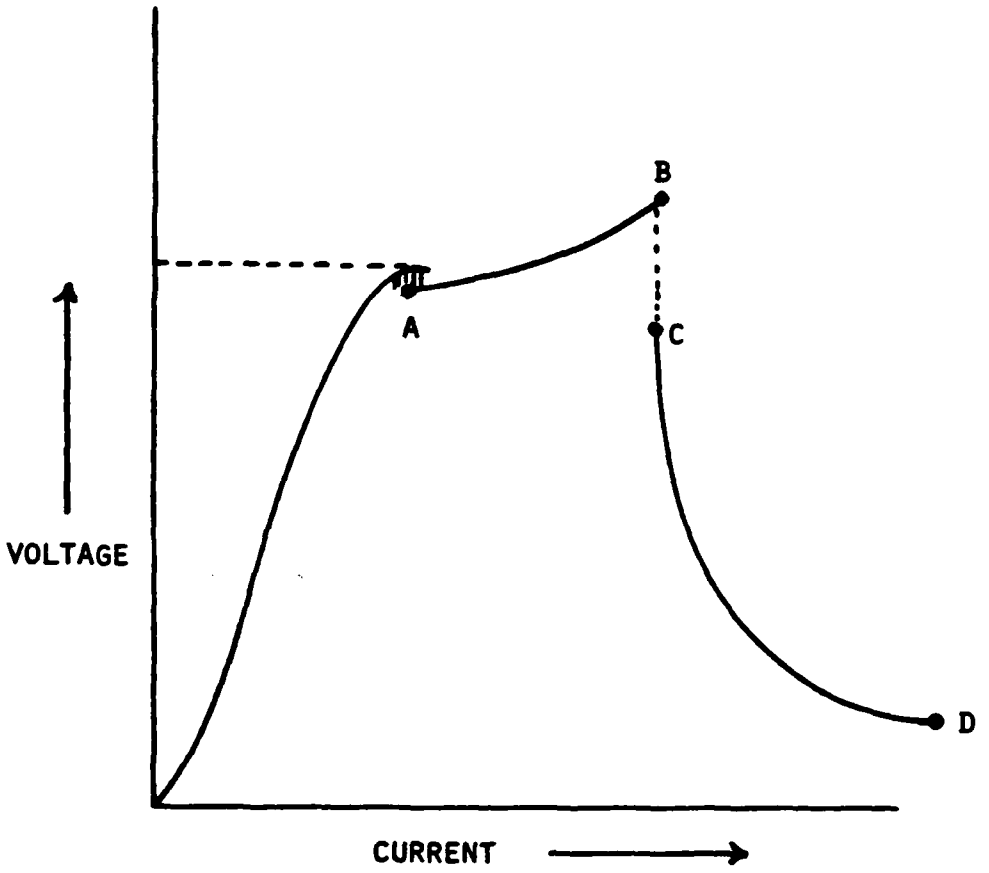

Figure 4. Typical Voltage-Current Relationship in a Gas Discharge.

emitted from the cathode (usually due to photoelectric emission) then the current, I, reaching the anode across a separation d is:

$$I = I_o \exp(\alpha d) \quad (1)$$

where α is the first Townsend ionization coefficient (cm^{-1}). This equation holds only as long as the currents are small enough so that space charge does not distort the field. The ionization coefficient represents the number of ionizing collisions for each electron per unit distance. Naturally, the number of ionizations will depend on both the field and the gas to be ionized. An empirical expression, equation (2), has been found to be a reasonable estimate of the ionization coefficient in a gas due to electrons accelerated by a strong field [8]:

$$\alpha = pA \exp(-B/E/p) \quad (2)$$

where p = pressure (torr)

E = field (V/cm)

A,B = Stoletow constants (see Table 1).

The constants A and B of equation (2) are termed Stoletow constants and are functions of the gas to be ionized. Table 1 presents the value of these constants for several gases. To calculate the amplification of the current, I/I_o, equations (1) and (2) can be combined as:

Table 1. Stoletow Constants (from [8]).

Gas	A($\frac{\text{ionizations}}{\text{cm-torr}}$)	B(V/cm/torr)	Range of E/p Valid (V/cm/torr)
Air	14.6	365	150 - 600
CO_2	20.0	466	500 - 1000
He	2.8	34	20 - 150
Ar	13.6	235	100 - 500

$$I/I_o = \exp(dp\ A \exp(-B/E/p)0) \qquad (3)$$

As ionization increases, the number of positive ions which strike the cathode begins to increase. At this point, secondary emission effects begin to supply electrons.

Included in this are the electrons released when positive ions strike the cathode. The growth of the current in static fields is usually given as [7]:

$$I = \frac{I_o e^{\alpha d}}{1 - \gamma(e^{\alpha d} - 1)} \qquad (4)$$

where I = current

I_o = initiatory photoelectric cathode emission

α = first Townsend ionization coefficient

γ = second Townsend ionization coefficient

d = electrode gap distance

Here γ represents the production of secondary electrons. (The several sources for these will be discussed later). It is important to note that α and γ are constants for a constant E/p at a given p where E is the field strength defined as voltage/d and p is the gas pressure [9]. Thus, when E/p is fixed, an increase in voltage is equivalent to increasing the spacing, d. Also, when there is no secondary emission ($\gamma = 0$), equation (4) becomes equation (1).

From equation (4), it appears that current can become infinite. In fact, current will only increase until the denominator becomes zero. At this point, the mathematically

"infinite" current actually sets the point at which sparking occurs. This is known as the Townsend Criterion for breakdown in uniformly static fields and is given as [7]:

$$\gamma(e^{\alpha d} - 1) = 1 \tag{5}$$

Since α and γ are fixed for a given E/p and p, the value of d which solves this equation, d_s, provides the sparking voltage -i.e., $V_s = Ed_s$. Above this voltage, the discharge becomes self-sustaining. Below, it is not self-sustaining and termed a Townsend Discharge.

The actual value for the sparking voltage depends on many factors (external circuit, electrode spacing, electrode material, etc.) but is usually several hundred volts [9]. Because the first and second Townsend ionization coefficients are both functions of E/p, it can be shown that the sparking or breakdown voltage is a function of pressure times distance [8, 9]. Known as Paschen's law, this is usually expressed as:

$$V_{sp} = f(pd) \tag{6}$$

A plot of V_{sp} versus pd has a distinct minimum known as the minimum breakdown potential. Irradiation of the cathode by an external source can also affect the value of V_{sp} [10]. Experimentally, the difference between sparking voltage with and without irradiation has been found to be proportional to

the square root of the current produced by the external source [10]. This factor provides a means of preionization which will be discussed shortly.

As can be seen from equation (5), both the first (α) and second (γ) Townsend ionization coefficients are important to breakdown voltage. The first coefficient is almost entirely a function of gas, gas conditions, and field strength. The second ionization coefficient, however, is the rate at which secondary electrons are produced and consequently is a function of the electrode material and design as well as the gas conditions. There are several secondary emission mechanisms which may be important. These include [7]:

a) positive ions incident on cathode
b) cathode emission due to incidence of photons
c) cathode emission due to incidence of excited atoms
d) gas ionization by positive ions
e) photoionization

The effects of thermionic and field emission are usually not considered as secondary breakdown mechanisms, although they may sustain discharges [7].

Glow Discharge

When the applied potential is greater than the sparking voltage, as is the case for the laser discharge, the electrical discharge beomes self-sustaining. At this point, there are two major classifications of discharges, the glow discharge and the arc discharge.

The glow discharge is that region of the voltage current characteristic curve marked by an increase in current with an increase in voltage (between points A and B in Figures 4). Usually this type of discharge occurs at pressures below atmospheric pressure with currents from 10^{-3} A and up [11]. The four basic parts to a glow discharge are shown in Figure 5. Of these regions, only the cathode dark space is required for a self-sustained discharge. Thus, it is this area that must be examined for insight into the stability of the glow discharge.

Since the cathode dark space can sustain a discharge without any of the other parts of the glow discharge, the conditions necessary for maintaining a self-sustained discharge must be met in this region alone. In other words, each electron leaving the cathode must interact with the gas in such a way as to cause a replacement electron to be liberated. The cathode dark space is a region of high positive space charge with a nearly linear charge distribution [11]. Although the field strength is very high near the cathode (4×10^3 V/cm), it is far short of the field necessary to pull electrons from the cathode. Thus, each electron leaving the cathode must initiate enough ionizing processes in crossing the region so that secondary emission effects (usually positive ions striking the cathode) will liberate a replacement electron. When this occurs, the discharge is self-sustaining with most of the voltage drop

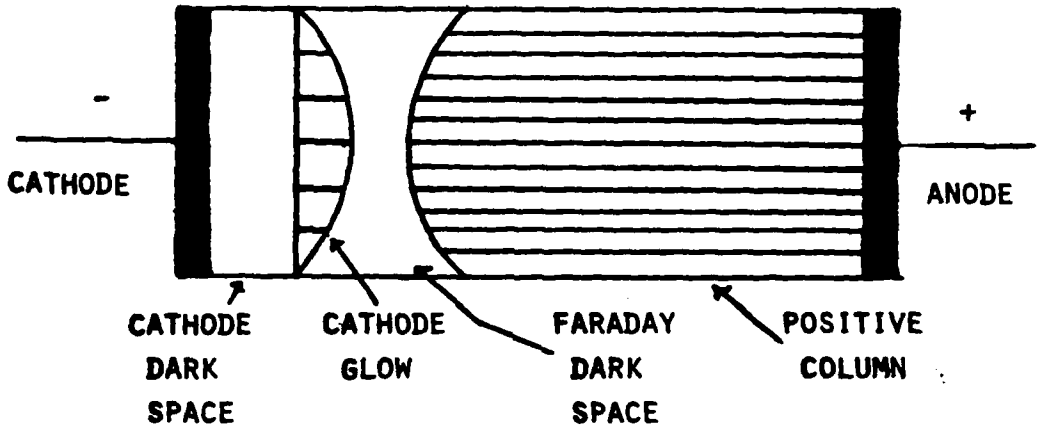

Figure 5. Major Parts of the Glow Discharge.

accounted for in the cathode dark space. This drop is known as "cathode fall."

The cathode fall can best be understood by considering a voltage source, V_s, applied to a discharge which is in series with a resistor, R (Figure 6). As discussed before, the sparking voltage is a function of the pressure distance product, pd, so that the voltage at which the discharge initiates is related to the gap distance. However, as the discharge progress a space charge is set up creating an effective anode in the gas at a shorter distance than the gap spacing [12]. This has the effect of lowering the spark voltage with the remainder of the voltage being dropped across the resistor producing the discharge current. As the current grows, the space charge increases, the gap decreases, the voltage is lowered and the current increases further. This progresses rapidly until the distance is such that the minimum sparking voltage is reached. Any decrease in spacing would now result in an increase in voltage across the cathode space charge region, and a decrease in current. Thus, the minimum sparking voltage represents the cathode fall.

Since the voltage drop across the entire discharge consists of the sum of the cathode fall, the voltage drop across the positive column and a small voltage drop near the anode, the gap voltage, V_D, will not simply be equal to the cathode fall. Rather from Figure 6, it is clear that

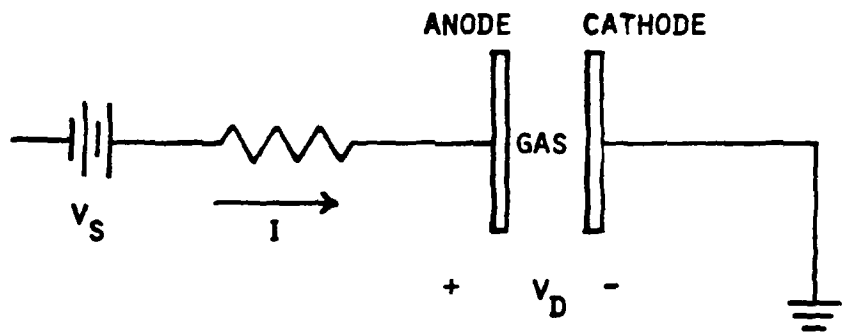

Figure 6. Simple Gas Discharge Circuit.

$$V_s - V_D = IR \qquad (7)$$

For the case when $V_s > V_{sp}$, there will be a current flowing and $V_D < V_s$. As V_s approaches V_{sp}, I approaches zero. Thus, V_D depends on V_s and is clearly also a function of pd. Figure 7 shows this dependence schematically. Measuring the minimum of either V_{sp} or V_D as a function of pd would thus serve as a measure of the cathode fall. However, in practice V_{sp} tends to be independent of the cathode at higher pd while V_D vs pd tends to be a very flat curve [12]. Thus, V_D vs pd provides a reproducible measure of cathode fall voltage. Also, it is possible to plot V_s vs I, which when extrapolated to I = 0, V_s approaches V_D and represents the cathode fall.

Once the cathode fall is established, an increase in current would seem to require an increase in this voltage. This is avoided by having the discharge spread across the cathode keeping the current density constant producing what is termed a "normal" glow discharge [11]. Once the entire surface is covered, the current density must increase with increasing current and an "abnormal" glow is obtained.

The thickness of the cathode dark space and the cathode fall are also constant in the normal glow discharge for a given cathode material and discharge gas [11]. The relationship to gas and cathode material is to be expected since all of these are related to the tendency for the gas to ionize and the ease at which positive ions can induce the cathode

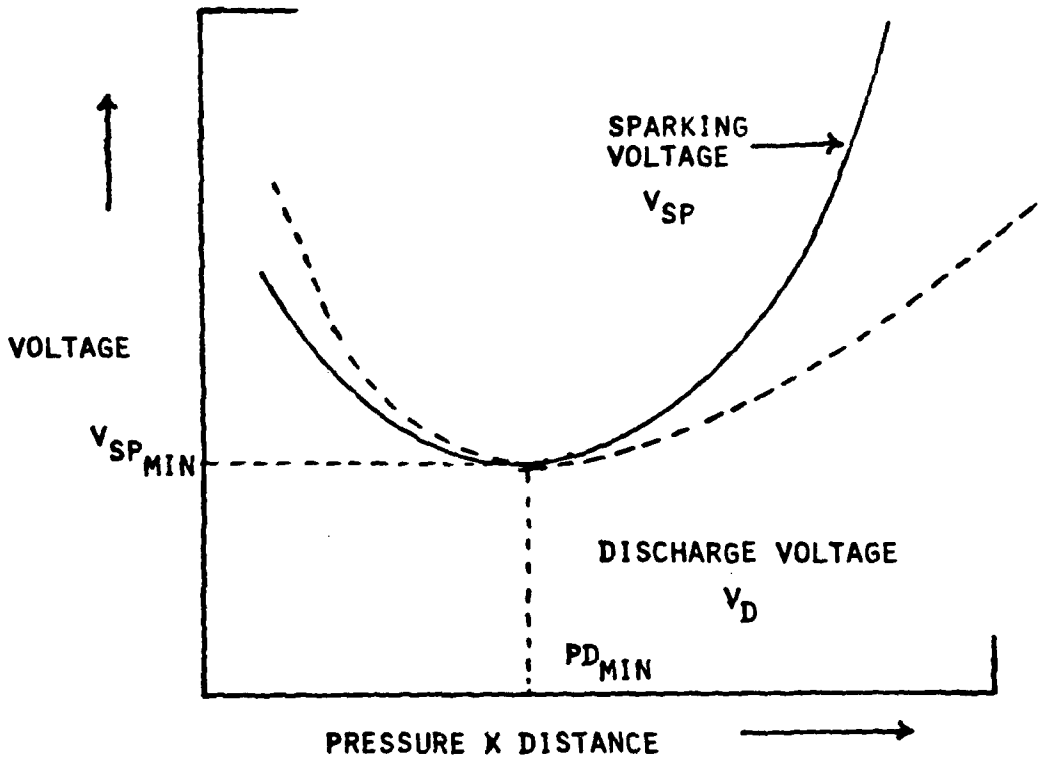

Figure 7. Paschen Law Curve for Sparking Voltage and Discharge Voltage.

to release electrons. Typical values of cathode fall for common cathodes and gases are shown in Table 2.

For the normal glow discharge, the cathode dark space thickness (d_n) and pressure (p) are related as:

$$pd_n = c \tag{8}$$

where c is a constant [8, 9, 11]. Values for c vary with gas composition and cathode material. Table 3 provides a partial list of these values. Also for the normal glow discharge, the current density (J_n) is proportional to the square of the pressure as:

$$J_n = kp^2 \tag{9}$$

where k is the constant of proportionality [8, 9, 11]. Table 4 presents values for J_n/p^2. The cathode fall for a normal discharge, like the current density and the dark space distance, depends on the efficiency of the cathode for producing electrons when struck by positive ions. Thus, it is not surprising that cathode fall can be related with high correlation directly to the cathode work function (for any given gas).

All of the values shown in Tables 2, 3, and 4 are only average values. Discrepancies occur because of the difficulty in measurement as well as in the experimental control. Gas impurities, for example, affect greatly the values observed

Table 2. Cathode Fall (Volts) (from [8]).

Cathode	Air	Ar	He	H_2	Ne	N_2	CO_2
Aℓ	229	100	140	170	120	180	-
Cu	370	130	177	214	220	208	460
Fe	269	165	150	250	150	215	-
Mo	-	-	-	-	115	-	-
W	-	-	-	-	125	-	-

Table 3. Values for C for Pd_n = C (cm-torr) (from [8]).

Cathode	Air	H_2	He	N_2
Aℓ	0.25	0.72	1.32	0.31
Cu	0.23	0.8	--	--
Fe	0.52	0.9	1.30	0.42

Table 4. Glow Discharge Cathode Current Density (J/p^2) (microamp/cm^2/$torr^2$) (from [8]).

Cathode	Air	H_2	He	N_2
Aℓ	330	90	--	--
Cu	240	64	--	--
Fe	--	72	2.2	--

[11]. Most importantly, these relationships are for the normal discharge region. In the abnormal glow regime, the cathode fall increases very rapidly with increased current or pressure, while the thickness of the dark space region decreases [11]. For plane cathodes, in common gases, the abnormal cathode drop can be given as [8, 11].

$$V_a = E + \frac{F\sqrt{J}}{p} \tag{10}$$

where: V_a = the abnormal cathode drop

J = the current density

p = the pressure

E,F = constants which depend on the gas and cathode.

Likewise the dark space thickness in the abnormal glow (d_a) is given by [8, 11]:

$$d_a = \frac{A}{p} + \frac{B}{\sqrt{J}} \tag{11}$$

where A and B are constants which depend on the gas and cathode. The experimental values may be altered by the generation of heat near the cathode region [8].

Arc Discharge

The voltage drop in a glow discharge is on the order of the breakdown voltage [11]. Once the cathode is completely covered (abnormal glow), the current density increases with the discharge current. The voltage also increases [8]. At some critical point, the discharge changes from a glow to

an arc resulting in a sudden increase in current density at the cathode [8]. The potential, V_D is now usually not more than 10 to 20 volts [11]. This corresponds to the region between points C and D on Figure 4. The maintenance of the discharge with such a low potential requires a change in electron emission processes at the cathode. For refractory materials, the increase in temperature during the abnormal glow regime will become sufficient to promote thermionic emission [8, 11]. For low melting cathodes, it has been suggested that field emission due to formation of a dense sheet of positive ions near the cathode is responsible for the increase in electrons.

The glow to arc transition can be induced either by increasing the current at a constant pressure or by increasing the pressure at constant current [8]. Irregularities at the cathode surface will cause the formation of arcs at the point where the field is the highest. Also, low work function impurities will permit glow-arc transition even from a normal glow discharge [8].

The voltage-current characteristics in an arc are not typically linear [11]. This is because of the dynamic nature of the conditions in the arc including temperature, ion density and electron energy. Only when the current is changed very slowly is the static voltage-current curve (Figure 4) followed exactly. A complete discussion of the behavior of arcs can be found in reference [11].

TEA Lasers

For operation of a molecular laser, high discharges must be uniform, large in volume and stable; should have the appropriate mean electron energy (related to E/p) to excite the desired vibrational states; and should have a high current density in order to achieve a high population inversion in a short time [3]. Unfortunately, uniform excitation of gases at elevated pressures is difficult. A low-pressure glow discharge changes characteristics as pressure is increased, and at about 50 torr, the glow transitions to an arc. Arc discharges are not suitable for efficient excitation of molecular lasers [3]. Clearly TEA laser conditions favor arc rather than glow discharge [13, 14]. Despite these inherent problems much effort has been expended to achieve stable high pressure TEA CO_2 lasers.

Conventional TEA Lasers

Although prior work had been done on the TEA CO_2 laser, Smith, et al. [6] were the first to combine this type laser with the main features of the waveguide laser. Their waveguide had a 1 mm square cross section and was 6 cm in length. The cathode was a solid copper block, while the anodes were thin (2 μm) copper strips located on a fused quartz substrate. The sidewalls were fused quartz slabs with polished sides. Their discharge circuitry involved simultaneously discharging individual capacitors of 100 μμF attached to each single anode strip. The capacitors were charged initially to 1.5 kV.

Charging was accomplished by means of a silicon-controlled rectifier. The peak current had an adjustable time duration from 1-10 μsec second was typically 1-2 A (given as the sum of the individual discharge currents). A mixture of CO_2, N_2 and He was passed through at "high" (not given quantitatively) flow rates. When the device was operated at about 400 Hz repetition rate, the discharge was more diffuse. This was attributed to "preionization" of the laser by the previous discharge pulse. Smith, et al. felt that the waveguide TEA laser offers the greatest opportunity for uniform discharge and minimum tendency to degenerate into arcs.

In later work, using a very similar device, Smith, et al. [15] operated at repetition rates of up to 40 k Hz using a thyratron pulser. They found that their device operated as a quasi CW device since gain persisted for a period of time after termination. The tests were run up to 1/3 of an atmosphere. The peak discharge current (total for all strips) for their device was 15 A using pulse widths of 1 μ second at 3 kV charging voltage. By increasing the nitrogen content of the lasing gas, the duration of lasing could be prolonged, at the expense of peak laser power.

One of the most comprehensive discussions on the limitations of the waveguide CO_2 laser came out of work by Papayaonou at the U.S. Army Electronics Command [16, 17]. The laser used in these investigations is shown schematically in Figure 8. For CW operation, each anode resistor had a

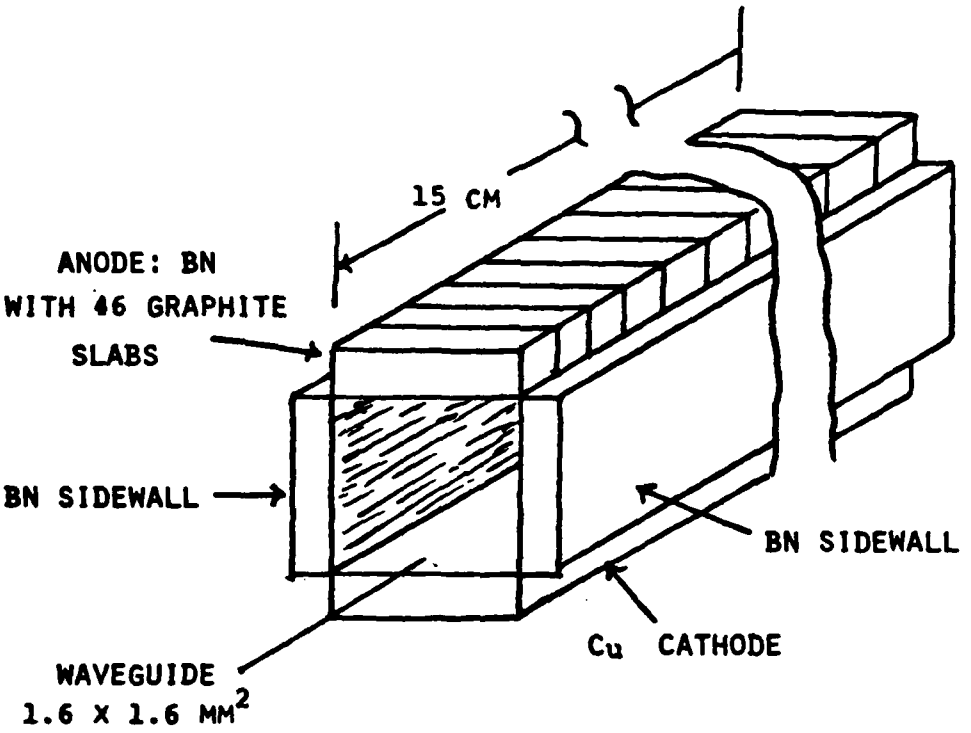

Figure 8. Schematic of a Waveguide Laser (from [16]).

1.5 MΩ ballast resistor to help maintain a stable CW discharge at higher pressures. The CW experiments were conducted with a closed cycle system with gas flow dwell times as short as 0.4 ms. The best results were at these higher flow rates. Visual observation of the discharges revealed a conical shaped luminous region with the anode as the vertex and the cathode as the base. As pressure increased to between 100-200 torr the discharge contracted radially and changes in cathode cooling, gas flow or gas mixture could not alter this contraction. Reversing the anode and cathode did not improve the discharge. At currents between 0.5 and 1.0 mA, a negative discharge resistance of 7 kΩ was observed. Apparent gains between 3 and 5 percent were measured for pressure between 80 and 250 torr at the near optimum discharge current of 30 mA (0.75 mA/slab). Visual observations of the pulsed discharge were similar. Optimum pressure for laser operation was higher when open flow was used with 70 to 85 torr optimum for the 55/28/17 mixture of $He/CO_2/N_2$ while 110 to 125 torr was optimum for 80/12/8. Laser power was reduced when water cooling of cathode was eliminated.

Papayaonou asserts that even when the discharge was restricted to a glow discharge by ballast resistors, the close spacing of the electrodes (1.6 mm) did not allow adequate length for discharge to expand and meet the sidewalls. Also, in CW discharges, the cathode fall is a large percentage of the voltage across the electrode (estimated to be between 35

and 82 percent of the total voltage). Thus, at low pressures, most of the energy is lost. At higher pressures, the contraction of the column becomes important. Papayaonou also calculated (using values taken from [8]) that very large power densities are placed into the waveguide resulting in high gas temperatures. The heating of the gases reduces gain and creates anisotropy in the index of refraction. Furthermore, for pulsed discharges, where the average current/slab is 125-250 mA, the discharge becomes an abnormal glow. This further increases the energy deposited into the cathode area. Papayaonou suggested that if the Townsend Second ionization coefficient of the cathode could be increased, larger current densities could be used while still maintaining a glow discharge. This would reduce the amount of heating in the cathode region. The Malter effect (discussed in a later section) was suggested as a possible solution. In addition, the current density could be reduced by increasing the uniformity of the anode discharge. This could be done by increasing the number of anode slabs per unit length.

In another effort for the U.S. Army, Mocker, et al. [18] reviewed the current state of the art in TEA waveguide lasers. From this review, they attempted three different waveguide configurations, a relaxation oscillation design, a solid electrode waveguide laser, and a multi-pin waveguide laser. Of major interest are the second two designs. Their waveguide consisted of two copper electrodes with quartz

slabs as the sidewalls. High voltage pulses were applied by means of a triggered thryatron. Initial results showed a strong preference for arcing at the ends of the electrodes, even at low pressure. At high pressure only arcing was observed. The electrodes were cleaned, smoothed, then uniformly roughened and there was a marked reduction in arcing. (This confirms the work of Karasiko and Shamin [19] who found that uniformly roughened electrodes were an improvement over smooth electrodes.) Arcing at low pressure (50 torr) occurred only occasionally, increasing as the voltage was raised above 5 kV. As pressure was increased, arcing increased as well. Examination of the electrodes showed a brownish discoloration where the strong arcing had occurred.

A multi-pin configuration was also tested. In this approach, 75 tungsten pins 0.004 inches thick were used with each pin connected to a load resistor. The uniformity of the discharge was good at 76 torr although individual filaments for each pin-slab did exist. At 280 torr, the uniformity was also good although at 390 torr, individual arcing took place. When the charging capacitance was reduced to 2.5 nF (from 15 nF) uniform excitation could be achieved at 450 torr. At atmospheric pressure, individual arcs existed.

Preionized TEA Lasers

Much of the arcing, non-uniform discharges and low gain reported are due in part to the fact that the fields required to provide a discharge at high pressure are far greater than

the optimum field (actually E/p) for laser excitation. However, it is possible to lower the potential required for sparking by creating ions in the gas. It was shown by White in 1935 [20] that the sparking potential is lowered when intense ultraviolet light is incident on the cathode. This was attributed to the release of electrons which subsequently created positive ions. This concept has been greatly extended and leads directly to the process of preionization- the separation of the charge carriers in the discharge from the magnitude of the applied field. This allows E/p to be optimized independently from the breakdown voltage.

One of the most common techniques for preionization is the use of two separate discharges. Laflamme [21] was one of the first to employ this "double discharge" technique successfully. In his work, he used two consecutive discharges, one to provide a source of electrons and one for the main discharge, Figure 9. The flat grid wire, G, is a common electrode to both discharges. Electrode T (the "Trigger electrode") is very close to G and is covered with a dielectric material. The third electrode, S, is at a larger distance from G than is T. As G is pulsed, the field between G and T grows faster than S and G, causing a discharge to start earlier. Although the current is small, the main discharge between G and S profits from the free electrons left in the vicinity of G.

While the others have employed different electrode

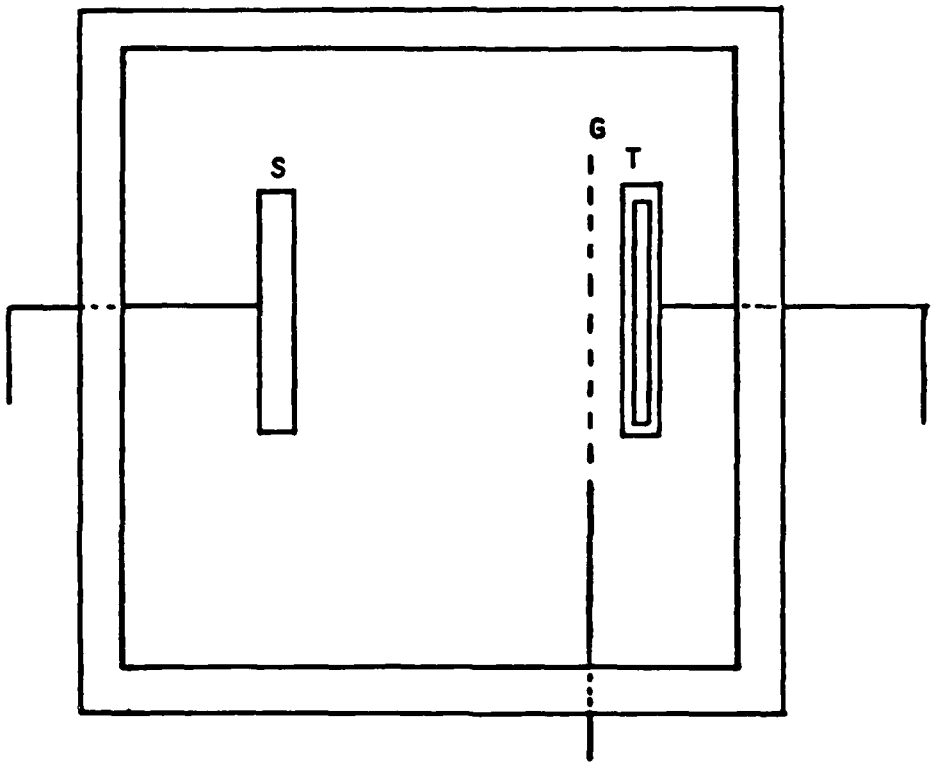

Figure 9. Electrode Configuration for a Double Discharge Laser ([29]).

configurations, the principle of the double discharge remains the same. References [13] and [22] through [28] as well as those discussed in detail below all use this type of preionization. An extensive review of work in this area can be found in references [2] and [3]. In most of the efforts, a high voltage discharge provides the ionization while a second, lower voltage discharge provides the field for inducing laser action. Because the high voltage discharge is much shorter than the low voltage discharge, only a small percentage of the total discharge energy goes into preionization. Yet enough ionization is achieved such that the breakdown energy is lowered significantly. Most of the complications with this technique come from the problem of switching the several kilovolts required for preionization while keeping the timing in the microsecond range.

Perhaps the best illustration of the preionization phenomenon is given by Jain, et al. [29]. In their work, they used a 100 n-sec high voltage pulse followed by an 18 μsec "DC" low voltage pulse of opposite polarity. A single pin (0.5 mm dia.) was used as the preionization cathode with solid copper as the cathode for the 18 μsec pulse. A 9.8 kΩ ballast resistor was used in the circuit to limit the current. They found that the short pulse behaved as an arc creating enough ionization to allow the reverse polarity discharge to establish a glow across the gap. Figure 10 depicts how the authors were able to control E/p by selection of the proper

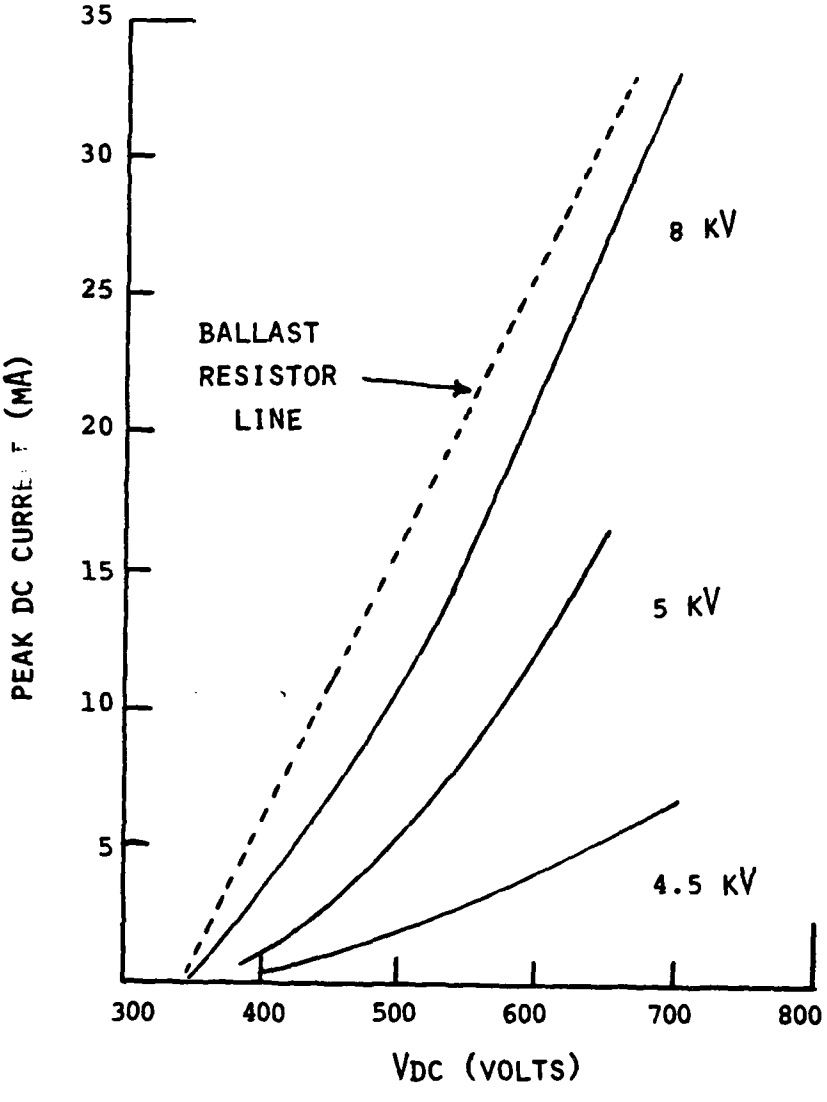

Figure 10. Peak DC (18 μsec pulse) Current Versus Applied DC Voltage for Various AC (100 msec) Voltages (from [29]).

high voltage pulse. Of the preionization cathodes tested, Fe, Ca, Ta, and W were particularly promising.

Many other efforts before and after Jain have also used the "double discharge" technique for providing preionization. Wood, et al. [4] used a 20 μsec duration pulse followed by a longer pulse of opposite polarity. Aluminum was used as the cathode for the preionization source, with the anode polished copper. The laser gas was 0.5/0.3/3, $CO_2/N_2/He$ flowing at 1 ℓ/min with pressure of 145 torr. Assuming a cathode fall of 460 V, the voltage across the positive column was calculated to be 50-100 volts, resulting in a E/p value of 3.4-6.9 V/cm torr. This is considered to be well below that necessary to initiate glow discharge in the absence of the preionization, but optimum for the CO_2 lasing. They attributed the high preionization to secondary emission from the aluminum cathode probably due to the "Malter effect" from the oxide layer on the cathode.

Smith, et al. [30] evaluated the role of E/p in the waveguide TEA laser. They used a short "ac" preionization with a longer "DC" excitation. Their laser consisted of a bottom wall of polished copper with glass slabs (polished edges) as the sidewalls. Metal wires through 0.75 mm holes in the lava top wall formed the other electrode. The preionization pulse had a duration of 100 ηsec, while the main "DC" source had pulses of 20 μsec. They found that the long pulse rapidly established a cathode fall of approximately 350 V in a region

less than 100 μm above the DC cathode (Cu block). Because of the small electrode spacing (2.0 mm), a large fraction of the total voltage drop was in the cathode fall region, resulting in a high dissipation of electrical power in this region. Two detrimental consequences were loss in efficiency due to the loss of energy in the region and heating of gas near the cathode which limits the gain of the laser. The fraction of the energy which gets into the positive column, F, was defined as:

$$F = \frac{Ed}{V_c + Ed} \tag{12}$$

where: E = the field in the positive column

d = the spacing between electrodes

V_c = the cathode fall voltage

Thermal saturation of the laser (when thermal effects negate the population inversion) occurs at 300 J/ℓ-atom, so that the energy at saturation is 300 F (J/ℓ-atom) in the positive column. Clearly as E/p increases, the energy at which saturation occurs must increase. But, for the gas mixture 1/0.5/4.4 of $CO_2/N_2/He$, as E/p increased from 4 to 8 V/cm-torr, the efficient excitation of the CO_2 molecules decreased. Smith, et al. found that that could make use of the higher thermal saturation value if a mixture of 1/1/3; $CO_2/N_2/He$ was used. Their results indicate that the maximum gain for this mixture is around 8.5 V/cm-torr. Difference between Al,

Ta, and Cu preionization electrodes were within experimental error. Based on their work, they recommend that large waveguide bores ($\sim$2 mm) should be used to minimize cathode fall effects. Also, operation should be at the highest E/p consistent with efficient excitation.

Dyer and James [31] also found that preionization was necessary for production of a high-energy density discharge. Pulsed discharges at high pressure passed through a glow phase prior to the formation of a constricted, highly conductive channel. Arc formation was marked by large amplitude oscillations in current and voltage waveforms, a result of the rapid change in loading provided by the discharge.

Another preionization technique has been the use of a high energy electron beam to directly supply the electrons. Two efforts from Las Alamos Scientific Laboratories, Fernstermacher, et al. [32] and Stratton, et al. [33], provide the best examples of this type. Here, the electrons were produced by a hot-cathode electron gun and were accelerated through a 0.001 inch Al vacuum window foil by application of a 150 kV, 10 μsec voltage pulse. The authors "injected" an electron current of 5 A (0.033 A/cm^2) into the gas and were able to sustain a discharge at 600 torr with only 3.5 kV across the 10 cm gap.

There is a distinct difference between the use of an electron beam to sustain a discharge and true preionization discussed above. In most of the electron beam sustained

discharges, the current amplification comes from energy of the beam itself. The CW fields are kept low so that field intensified ionization does not occur. This prevents run away current growth and arcs. However, the amplified current pulse coincides exactly with the electron beam pulse. In the double discharge techniques, the ions produced by the first discharge are accelerated by the field, causing an increase in current and secondary emission. These discharges then became self-sustaining even after the initial discharge is through. This technique is not done with CW fields, as arcs would develop. In fact, when the fields used in a e-beam sustained lasers are increased, arcing becomes a problem unless these fields are also pulsed [3].

Other methods for achieving improvement in discharge characteristics are not well understood, nor as successful. One such technique is using the "Malter Effect." It was found [34] that thin oxide films will aquire a positive charge during positive ion bombardment. This creates an intense field in the film which ionizes electrons that are then accelerated by the field. At higher currents field emission may predominate making the current independent of the gas pressure [7]. Also, as discussed previously, uniformly roughened electrodes seem to eliminate random surface perturbations and stabilize the electrical discharge [19]. The use of low ionization additives has also been known to be effective [38]. Still others have used current limiting

techniques such as high resistance electrodes or large series resistors in order to maintain a glow discharge [36, 37, 38]. Unfortunately, this technique results in a large loss of power due to the resistive losses.

Field Emission from Oxide-Metal Composites

It is very likely that unidirectionally grown oxide-metal composites can offer a technique for supplying a uniform source of electrons through field emission and thus, these composites may offer a solution to the type of problems which plague TEA CO_2 laser operation. This section presents a description of the composites and their field emission characteristics.

Field Emission

Field emission is the process of electron emission from a metal or a semiconductor into vacuum owing to the presence of a high electrical field at the surface. These free electrons "tunnel" through the metals surface potential when the latter is thinned by the high field. A great many references provide details on the theory of field emission and the theoretical analysis presented below [39, 40].

The theoretical analysis which is most often used to describe field emission is the Fowler-Nordheim equation. This equation was derived by calculating the thinning of the potential barrier for an applied field and the tunnelling through that barrier. The details of that derivation are not

presented here, but lead to the following equation:

$$J = \frac{AE^2}{t(y)} \exp\left(\frac{-B\phi^{3/2}}{B}\right) f(y) \qquad (13)$$

where: J = field emission current density (A/cm^2)

E = electrical field at surface (V/cm)

ϕ = work function (electron volts)

y = shottkey lowering of work function barrier

($y = 3.79 \times 10^{-4} E^{1/2}/\phi$)

f(y),t(y) = computed elliptical functions (see [39])

A, B = combined physical constants with numerical value of 1.54×10^{-6} and 6.83×10^{7}, respectively.

For the purpose of this work, the important factor to realize is that the high fields which permit the oxide metal composites to be field emitters are created by a field enhancement at the very small tips of the metal pins. This enhancement can be related to a geometrical factor β defined as

$$\beta = 1/r \qquad (14)$$

where r = the radius of the pin tip. This enhancement factor β then can be used to relate the voltage applied, V, to the field, E, as:

$$E = \beta V \qquad (15)$$

Combining equations (13) and (15), dividing by V^2, and taking the log of both sides puts the Fowler-Nordheim equation in the

form:

$$\log J/V^2 = A - B/V^2 \tag{16}$$

where V is the voltage applied. This equation is a straight line where the slope and intercept are functions of the work function, ϕ, and the geometric parameter, β.

Another way of relating enhancement to the voltage is to use a dimensionless field enhancement factor, γ, as

$$E = \gamma E_A \tag{17}$$

where: E = the enhanced field

E_A = the applied field

Creating the fields required for field emission (3×10^7 V/cm) is not feasible unless β (or γ) is large. Usually, narrow wire tips are used. However, at the Georgia Institute of Technology, work has been underway for several years using unidirectionally grown oxide-metal composites as field emitters [41]. These composites will be discussed next.

Oxide-Metal Composites

Although the growth of many oxide metal composites have been attempted, the two which have shown the most promise are Gd_2O_3-Ce_2O_3-Mo and UO_2-W. (The growth of unidirectional composites is presented in Appendix A.) The results of the unidirectional growth process is a structure consisting of an oxide matrix with single crystal metal pins. The pin densities of these composites range from 10^6 - 10^7 pins/cm^2

with pin diameter of 3000-4000 Å. Because of the arrangement of pins, the composites would be expected to act much like the multipin electrodes described previously. But, with the large number of pins, the potential for uniformity of the discharge is far greater with the composites. Perhaps a more significant advantage of the composites is that the pins can be lengthened and/or pointed so that an optimum geoemtry for field emission can be achieved, Figure 11. Ohlinger [39] using fields on the order of 10^5 V/cm, measured field emission from pointed exposed pin UO_2-W composites as high as 1.2 A/cm^2.

The second promising use of the unidirectionally grown composites is as a low voltage field emission electron source for preionization. Figure 12 shows an example of the low voltage field emitter (LVFE) developed at Georgia Tech [41]. (The details of manufacture are summarized in Chapter III.) When the extractor is grounded and a negative voltage put on the pins, the small diameter hole and sharp pins lead to high fields at the tip. These fields have been estimated to be as high as 10^8 V/cm at the tip of the pointed pins when only 100 V is applied [40]. When emitting areas on the order of 1 x 10^{-4} cm^2 are used, emission current densities as high as 30 Å/cm^2 have been reported [40].

(a)

(b)

Figure 11. Typical Exposed Pin Cathodes. (a) X5200, (b) X1200, from [41].

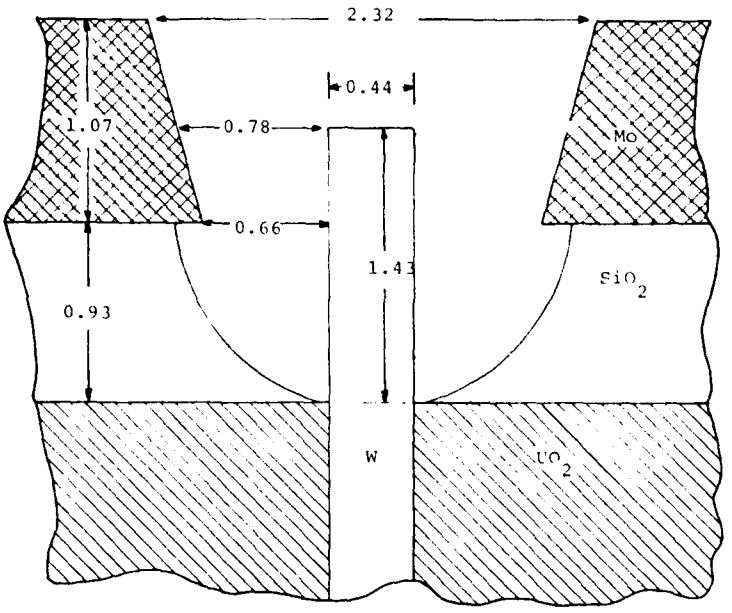

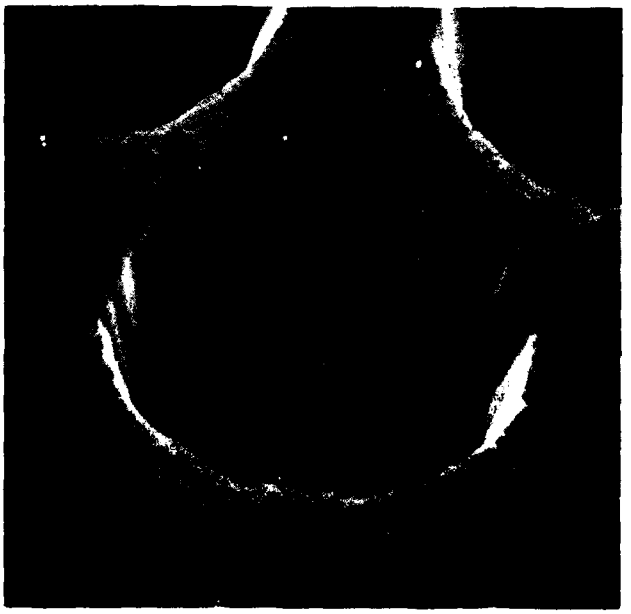

Figure 12. The Low Voltage Field Emitter (LVFE) Structure (dimensions are in microns).

CHAPTER III

PROCEDURE

The research conducted in this study was divided into two areas. In the first, unidirectionally grown composites were tested as electrodes for CO_2 TEA lasers. Polished and exposed pin composite electrodes were fabricated and tested for cathode fall uniformity and stability. Comparisons of these discharge properties with those of an aluminum electrode were made. In the second area, Low Voltage Field Emitters (LVFE) were examined as an electron source for control and/or preionization of a gas discharge. Included in this examination was an evaluation of high pressure emission, the use of emission to control gas discharges, and the survivability of the emitters in the high pressure environment.

This section provides details on the test apparatus, electrode fabrication and testing for both areas described above.

Unidirectional Composite Electrode Discharge Test Apparatus

The electrical and visual discharge characteristics of the composite electrodes were evaluated using a flow system, Figure 13, consisting of a glass T into which the discharge assembly, Figure 14, could be inserted. The water cooled

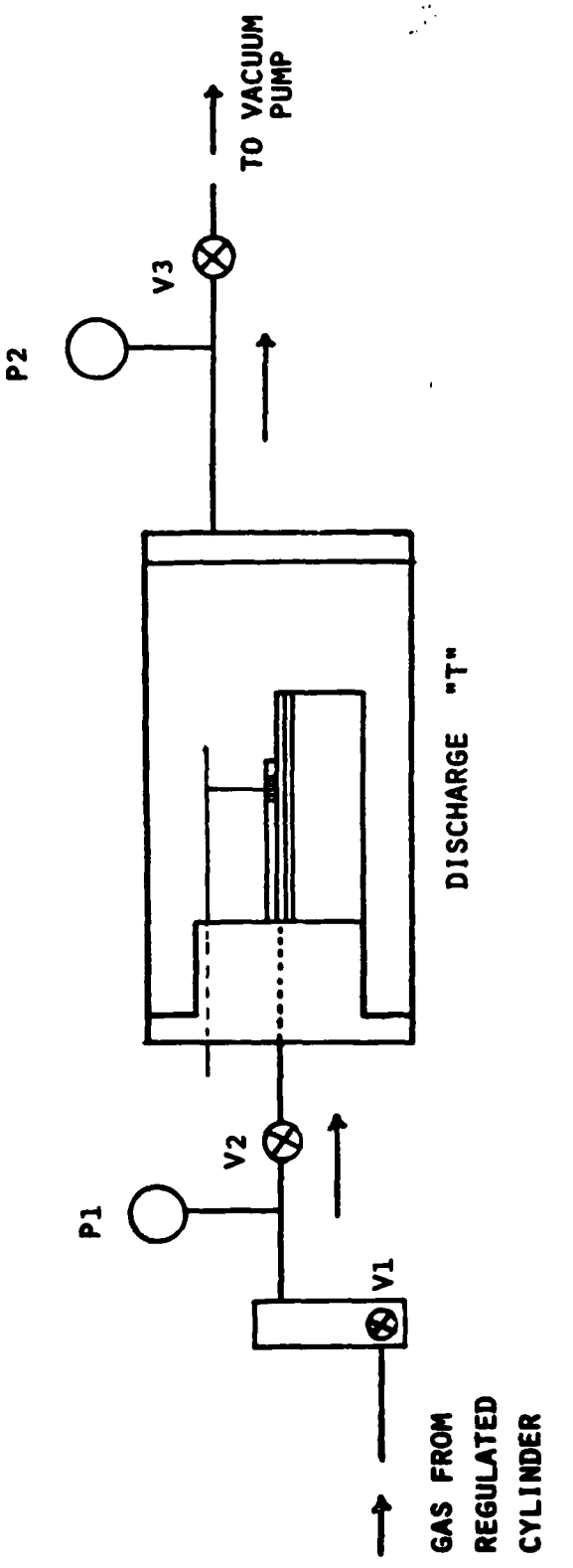

Figure 13. Schematic of Composite Electrode Discharge Apparatus.

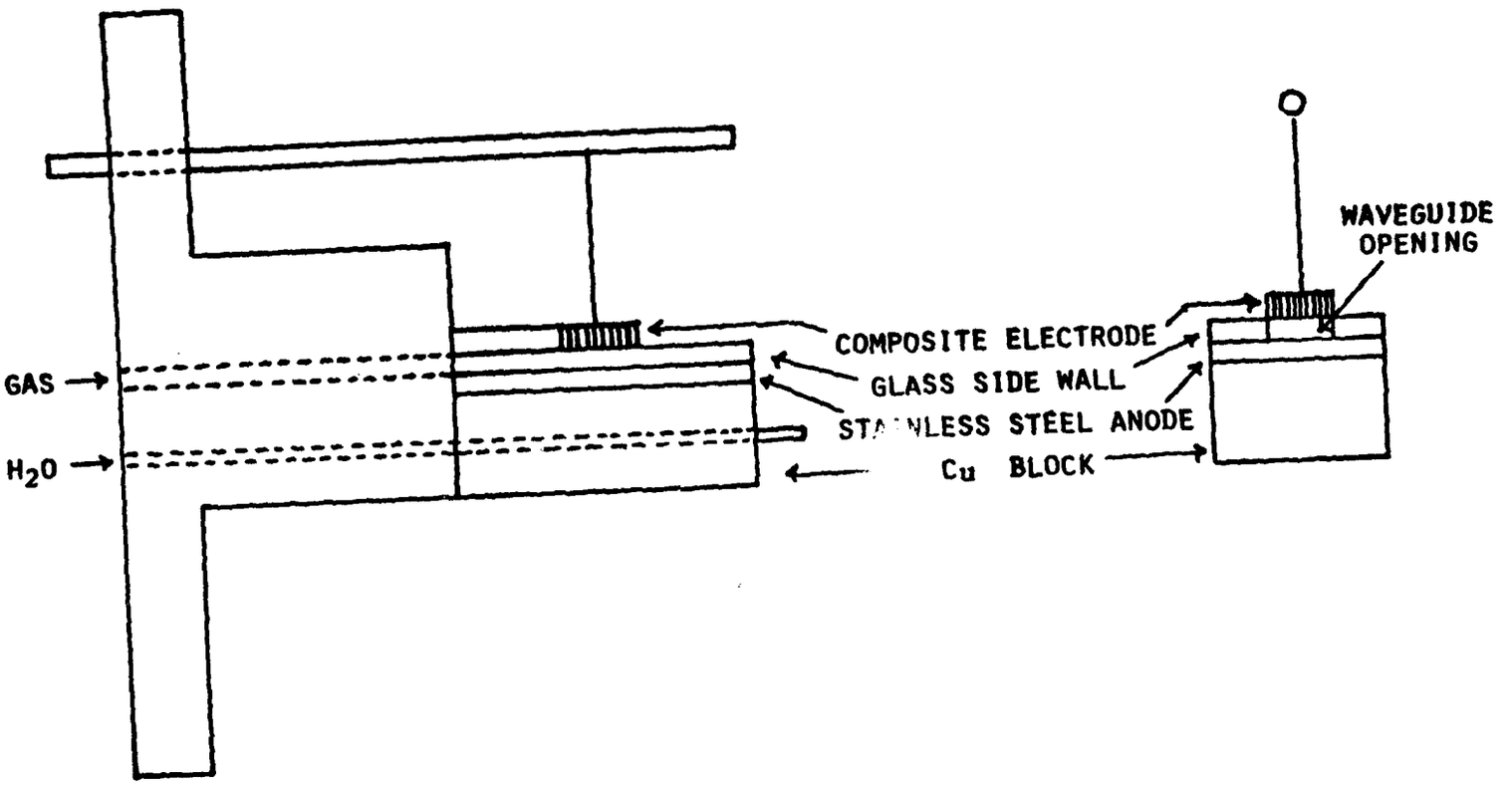

Figure 14. Schematic of Composite Electrode Waveguide Configuration.

copper block served as a base for a stainless steel plate electrode. The composite in this configuration rested on top of glass sidewalls which provided both the channel for the gas flow, and the anode-cathode spacing for the discharge. A pair of 1 mm microscope slides or 3 mm plate glass slabs were used as sidewalls for most tests. The sides of these glass pieces were polished so that the discharge could be observed. Electrical connection to the composite electrode was made using a wire silver pasted to the back of the composite and spot welded to an aluminum bar which passed through the plexiglass. Electrical contact to the copper was made through the water cooling tubes. The discharge assembly was designed so that the composite electrode would be centered in the glass T. The port at the stem of the discharge was closed with a clear plexiglass disc to allow observation of the discharge.

The gas used throughout the composite electrode testing was a laser gas mix of 12.5% N_2, 12.5% CO_2, 75% He. The gas flow system used for the discharge tests, Figure 13, provided a flow from a regulated gas cylinder, through a flow meter, into the discharge chamber, and finally evacuating into a vacuum pump. The pressure on the downstream side of the flow meter was kept at atmospheric pressure to ensure that the flow-rate readings would be valid. This pressure was monitored with a barometer (P1). A value (V2) provided the pressure drop between atmospheric pressure and the desired chamber

pressure. A second barometer (P2) was used to monitor the chamber pressure. Finally, a value (V3) upstream from the vacuum pump throttled the vacuum pump to equilibrate evacuation rate with flow rate. The operation characteristics of this system were limited by the volume of gas the vacuum pump could handle. However, the limitation was not severe.

Composite Electrode Fabrication

In the discharge tests, one electrode was always a stainless steel plate polished to a 1 μm finish. The electrode was either an aluminum control electrode or a unidirectionally solidified composite test electrode. The growth and properties of the two composites, UO_2-W and Gd_2O_3-Ce_2O_3-Mo have previously been discussed. This section details preparation of experimental composite electrodes starting with composite slices cut perpendicular to the metal fiber axes.

Slices of these composites 2-4 mm thick were core drilled in a crack free area to form a cylinder 8.2 mm (0.325 in) in diameter. A matching hole was then drilled in a 1 mm thick alumina substrate and the composited was mounted into the substrate with epoxy so that the front surface of the composite was flush with the alumina, Figure 15. After curing the epoxy for 24 hours at room temperature, the composite-alumina electrodes were ground sequentially with 180, 320, and 600 grit silicon carbide paper. In most tests the final polish was with 1 μm diamonds paste. However, in some tests an additional 0.3 μm Al_2O_3 polishing was performed. To

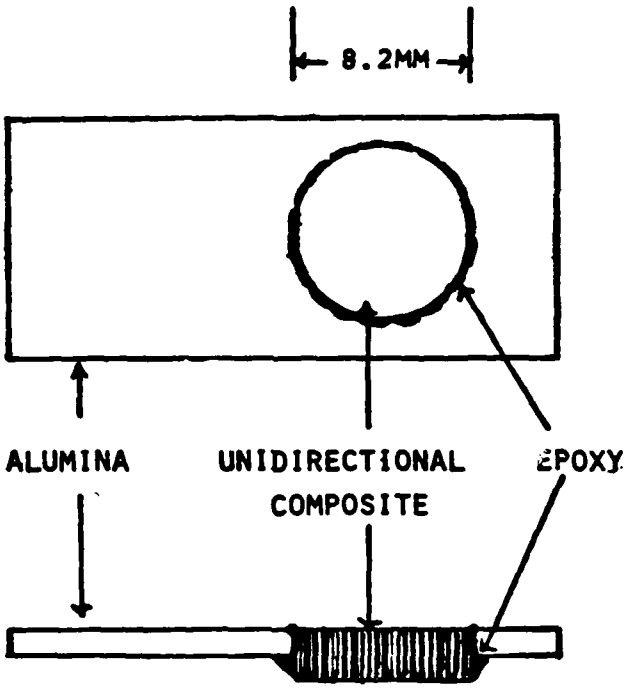

Figure 15. Composite Electrode Fabrication.

prepare the aluminum control electrode, an aluminum rod 2 cm long machined to the desired 8.2 mm diameter was epoxied into the aluminum substrate and polished to a 1 μm finish as described above.

Up to this point, preparation of both composition composite electrodes were identical. However, for tests requiring exposed pins, it was necessary to preferentially etch the composites and this process was different for the two types.

Concentrated sulfuric acid will dissolve the oxide matrix of the Gd_2O_3-Ce_2O_3-Mo composite while leaving the metal pins unetched [42]. Thus, Mo pins of this composite were exposed by etching the polished electrode with sulfuric acid. Due to severe attack, it was necessary to protect the epoxy from the acid. The epoxy surrounding the composite was coated with a parafin wax and then sulfuric acid was dropped on the composite to form a pool contained by the wax. By trial and error, it was found that 40 minutes exposure to the acid produced pins about 8 μm long. The resultant pins had cylindrical tips. Although reference [42] included a technique for pointing the pins, this proved unsuccessful and only cylindrical pins were used in the tests.

Far more effort has gone into work to perfect lengthening and pointing etches for the UO_2-W composites [41, 43]. The chemical composition of both etches are shown in Table 5. The lengthening etch acts like the sulfuric acid

Table 5. Chemical Composition of UO_2-W Etches.

	Lengthening Etch (Vol%)	Pointing Etch (Vol %)
Acetic Acid, Glacial	28.6	26.5
Nitric Acid	8.6	18.5
Hydrofluoric Acid	5.7	15.3
Saturated CrO_3	57.1	39.7

etch described above. The UO_2 matrix is dissolved leaving cylindrical metal pins. The pointing etch, on the other hand, attacks the tungsten pins as well as the oxide matrix leaving pins that have been lengthened and pointed. Application of these etches was done in an identical manner to the sulfuric acid etch described above. Pins were pointed then lengthened using the etches successively, each for 40 minutes. This produced pins that were long and pointed, Figure 11.

Discharge Tests-CW

The CW discharge tests were made in the test equipment previously described; the electrical test circuit for the tests is shown in Figure 16. The power source was capable of a maximum of 25 mA at 3 kV and the current limit was provided by a series resistor, R_s, which could be varied. The circuit current, I, was measured using a milliampmeter in series with the discharge. Applied voltage, V_s, and voltage drop across the discharge, V_D, were measured utilizing a 1000 x voltage probe. All tests were begun by evacuating the chamber and adjusting the flow rate as discussed previously. The valve to the vacuum pump was throttled to obtain the desired chamber pressure. Only minor adjustments were required throughout a run to maintain a desired flow rate and pressure.

The principal measurement made in the CW tests was the determination of the cathode fall voltage for the various electrodes. This had to be accomplished during a normal

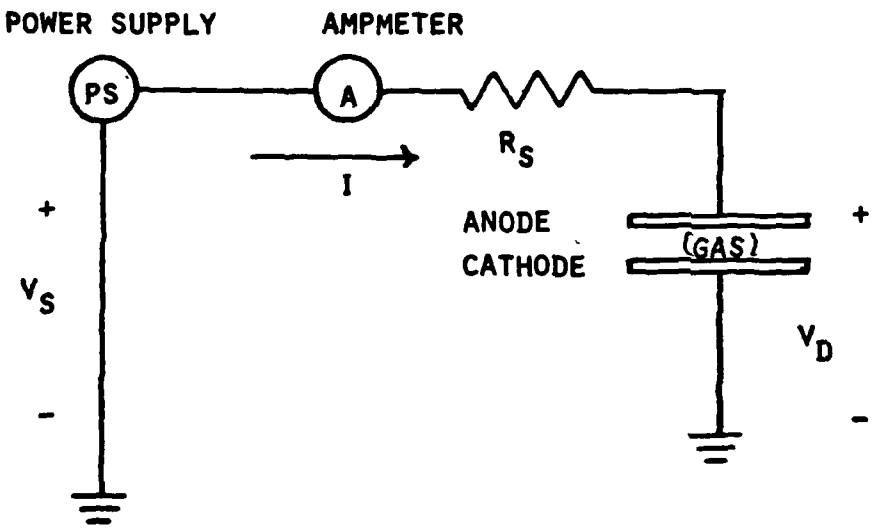

Figure 16. Composite Electrode CW Discharge Circuit.

glow discharge. The "normal" glow discharge was ascertained by increasing the current and observing the spread of the discharge across the surface of the cathode. The spreading indicated a constant current density was being maintained, a characteristic of a glow discharge.

Although the "normal" cathode fall remained constant with increasing current, the overall voltage drop was seen to fall. This is because the resistance of the gas decreased as the current increased. Once the entire surface of the cathode was covered with a discharge, a rise in cathode fall ("abnormal" cathode fall) with increasing current occurred as the current density no longer could remain constant. This indicated the "abnormal" glow regime, a regime which had to be avoided or the cathode fall measurements would be too high.

In making cathode fall measurements, the operating parameters were adjusted to insure a glow discharge. Of primary importance was the circuit current, for it is the current which determines the discharge characteristics, Figure 4. The current was controlled primarily by the series resistor, the value of which was critical. Another factor affecting the type of discharge was the pressure. At high pressure, it was difficult to spread the discharge across the entire surface of the cathode and often an abnormal discharge or an arc was initiated from only a small portion of the cathode.

The ultimate goal of this effort was to find a cathode that can operate with low resistances and at high pressure and still maintain a glow discharge. However, for the cathode fall tests, high resistances (between 68-500 kΩ) were used. In addition, the tests were run at low (<150 torr) pressures. This insured accurate cathode fall values for all of the cathodes tested. Actually, it is the pressure times distance which determines the discharge stability. Thus, the anode-cathode separation distance was usually 0.1 cm for these tests.

Cathode fall measurements were made for each of the cathodes listed in Table 6. For each, data for the measurement consisted of recording the circuit current, I, and the voltage drop across the discharge, V_D, for various applied voltages, V_s. Pressure, cathode-anode spacing, and series resistance were varied for each cathode within the bounds discussed above. Once in the proper regime, the normal cathode fall was measured in two ways. First, the voltage drop across the discharge gap was measured as a function of pressure times gap distance, pd. As pd decreased, the voltage drop approached the cathode fall voltage. The second technique involved measuring the discharge current as a function of applied voltage. The minimum sparking voltage, estimated as the voltage at which current extrapolated to zero, served as an additional estimate of the cathode fall voltage.

Table 6. Electrodes for CW Cathode Fall Tests.

Electrode	Description
AL-1	Aluminum
G-1	Gd_2O_3-Ce_2O_3-Mo, polished
G-1E	Gd_2O_3-Ce_2O_3-Mo, exposed pin
U-1	UO_2-W, polished
U-1E	UO_2-W, exposed pin

Discharge Tests - Pulsed

The pulsed discharge tests were made in the same discharge test equipment used for the CW discharge tests. Flow rate and pressure were adjusted as previously described. The circuit for the pulse tests is shown in Figure 17. The pulses were generated by a Cober High Power Pulse Generator (606P) pulse generator capable of 2500 V pulses over a large range of duty cycles. The current was measured using a small resistor, R_m, while the voltage pulse was measured using a 100x voltage probe. After a discharge occurred, the voltage probe measured the voltage drop across the discharge and the source voltage, V_s, had to be calculated by adding back the voltage drop across the total series resistance, $R_s + R_m$.

The first tests made with the pulsed circuit were repeats of the CW cathode fall tests. The considerations for cathode fall measurements were identical to those for the CW tests with the addition of pulse length. Short pulses make a discharge inherently more stable, but prevent the use of large series resistors. For most of the tests, 100 μsec pulses provided a good compromise. As in the CW tests, the cathode fall data consisted of measuring the voltage applied, the voltage drop across the discharge, and the current in the discharge.

After completion of the cathode fall tests in the pulsed mode, sparking voltage and stability tests were made on three electrodes, the aluminum, the polished UO_2-W, and the UO_2-W

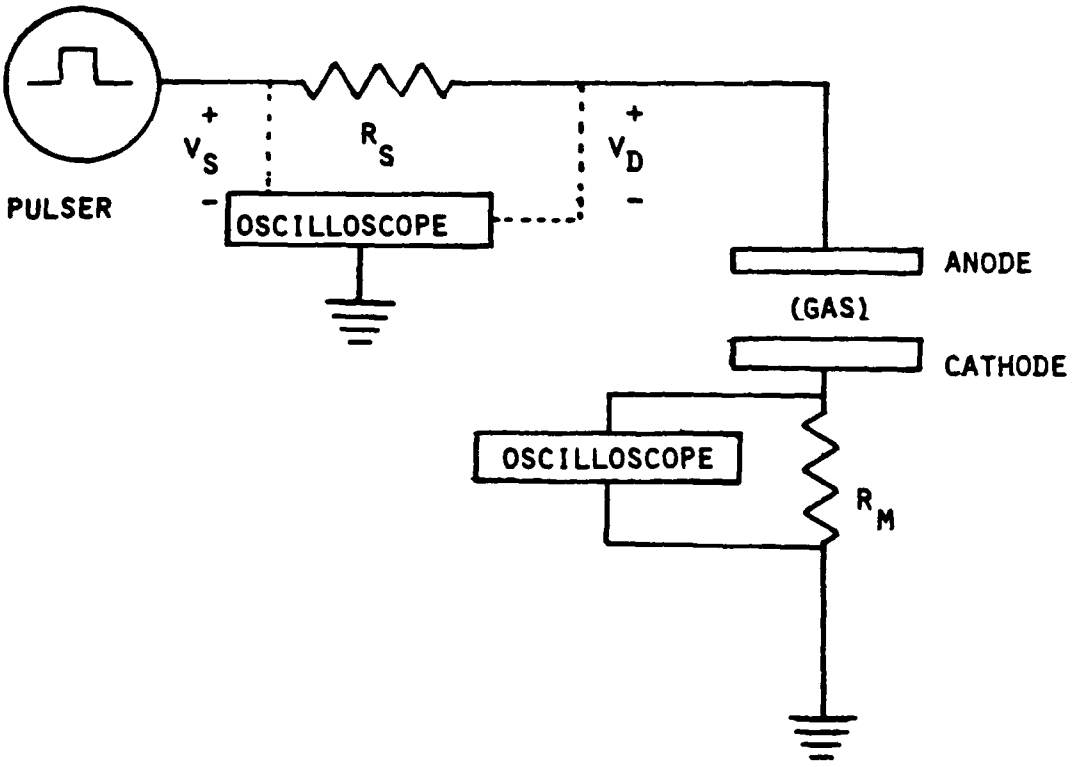

Figure 17. Composite Electrode Pulsed Discharge Circuit.

etched electrodes. The sparking voltage tests measured the minimum voltage required to initiate a discharge as a function of pressure. The same pulsed circuit previously described was used. Pulses for this test were kept short typical of TEA laser operation. This necessitated using low (4 kΩ) series resistance. Even using a 0.1 cm gap, pressures higher than 560 torr could not be used due to the limitation of the power supply voltage. The stability test of each cathode was somewhat subjective in that the discharge had to be visually examined for uniformity. These tests were performed in conjunction with the sparking voltage tests. At a specific pressure, the voltage was raised until a discharge occurred. This was taken as the minimum sparking voltage. Then the voltage was raised further and the discharge examined. A stable discharge should spread uniformly over the entire cathode area while an unstable discharge will tend to localize into an arc. For each electrode, the pressure at which the discharge was no longer stable was recorded, along with other visual observations about the discharge itself. In addition, the trace on the oscilloscope was used to evaluate the discharge stability.

LVFE Preionization Source

Preionization Apparatus

The preionization tests were all accomplished using adaptations of the sample holder configuration used by Hill

[40] for the vacuum field emission work. Figure 18 shows the three post flange arrangement used for simple field emission work. This flange allowed electrical connection to the cathode, the extractor, and the collector. Manufacture of the Low Voltage Field Emitter (LVFE) is discussed in the next section. Once produced, the emitter was mounted onto a spring loaded stainless steel rod using silver paste. This provided electrical contact between the tungsten pins and the rod. Next, the extractor was screwed into place with the active area of the LVFE centered in the recessed hole. The rod was then raised until contact between the moly film on the LVFE structure and the extractor was made. Contact was verified with an ohm-meter. At this point, the rod was lowered again to protect the chip while the collector was positioned. Collector-cathode distances were varied between 1 and 2 mm. Once the collector was secured with a lock nut, the chip was raised into position and contact rechecked. The flange was now ready for use.

For this simple cathode-extractor-collector geometry, the circuit used was identical to that of reference [40], Figure 19. Oscilliscopes were used to measure the voltage to the pins, the leakage current, and the emission current. A 10x voltage probe was used to measure pin voltage on the oscilliscope; pulses were generated in the same manner as in the pulsed discharge tests. A 68 kΩ resistor was placed between the pulser and the pins to limit the current in the

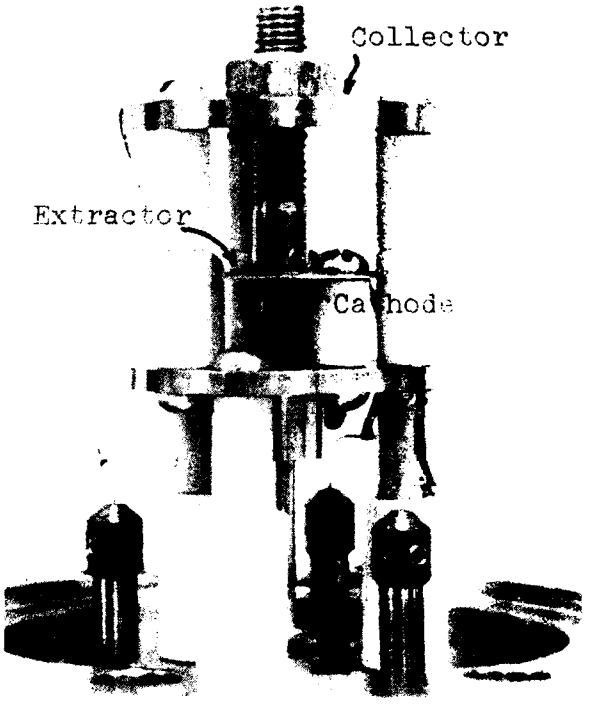

Figure 18. Photogragh of Emission Test Fixture Mounted on Conflat Flange, Showing Electrical Connections.

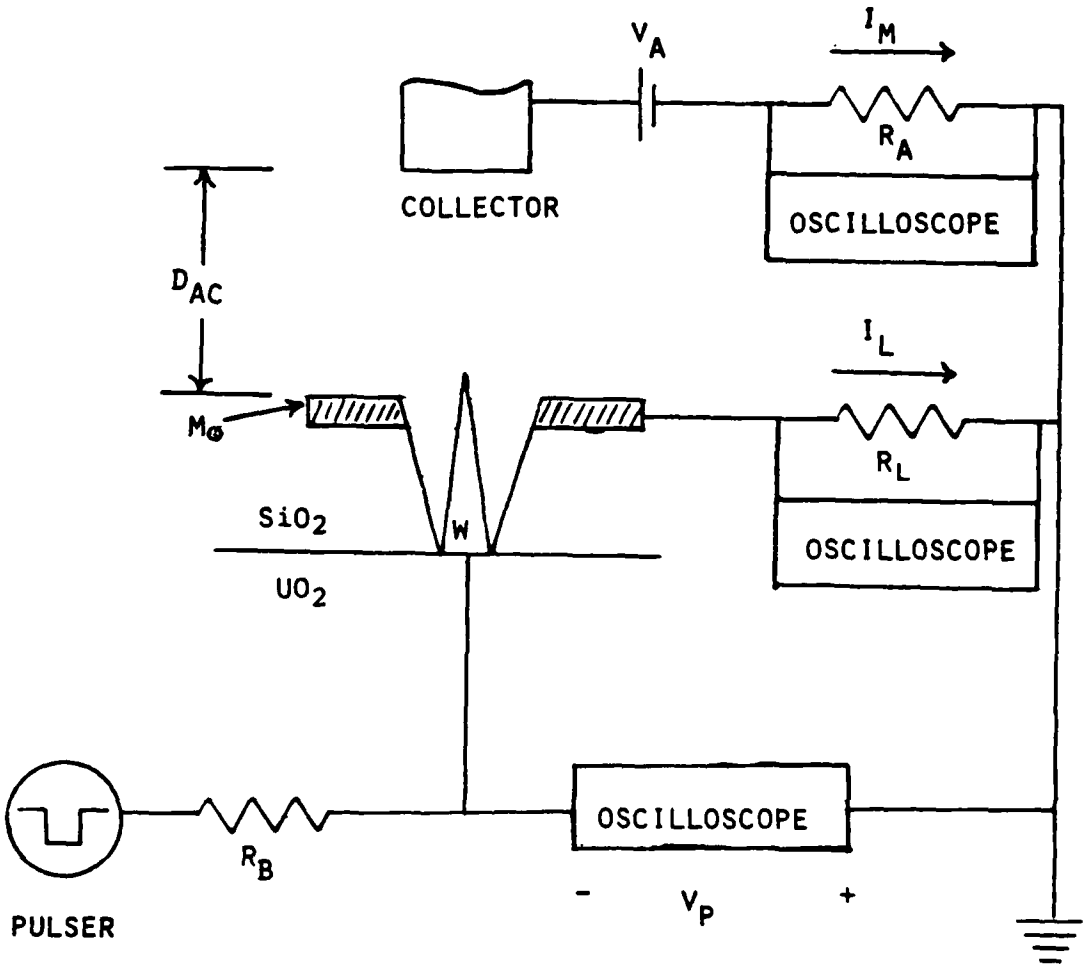

Figure 19. Circuit for Two Electrode LVFE Preionization Configuration.

event of a short in the insulator film. The leakage current was always in the range which could be monitored with a 500 Ω resistor. The resistor used in the emission current circuit was varied depending on the magnitude of the emission. Naturally, as small a value as possible was chosen to minimize current lag due to charging. The value of the bias battery was varied between +67 and +300 volts depending on the test.

In addition to the two electrode configuration discussed above, several tests were run in a "three electrode" configuration, Figure 20, in which the collector was replaced with a wire mesh (50% transparent) and the collector was placed in an anode position above the mesh. This allowed the mesh to be kept at a constant collector voltage, while the anode voltage could be varied independently. Distances between the cathode and the wire mesh varied between 1 and 4 mm while the anode mesh distance was varied between 0.5 and 2 mm.

Two circuit arrangements were used in the "three electrode" tests, Figure 21. In the first, the source, s, was a battery which biased the anode positive with respect to the wire mesh collector. In the second, the source was changed to a DC power supply. Again values of the resistors were varied depending on the tests.

For both the two and three electrode configurations, the mounting flange was inserted in place of the plexiglass

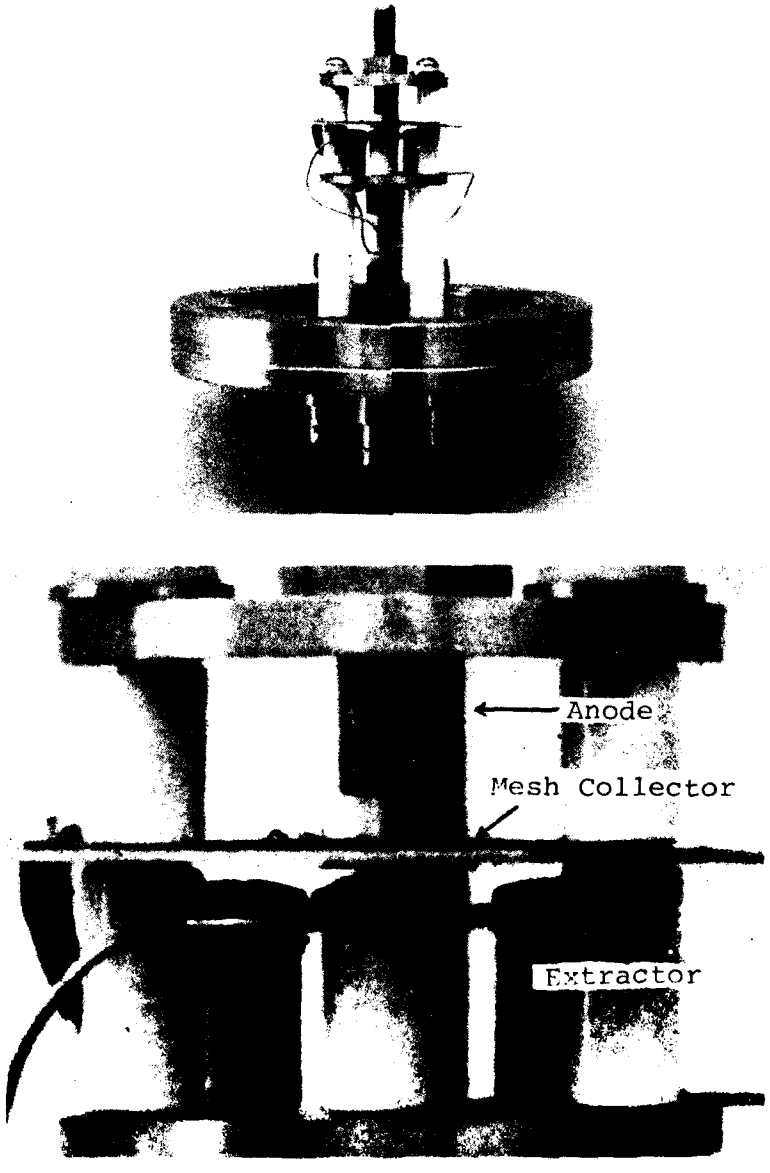

Figure 20. Photograph of (a) Three Electrode Discharge Test Fixture Mounted on Conflat Flange, X0.5 and (b) View of Three Electrode Configuration, X3.

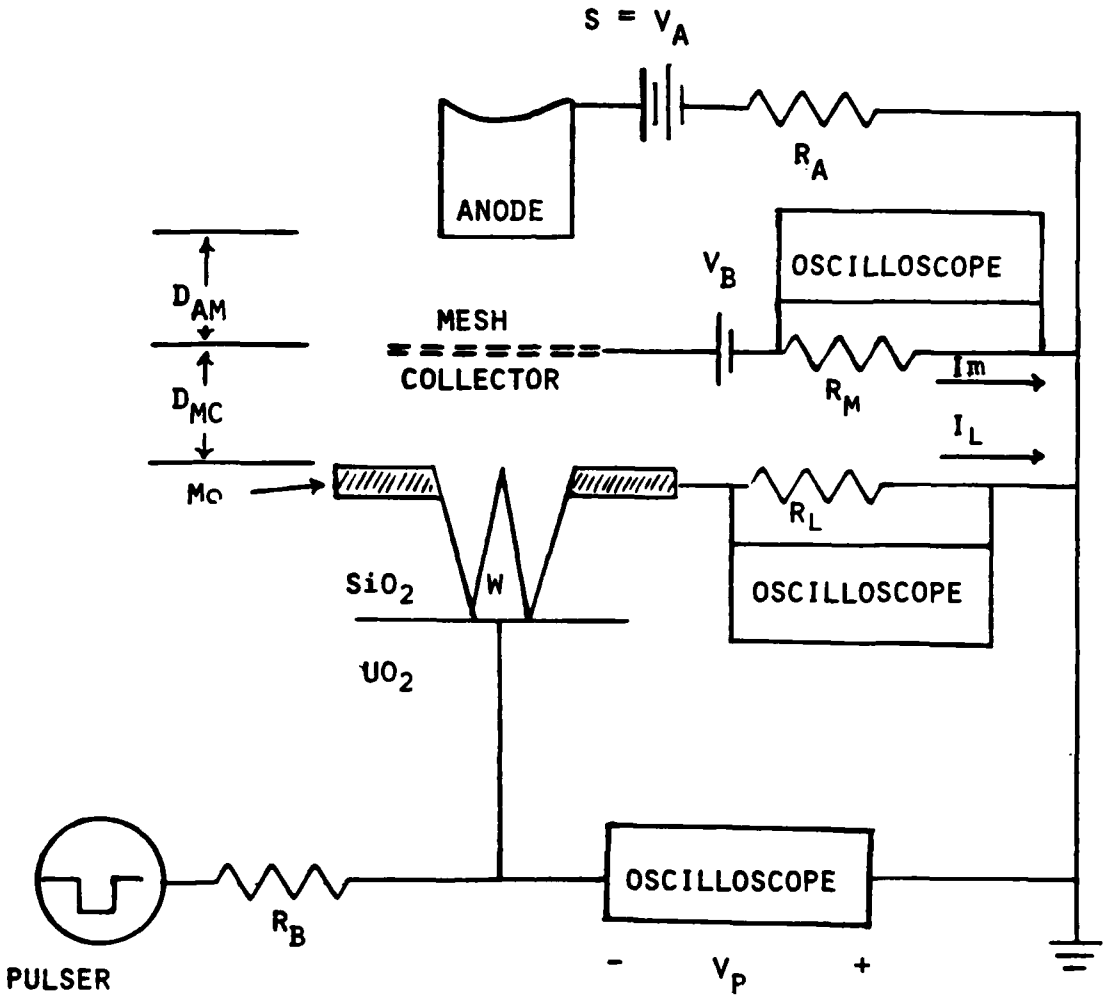

Figure 21. Circuit for Three Electrode LVFE Preionization Configuration.

window in the glass T previously described, Figure 13. Negative pressure was used to hold the flange in place since it was not actually designed to bolt onto the glass T. Even so, pressures as high as 600 torr could still be maintained. The third electrode required a fourth lead which was brought into the "T" via the stainless steel rod shown in Figure 14. At the start of each test, the chamber was evacuated and back filled with helium to the desired pressure. As in the discharge tests, a balance between the vacuum throttle and the incoming gas was used to maintain pressure. In these tests, the flow rate of the gas was not critical since the gas did not flow by the sample.

In addition to the tests described above, several tests were run in a vacuum chamber pumped to a mid 10^{-6} torr with a diffusion pump and a freon baffle. After the low pressure tests, the chamber was sealed off and filled to the desired high pressure. These tests were all run with the three electrode configuration.

LVFE Fabrication

This section summarizes the procedure for producing the Low Voltage Field Emission cathodes. An extensive discussion of the fabrication method can be found in references [40] and [41].

The substrate for these cathodes was a disc 4.2 mm in diameter, 1-2 mm thick cut from a crack free area of a UO_2-W composite slice. The area from which the disc was cut was

selected for pin uniformity and the presence of near perpendicular fibers. The cut discs were annealed in H_2 for two hours at 1200°C to reduce any WO_x phases to W. The discs were then polished to a 1 μm finish.

Pointed fibers extending above the UO_2 matrix were produced by etching the disc in the pointing etch, Table 6. The disc was held using plastic tweezers and immersed in the etch. The etch was in a shallow dish which was rotated at a controlled RPM so that the liquid moved toward the polished side of the disc. This technique produced matrix surfaces which were consistently smooth. Times of 15-30 minutes at speeds of 1-3 cm/sec produced pins which were from 3-6 μm long and pointed to radii varying between 50 Å and 250 Å.

After etching, each disc was examined in the SEM to insure that the pins near the center were uniform, near perpendicular, and sufficiently pointed. If so, an active emitting area was formed on the disc, Figure 22. This was done by protecting a circular group of pins with a parafin wax then dissolving the unprotected pins with an alkaline potassium ferrocyanide solution (0.5 g NaOH, 1.5 g $K_3Fe(CN)_6$ in 10 ml H_2O). Before the pins were dissolved, the back of the disc was covered with wax to protect the exposed pins that would ultimately be used to make electrical contact. The most complex part of this procedure was the placement of the parafin drop. The equipment for this, designed by Hill [40], consisted of a syringe which had been mounted in place of the

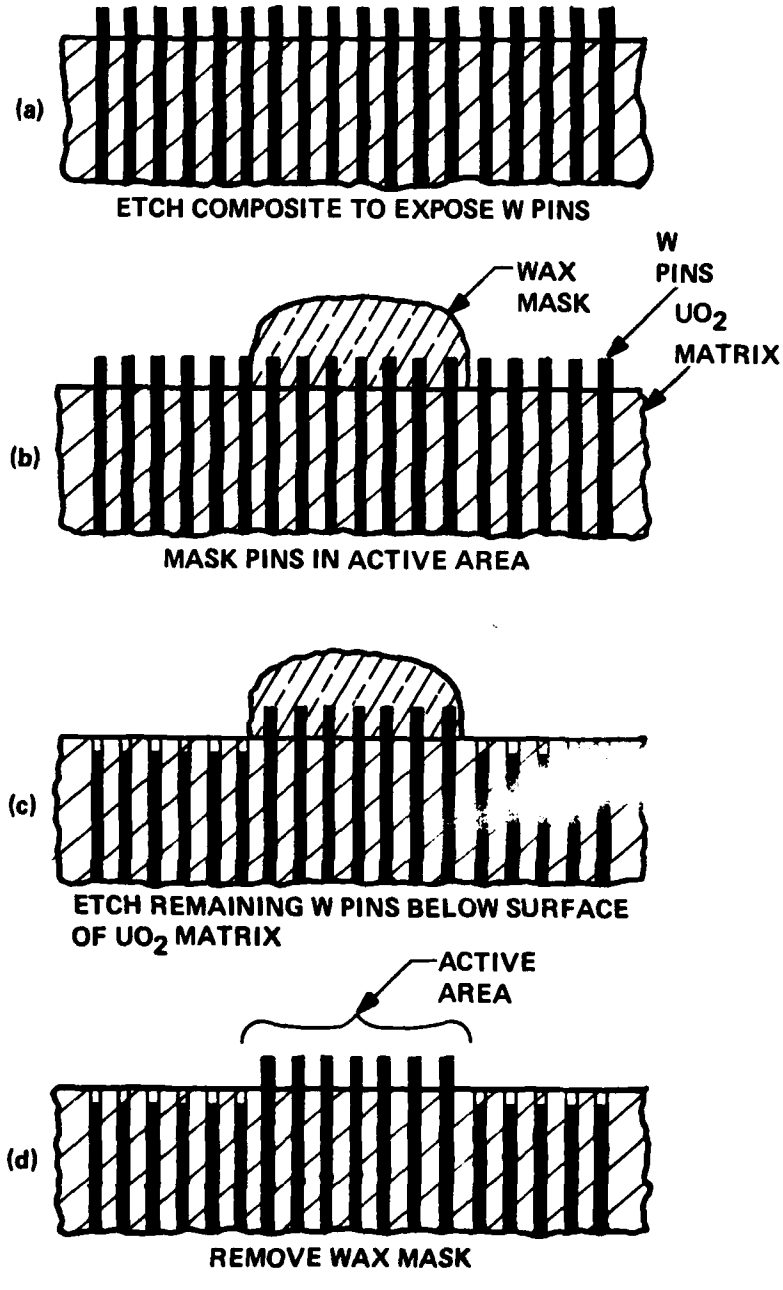

Figure 22. Schematic Diagram Illustrating the Steps in The Formation of the Active Area.

barrel of microscope. Using a micrometer attached to the syringe plunger, a small drop of wax was released from the syringe onto the disc. The entire operation was done under a 30x binocular scope. Average active areas produced by this technique were around 1-2 x 10^{-3} cm^2.

Once an active area had been formed, silica and molybdenum were sequentially vapor deposited at normal incidence to the UO_2 matrix. A schematic of the vapor deposition chamber is presented in Figure 23; the specifics of this deposition process are presented in references [40] and [41]. The LVFE structure was formed from the vapor deposition as illustrated in Figure 24. Although cylindrical pins are shown, the technique was identical with pointed pins. The first step shows the results of the etching and active area formation process discussed above. Step 2 shows how the silica and molybdenum form cones on the pins which shadows the composite surface. The composite disc is then rinsed for about 5 seconds in HF and shaken in distilled water for about 15-30 seconds. This resulted in the removal of the vapor deposited cones, leaving holes around each pin. These steps are also illustrated in Figure 25 which shows SEM photographs for the process.

The dimensions of the pin-extractor configuration which resulted from the deposition depended on the pin height and the thickness of the insulator film. Reference [44] presents a detailed discussion of the effect of these parameters.

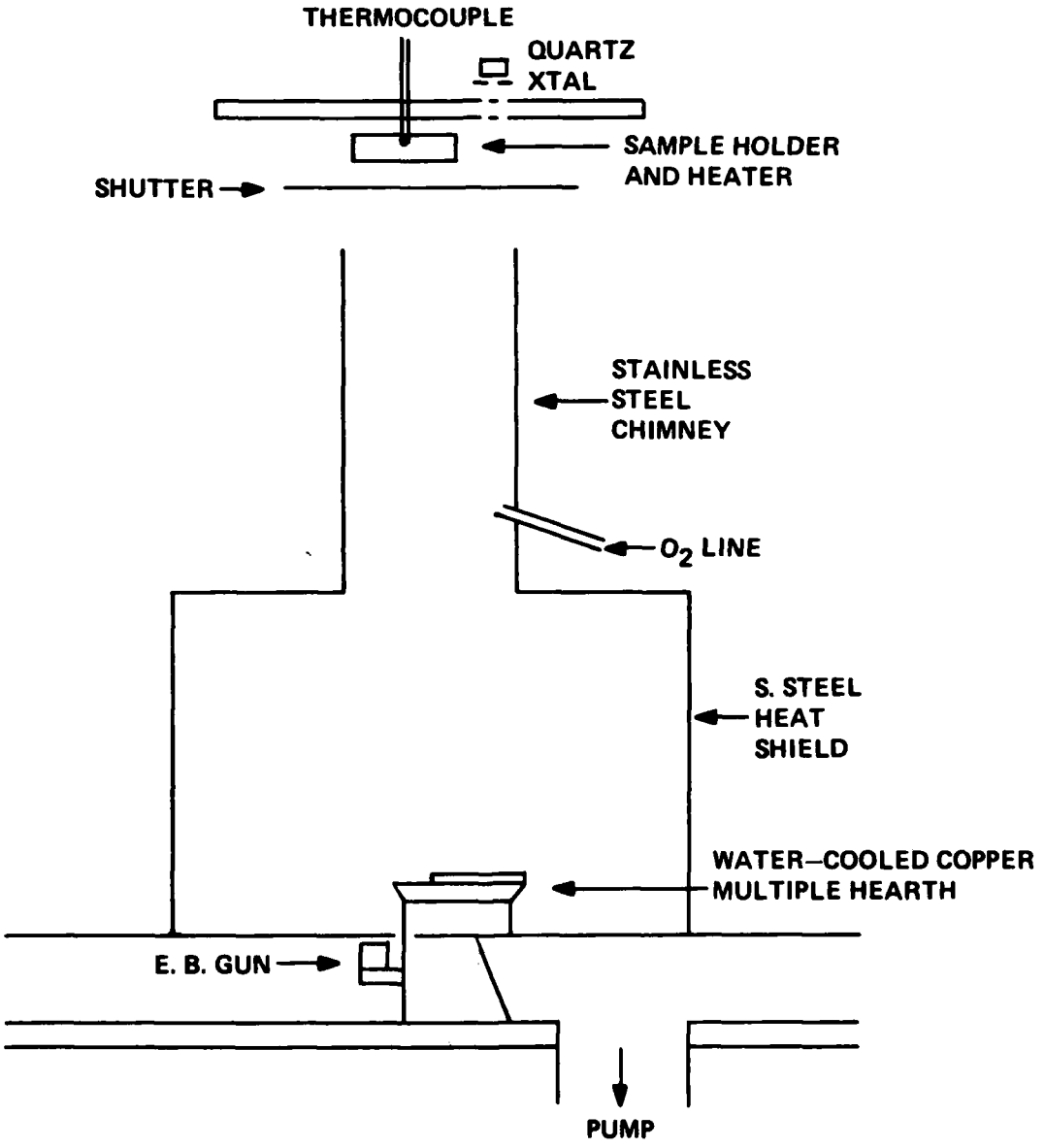

Figure 23. Schematic Diagram of Vapor Deposition System.

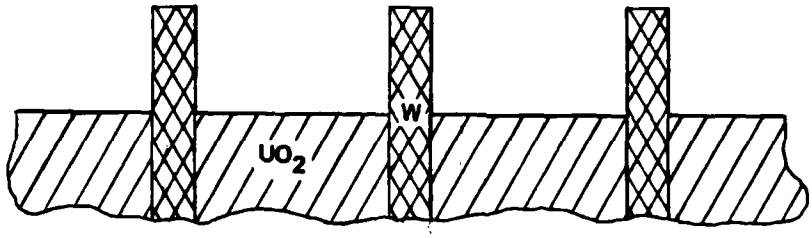

Step 1. Etch a polished UO_2 – W composite to produce free standing W pins (cathodes).

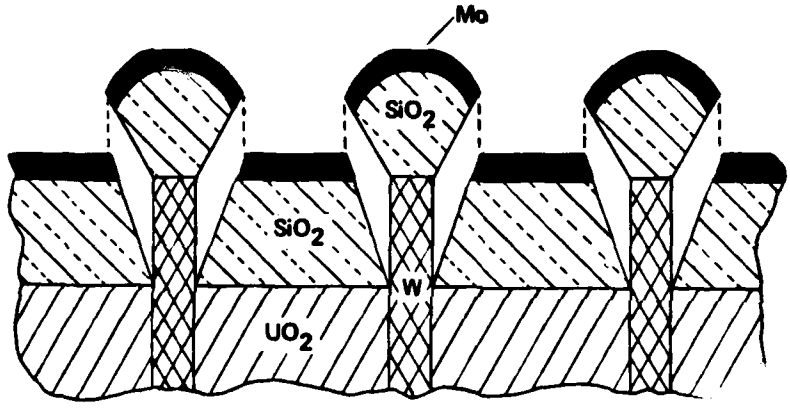

Step 2. Vapor deposit SiO_2 and Mo parallel to fiber axes to the desired thickness

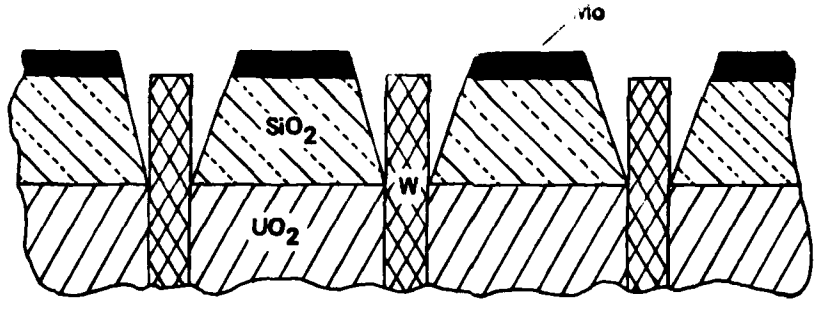

Steps 3 and 4. Ultrasonically vibrate in H_2O to remove cathode cones and clean remanent SiO_2 from cathode with hydrofluoric acid.

Figure 24. Schematic Diagram Showing the Steps in the Formation of the LVFE Structure.

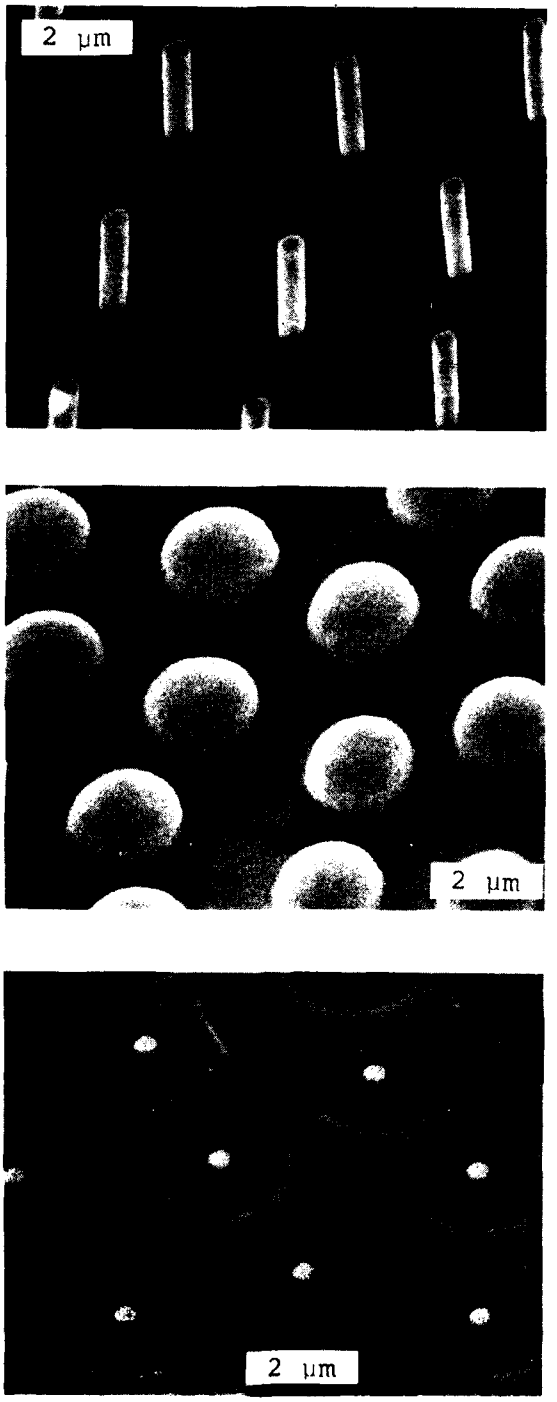

Figure 25. Examples of the LVFE Structure During Each of the Fabrication Steps Illustrated in Figure 24.

For this effort, very little variation was used in the deposition with silica layers about 2.0 μm and the molybdenum layer about 0.5 μm.

Preionization Testing

The specifics of each preionization test varied greatly depending on the goal of that particular test. The purpose of this section is to describe the general techniques used throughout. Any important deviations from the tests described below will be presented in Chapter IV.

One of the major concerns in this phase of the research was the measurement of field emission. For the low pressure (mid 10^{-6} torr) measurements, the procedure followed was similar to that used by Hill [40] with one important difference. In that work, the cathodes were conditioned over a long period of time in order to maximize emission current. Since the goal of this work was not to maximize emission, conditioning time was shortened to several hours using the following scheme. With the circuit set up as previously described (three electrode configuration), the pulsed (100 μsec/50 Hz) voltage on the pins was raised until emission was between 5 and 10 μA. The current was measured by detecting the voltage drop across a series resistor with an oscilloscope. The voltage was held for about 30 minutes, then raised 20 volts. The new voltage was also held for about 30 minutes before it was raised again. At each voltage, a series of current vs voltage data points was taken to provide the data necessary

for a Fowler-Nordheim plot. The conditioning continued until emission was stable and if possible until there was measurable emission at voltage values under -100 V. Typical voltage/current oscilloscope traces are shown in Figure 26.

All of the low pressure tests were made with the three electrode configuration using the diffusion pump vacuum chamber. Conversely, the high pressure tests (0.03 - 760 torr) were made in both the vacuum chamber and the discharge 'T' using the two electrode as well as the three electrode configuration. The pressure was established in the discharge 'T' in the same manner as for the discharge tests. To pressurize the vacuum chamber, the diffusion pump and baffle were shut off and the quick-cool water lines connected. After about 20 minutes, when the diffusion pump had cooled sufficiently, the valve between the chamber and the fore pump was closed and the valve between the gas supply and the chamber was opened. The chamber was filled with helium to 760 torr.

The field emission tests at high pressure were significantly different than the low pressure tests. Most often, the voltage was raised only until stable emission was detected using a 220 kΩ or 100 kΩ series resistor. In general, the voltage was kept as low as possible in order to minimize both destruction to the cathode and arcing. No conditioning was done at high pressures.

After the emission at high pressure was measured, many of the cathodes were tested as a preionization source for a

AD-A091 407 AIR FORCE INST OF TECH WRIGHT-PATTERSON AFB OH F/G 20/5
UNIDIRECTIONAL COMPOSITES AS ELECTRODES/PREIONIZATION SOURCES F--ETC(U)
DEC 79 S G WAX
UNCLASSIFIED AFIT-CI-79-249D NL

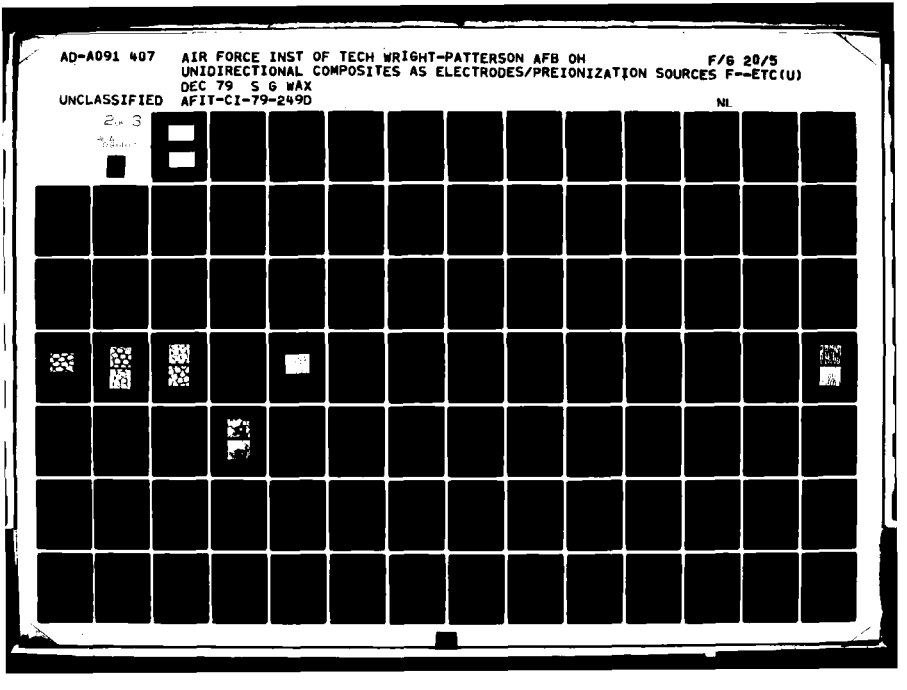

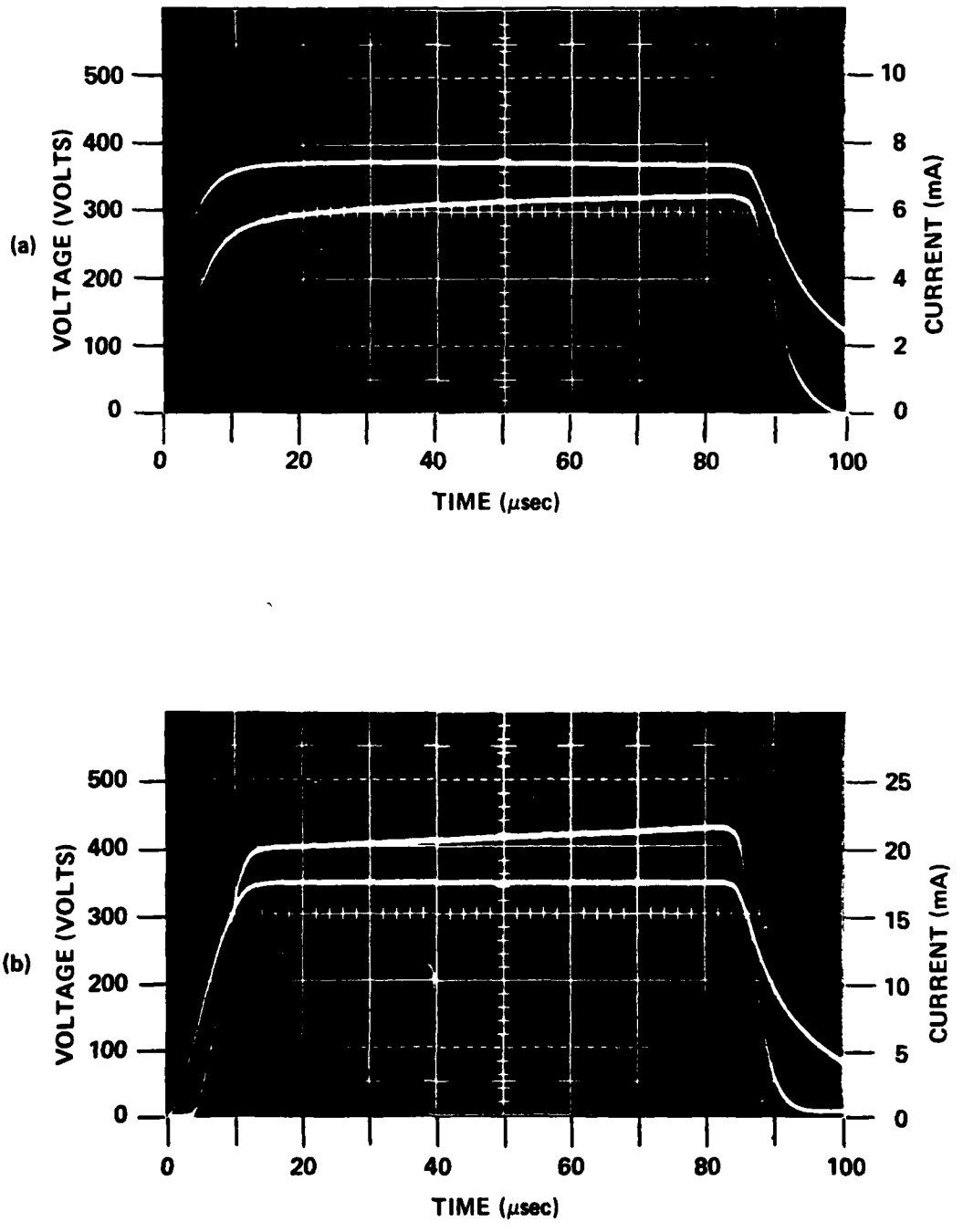

Figure 26. Oscilloscope Traces of Extractor Voltage and Emission Current

discharge. In the two electrode configurations, the collector was the anode for the discharge, Figure 19. The voltage applied across the gap was the value of the battery minus the negative pin voltage. Current direction was identical to emission and thus discharge current was measured exactly as emission. In the three electrode configuration, Figure 21, the collector served as the cathode for the discharge, and the third electrode served as the anode. The voltage across the discharge was the difference between the positive voltage placed on the anode and the positive collector voltage. A discharge in this configuration resulted in a flow of electrons away from the collector, opposite the flow due to emission. When the discharge currents were larger than the emission, the current detected across the series resistor was of opposite polarity to emission. This polarity change was used to detect the onset of a discharge. As previously discussed, either a battery or a DC power supply was used to provide the anode voltage. However, all of the quantitative data was taken using the DC power supply. For most of the tests, the pin voltage was held constant and discharge current was measured as a function of anode voltage up to the sparking voltage. If there was no discharge at a particular anode voltage, then emission was measured. In some tests, when the cathode was emitting well at low voltages, discharge current was measured as a function of pin voltage at each anode voltage. In either case, during the discharge test, lower

values of anode voltage were rechecked to detect any hysteresis due to cathode deterioration.

CHAPTER IV

RESULTS AND DISCUSSION

This chapter presents a discussion of the results of the two phases of this research, the use of LVFE cathodes as a preionization source for lasers and the use of unidirectionally grown oxide-metal composites as laser electrodes. Although the preionization tests were performed second, they made up the bulk of the effort and consequently these tests are discussed first.

LVFE Cathodes as Preionization Sources

In evaluating the use of low voltage field emitters as a preionization source for lasers, three factors had to be considered. First, would the cathodes emit sufficiently at typical laser operating pressures? Second, could the emitters be used to control a discharge? Finally, could the cathodes survive the potentially harsh environment necessary for field emission at high pressure? This section addresses those questions in light of the results of the LVFE tests performed. Table 7 presents a summary of the test configurations. Appendix B is a test by test description of all the LVFE tests. References in this section to tables beginning with "B" (e.g., Table B-1) can be found in that appendix.

Table 7. Test Configurations for LVFE Cathode Testing.

Test #	Cathode	Configuration[1]:	R_A (KΩ)	R_m (KΩ)	D_{Am} (cm)	D_{mc} (cm)	D_{Ac} (cm)	V_A (V)	V_B (V)
HP-1	S-11C	A	10	-	-	-	0.1	67/300	-
HP-2	S-11C	A	Same as HP-1						
HP-3	L-44C	A	Same as HP-1						
HP-4	E17-1	A	100	-	-	-	0.1	67/300	-
HP-5	E17-1	A	Same as HP-4						
HP-6	L19B	A	Same as HP-4						
HP-7	E20-1	A	Same as HP-4						
HP-8	(No Test)								
HP-9	E20-1	A	Same as HP-4						
HP-10	E17-2	A	Same as HP-4						
HP-11	E20-1	B	100	10	0.1	0.1	-	300	67
HP-12	(No Test)								
HP-13	L19D-A	B	-	220	0.1	0.1	-	300	67
HP-14	E13-2	C	-	220	0.1	0.16	-	Variable	67
HP-15	JP9-1	C	500	220	0.1	0.32	-	Variable	67
HP-16	JP9-1	C	Same as HP-15						
HP-17	JP9-1	C	Same as HP-15						
HP-18	L19E	C	-	220	Anode-mesh Connected		0.32	-	67/300
HP-19	JP9-3	A	220	-	-	-	0.32	67	-
HP-20	L19D-B	A	220	-	-	-	0.15	67	-
HP-21	L19D-B	C	500	220	0.1	0.32	-	Variable	67
HP-22	JP9-2	C	500	Variable	0.1	0.32	-	Variable	67
HP-23	JP9-2	C	Same as HP-22						
HP-24	E1-2	C	Same as HP-22						
HP-25	ER+E	C	Same as HP-22						

(1) A - Two Electrode, Figure 19; B - Three Electrode/S = Battery, Figure 21
C - Three Electrode/S = DC Power Supply, Figure 21.

Field Emission at Laser Gas Pressures

Field emission from the LVFE cathodes in a vacuum has been well established [40]. However, stable emission at or near atmospheric pressure must be demonstrated if the LVFE structures are to be used for laser preionization. To assess emission at elevated pressure, an attempt was made to measure field emission at pressures between 500 and 760 torr for every cathode fabricated. A summary of the results of these emission tests are shown in Table 8. The test and test conditions shown for each cathode are for the highest pressure at which emission was measurable, i.e., >0.25 μA. All but four cathodes displayed measurable emission at 500 torr or greater indicating that emission at high pressure is indeed feasible. However, the nature of field emission from the LVFE cathodes into a gas requires additional discussion.

Field Intensified Ionization. Of the four cathodes that failed to provide measurable emission at pressures greater than 500 torr, three of these had emission that was measurable at pressures above 10 torr, still a relatively high pressure. (The fourth was not tested at less than 760 torr.) In this relatively low pressure range (10-200 torr), a great many ionizations occur producing additional electrons which amplify the current. Because the number of ionizations depend on the field which accelerates the electrons, the amplification of the current is termed "field intensified ionization." The phenomenon of field intensified ionization was most

Table 8. LVFE Cathode Emission Summary.

Cathode (Test)	Maximum Pressure for Emission (torr)	Maximum Emission (μA)	Maximum Emission Density (mA/cm^2)	Voltage at Max. Emission (V)	Minimum Voltage to Initiate (V)
S-11C (HP-1)	500	3	5.6	-100	-60
E17-2 (HP-4)	500	16	24.5	-100	-60
L19B (HP-6)	500	3.7	3.9	-90	-80
E20-1 (HP-7)	500	6.0	12.7	-100	-80
L19D-A (HP-13)	15	181	233	-80	-60
E13-2 (HP-14)	500	1.8	2.2	-50	-30
JP9-1 (HP-15)	500	0.7	1.0	-100	-64
L19E (HP-18)	34	0.9	0.63	-180	-140
JP9-3 (HP-19)	500	3.6	4.3	-175	-120
L19D-B (HP-20)	222	2.7	3.2	-170	-170
JP9-2 (HP-23)	760	9.0	4.4	-160	-50
E1-2 (HP-24)	10^{-6}	75	56	-200	-150
ER+E (HP-25)	760	<.25	<.3	-120	-120

clearly observed with test HP-15 in which emission current measured at the collector was recorded as a function of gas pressure, Table 9. Equation (3), repeated below, is an empirical approximation for the number of ionizations that results from each electron as a function of gas composition, pressure, voltage, and distance. Using this expression and the constants for Helium (Table 1), theoretical calculations

$$I = I_o \exp(pAd \exp(-B/E/p)] \qquad (3)$$

of I were made for three different voltages: 90 V (the pin voltage on cathode JP9-1), 157 V (90 V plus the 67 volts on the collector), and 225 V (a voltage to bound the high side). The curves in Figure 27 were generated by calculating I_o (Eq. (3)) from the 36 torr, 22.7 μA measurement. It can be seen from Figure 27 that the 157 V potential provides a very good theoretical estimate for the experimental data and shows fairly conclusively that the accelerating voltage for the electrons that are emitted is the difference between the positive voltage on the collector and the negative voltage on the pins and not the potential difference between the extractor and the cathode.

Because the current at low pressure included the ionization current, it is clear that low field emission currents can be more readily measured when ionization is high. Field intensified ionization does not explain completely, however, the lack of high pressure emission from some samples.

Table 9. Field Emission Current vs Pressure for Cathode JP9-1, Test HP-15.

Pressure (torr)	Emission Current[1] (μA)	Pressure (torr)	Emission Current[1] (μA)
36	22.7	52	9.1
54	4.5	57	6.8
59	2.7	62	2.7
72	4.5	207	1.8
259	0.9	362	0.7
465	0.1		

[1] -90 V on pins, +67 V on collector.

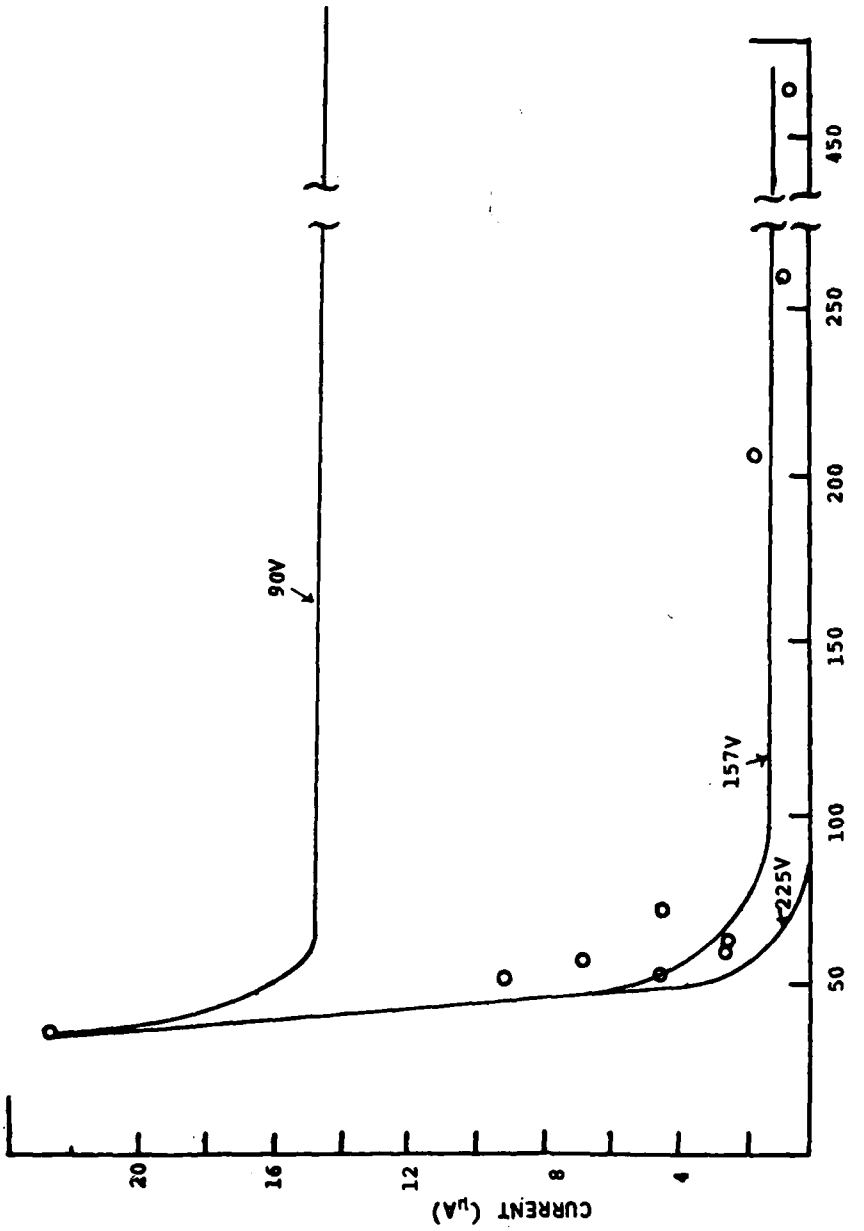

Figure 27. Empirical Versus Experimental Field Intensified Ionization as a Function of Pressure (Data from Table 9).

Cathode L19D-A (HP-13) is the most dramatic example of this. For the conditions of that test (-80 V on the pins, +67 V on the collector, 15 torr, 0.1 cm separation) an amplification of $I/I_o = 24$ can be calculated from equation (3). Yet, with an emission of 181 μA at 15 torr, emission at 760 torr should have been about 7 μA. This leads one to believe that higher pressure may have a deleterious effect on emission. Further evidence of this was provided in Test HP-23 where the 10^{-6} torr emission and even the .030 torr emission were both significantly higher than that for 760 torr emission for the same cathode, Table 10.

Space Charge Current Limit. There are several possible explanations for the lower emission at higher pressures. One of the most likely contributors to the low emission is the presence of space charge. When current densities are high, electrons emitted from a field emitter collect in the neighborhood of the cathode creating a negative space charge region and inhibiting the emission of other electrons. This occurred to some degree in the vacuum testing of the LVFE cathodes [40]. The result of space charge is a deviation from the Fowler-Nordheim equation with the data curving down from the straight line that that equation predicts. Figure 28 shows a Fowler-Nordheim plot for the 1092 minute 10^{-6} torr data for JP9-2 (HP-23) and the 10^{-6} torr data for cathode ER+E (HP-25). Both plots appear to be reasonably typical of that expected from vacuum field emission data, although there does

Table 10. Field Emission Current vs Applied Voltage for Selected Pressure, Cathode JP9-2, Test HP-23.

Voltage Applied (V)	Emission Current (μA)[1]		
	10^{-6} torr	.030 torr	760 torr
100	400	--	2.7
130	--	125	--
150	620	600	9.0

[1] +67 V on collector

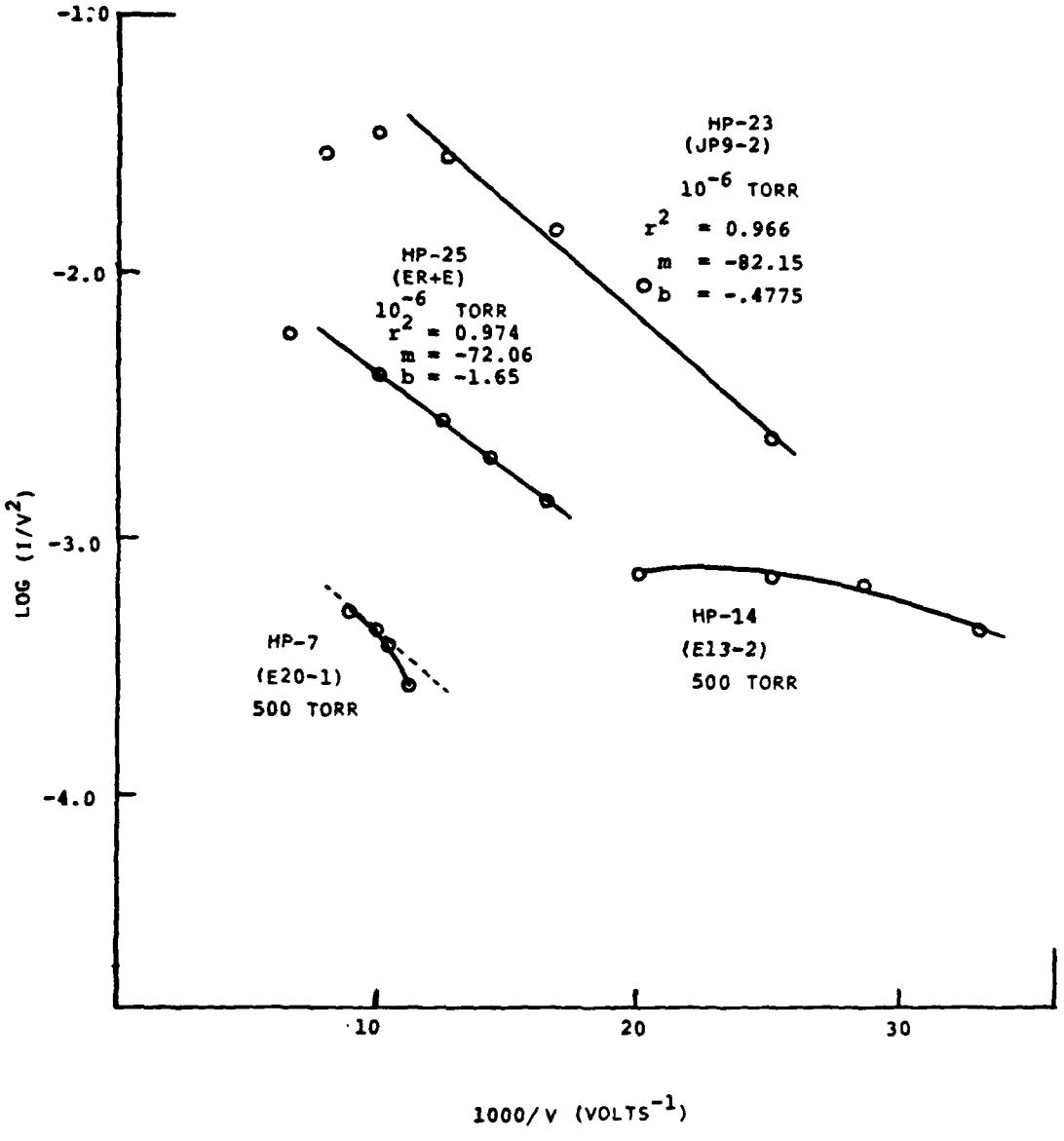

Figure 28. Fowler-Nordheim Plots for Selected Emission Tests.

seem to be a tendency for space charge at the higher voltages. Neither of these cathodes emitted well enough at 760 torr for high pressure V-I data to be taken. However, 500 torr data from tests HP-7 (cathode E20-1) and HP-14 (cathode E13-2) were available, Figure 28. Cathode E13-2 clearly showed space charge effects. For cathode E20-1, it is difficult to determine whether the initial data point was incorrect (dotted line) or whether space charge existed (solid line). Unfortunately, insufficient V-I data was available at high pressures to ascertain whether space charge was limiting the current in other high pressure tests.

Space charge effects in high pressure gases are much more evident than in a vacuum [8]. Under high pressure conditions, the electrons emitted will reach their drift velocity very quickly. Cobine [8] presented an equation for space charge at high pressure for any gas region in which current is carried by ions of one sign:

$$J = \frac{9.95 \times 10^{-14} \, KV^2}{x^3} \qquad (18)$$

where: J = current density (A/cm^2)

V = voltage across the gap (V)

x = gap distance (cm)

K = mobility of electrons in gas (cm/sec/volt/cm)

Using K = 1000 and a field of 1 V/cm, he estimated that the space charge limited current for atmospheric pressure across a

one cm gap would be $\sim 10^{-4}$ $\mu A/cm^2$, while for vacuum the same field and gap would result in a limit of 2.33 $\mu A/cm^2$. Thus, space charge could limit the current by orders of magnitude below the vacuum emission. In Appendix C, an attempt was made to estimate the magnitude of current limit expected for the high pressure runs. The results are summarized in Table 11. Although the correlation coefficient between maximum current density and theoretical space charge was not a strong one (0.573), it indicated that there was some relation between measured currents and space charge effects.

LVFE Cathode Conditioning. Another possible explanation for the lower emission measured at high pressure was that the LVFE cathodes were never conditioned at high pressure. It was found that a slow increase of voltage with time, "conditioning," was necessary to maximize vacuum emission [40]. While never done intentionally, several instances of inadvertant conditioning at high pressure indicated that this process may be as critical to high pressure emission as it is for vacuum emission. In test HP-20, cathode L19D-B emitted measurably at 220 torr only after emitting at lower pressure for a time. Additional conditioning was observed in test HP-23 when an inadvertant high voltage was applied to the cathode due to the sudden burning out of the short. This high voltage resulted in an emission current at 760 torr which was still measurable when the pin voltage was lowered to -100 V. Prior to the short, the same cathode did not

Table 11. Space Charge Estimate for Cathode Emission.

Cathode	Voltage (V)	Gap (cm)	Pressure (torr)	E/p V/cm^2-torr	K $\frac{cm/sec}{V/cm}$	Theo. Space Charge mA/cm^2	Max. Current Density mA/cm^2
E17-1	167	0.1	500	3.3	1443	4.0	24.5
L19B	157	0.1	500	3.2	1484	3.6	3.9
E20-1	167	0.1	500	3.3	1443	4.0	12.7
E13-2	117	0.16	500	1.5	1751	0.6	2.2
JP9-1	167	0.32	760	0.6	1113	0.09	1.0
JP9-2	227	0.32	760	0.9	1170	0.18	4.4
ER+E	187	0.32	760	0.8	1284	0.14	0.3
						(r^2 = 0.573)	

emit at 760 torr up to -150 V. In an attempt to capitalize on the conditioning of the cathodes, a diffusion pump system was set up and the cathodes were run at 10^{-6} torr. Unfortunately, emission at 10^{-6} torr did not affect emission at higher pressures, probably due to the length of time (20 minutes) required to raise the pressure from 10^{-6} torr to 760 torr.

Contamination of LVFE Pins. The last mechanism for emission decreases at high pressures that will be discussed is the possibility that the emitter pins were contaminated by foreign substances. In test HP-22, emission at 10^{-6} torr showed consistent degradation after about 270 minutes of operation, Table B-16. However, when put back into the vacuum and rerun, emission was higher than previously recorded, Table B-17. Since the 10^{-6} torr pressure was achieved with a diffusion pump, it is possible that pump oil could have contaminated the pins. This would also help account for low emission from high pressure runs (HP-23-HP-25) made in the vacuum testing system. In addition, the discharge system was not completely free of contaminants either, and it could not be evacuated to less than 5 torr. Impurities in the gas or in the chamber itself could certainly have affected performance.

Regardless of the effect of the three factors discussed above, the fact remains that field emission current densities on the order of 10 mA/cm^2 were achieved at high pressure.

Optimizing the configuration to reduce space charge, conditioning the pins, keeping the system free of contaminants and, of course, constructive changes in pin uniformity/geometry can only improve the output. What had to be considered next was whether emission into high pressure gases would be useful in improving laser discharge characteristics.

LVFE Preionization of a Discharge

In the examination of LVFE arrays as a preionization source for laser discharges, two different electrode configurations were used. Although these have been discussed previously, a review of current flow in each will help clarify the following discussion. In the two electrode configurations, Figure 29a, the magnitude of the current is the sum of the electrons from the field emitter plus any electrons produced by ionization in the gas or secondary emission from the cathodes, i. e.,

$$I_m = e_e + e_i + e_s \qquad (19)$$

where: I_m = total current measured (at collector)

e_e = electron current from emission

e_i = electron current from ionization

e_s = electron current from secondary emission.

Regardless of the magnitude of the current, the electron flow was always toward the collector and the current measured was always negative. For the three electrode case, Figure 29b, a mesh of transparency M was inserted between the old

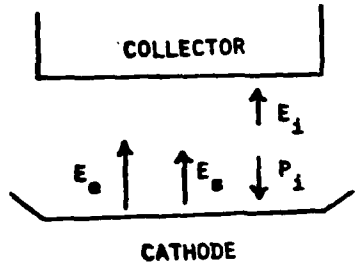

$I_M = E_e + E_S + E_i$

(a)

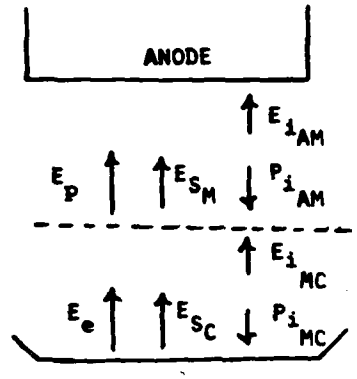

$I_M = (1-M)(E_e + E_{S_C} + E_{i_{MC}} + P_{i_{AM}}) - E_{S_M}$

(b)

E_e - ELECTRON CURRENT FROM FIELD EMISSION

E_i - ELECTRON CURRENT FROM IONIZATION

- $E_{i_{AM}}$ - BETWEEN ANODE AND MESH
- $E_{i_{MC}}$ - BETWEEN MESH AND CATHODE

P_i - POSITIVE ION CURRENT FROM IONIZATION

- $P_{i_{AM}}$ - BETWEEN ANODE AND MESH
- $P_{i_{MC}}$ - BETWEEN MESH AND CATHODE

E_S - ELECTRON CURRENT FROM SECONDARY EMISSION

- E_{S_M} - FROM MESH
- E_{S_C} - FROM CATHODE

E_p - ELECTRON CURRENT PASSING THROUGH THE MESH

I_M - CURRENT MEASURED AT COLLECTOR

M - TRANSPARENCY OF MESH

Figure 29. Current Flow in (a) Two Electrode and (b) Three Electrode Configurations.

collector (now termed the "anode") and the cathode, with the current measured at the mesh (now the "collector"). The magnitude of the current at the collector mesh was a complicated expression which depended on ionization and secondary emission on both sides of the collector. However, assuming that between the cathode and the mesh there are no ionizing collisions (low field) on secondary emission, the equation can be simplified to:

$$I_m = (1 - M)(e_e + P_{i_{Am}}) - e_{s_m} \qquad (20)$$

where: I_m = total current measured (at mesh)

M = mesh transparency

e_e = electron current from field emission

$P_{i_{Am}}$ = positive ion current from ionizations between anode and mesh

e_{s_m} = secondary emission current from mesh.

Because the emission current, e_e, and the positive ion current $P_{i_{Am}}$, have opposite signs, the sign of the discharge current will depend on the magnitude of each. When there are no (or few) ionizations, $e_e > P_{i_{Am}}$ and the current will be negative (termed "emission"). When there is sufficient ionization, $P_{i_{Am}} > e_e$ and the current will be positive (termed a "discharge"). Thus, in the mesh electrode configuration, the sign of the current can be used to detect a discharge.

Two Electrode Testing. In the two electrode

configuration tests, the effect of anode voltage was observed by a jump in emission current as the voltage on the collector was changed. In test HP-1, the total emission current increased from between 2-3 μA to between 10-20 μA when the collector voltage was increased from +67 to +300 V. This test was in laser gas and resulted in a collection of material, probably carbon, at the pin tips. Helium was used in all subsequent tests.

The first visible observation of a discharge caused by field emission from a LVFE came in test HP-4. With +67 V on the collector, an emission current of 16 μA (24.5 mA/cm^2) was measured. When +300 V was put on the collector, a stable purple ionization column was observed between the LVFE active area and the collector. The current in this column was up to 200 μA (100 mA/cm^2) with only -60 V on the pins. Similarly, cathode E20-1 emitted only between 4-6 μA (8.5 - 12.7 mA/cm^2) with +67 V on the collector (HP-7), but with +300 V on the collector (HP-9), the current was up to 350-400 μA (745 - 852 mA/cm^2). As before, a stable column of ionization was visible. With no voltage in the pins, +350 V on the collector was required to initiate even a very erratic discharge. Most important, this discharge was from the corner of the collector to an edge of the extractor, not from the active area. This shows that the current flow described above was a direct result of the field emission and in fact coincided with the pulse of the field emitter. An attempt

was made to correlate the measured current at the high field condition (+300 V on collector) with the field emission at the low field condition (+67 V on collector). Test HP-7 and HP-9 can be used for this correlation since both tests were made with the same cathode, E20-1. From equation (19), it can be seen that when there is no secondary emission ($e_s = 0$) the measured current is the sum of the ion current plus the emission current. If field intensified ionization was responsible, the total current would be:

$$I_m = Ae_e \tag{21}$$

where: $A = I/I_o$ and is calculated from equation (3). When the Fowler-Nordheim equation is applied, it can be seen that:

$$\log \frac{I_m}{V^2} = \log \frac{e_e}{V^2} + \log A \tag{22}$$

For constant anode voltage, A is a constant and consequently, the measured current when plotted versus 1/V will have the same slope as the Fowler-Nordheim plot for field emission, but an intercept which is increased by a factor of log A. Figure 30 shows both the low field (HP-7) and the high field (HP-9) Fowler-Nordheim plot. As previously discussed, it was difficult to tell whether HP-7 was affected by space charge or not. Consequently, the actual Fowler-Nordheim line could not be determined. However, if space

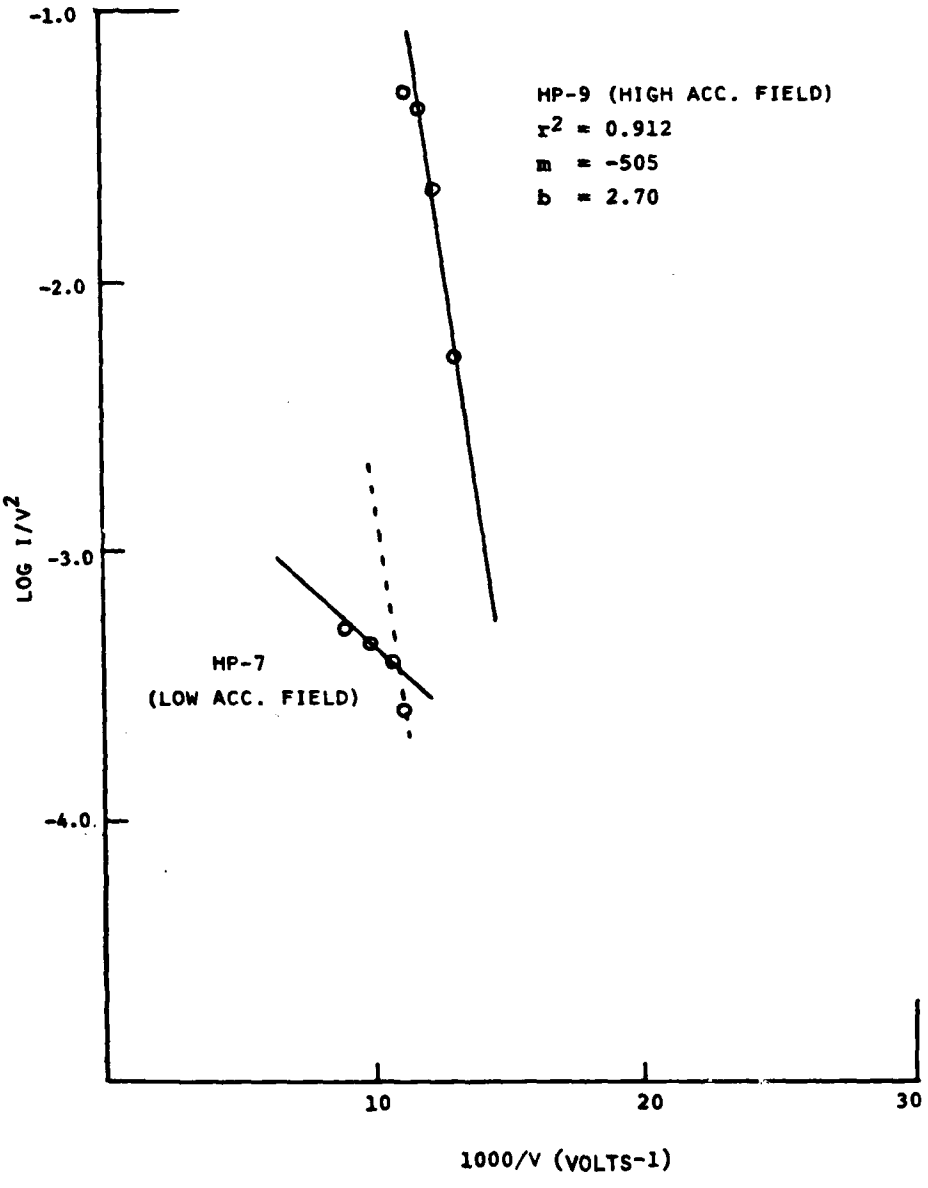

Figure 30. Fowler-Nordheim Plot of Measured Current from Cathode E20-1 at Low and High Accelerating Fields.

charge is assumed, it is not unreasonable that the correct Fowler-Nordheim line is parallel to the high field data. That the high field data fits the Fowler-Nordheim relationship so well was an indication that the relative current magnitude between the electrodes was in direct response to field emission.

The two electrode configuration did demonstrate that high current could be made to flow across spacings that would not be conductive were it not for an outside source of electrons. Thus, the ability to control current in a field independent of the breakdown characteristics was demonstrated. However, as will be discussed later, high current levels at high fields in the neighborhood of the cathode produced extensive damage to the cathode. For this reason, the two electrode configuration was discontinued and the three electrode configuration was used in all subsequent tests.

Three Electrode Testing. It was with the three electrode tests that the first preionization of a discharge in the conventional sense was attempted. Cathode E20-1, used for the first test (HP-11), showed no emission until -220 V were placed on the cathode pins, and then emission was only 1 μA (2.1 mA/cm^2). When a potential of +533 V was placed across the 0.1 cm anode - collector separation, the current passing through the wire mesh was sufficient to allow a discharge current of 5 μA visible as a faint column from anode to collector above the active area of the emitter. With +300

V across the gap, only a slight unmeasurable discharge occurred, and no discharge occurred with +233 V on the anode. At those voltage, no current was measurable unless field emission was present. Thus, this test was the first to show that field emission could provide electrons to produce a current flow between two other electrodes and was typical of most tests which were run with the three electrode configurations. Table 12 presents a summary of the successful discharge tests. Figure 31 is a graph of results shown as current versus anode voltage at constant pin voltage. The intercept of the curves was assumed to be the minimum voltage at which a discharge could be initiated at any pressure. This value of about 280 V, equivalent to the cathode fall voltage for those conditions, was larger than the theoretical value of about 160 V for a normal glow discharge which indicated that the discharges were not in the normal regime. This will be discussed later.

It was the last two discharge tests (HP-24 and HP-25) which demonstrated the independent control of field and current which is desired in a preionization scheme. The cathodes in those tests both emitted at 10^{-6} torr, but at 760 torr, cathode E1-2 (HP-24) showed no measurable emission while ER+E (HP-25) showed only trace emission ($\sim$0.25 μA). However, in the discharge tests, it was found that the discharge current was a function not only of the anode voltage, but also of the voltage to the field emitter, Appendix B,

Table 12. Summary of Three Electrode Discharge Tests.

Test	Cathode	Pressure (torr)	Maximum Discharge Current Density (mA/cm^2)	Pin Voltage (V)	Emission Without Discharge (μA)
HP-14	E13-2	500	18	-(40-60)	0.7
HP-16	JP9-1	350	13.6	-100	0.5-0.7
HP-17	JP9-1	31	159	-175	1.8
HP-21	L19D-B	13	36.4	-225	0.9
HP-24	E1-2	760	10	-150	Not Detected
HP-25	ER+E	760	18	-(60-140)	<0.25

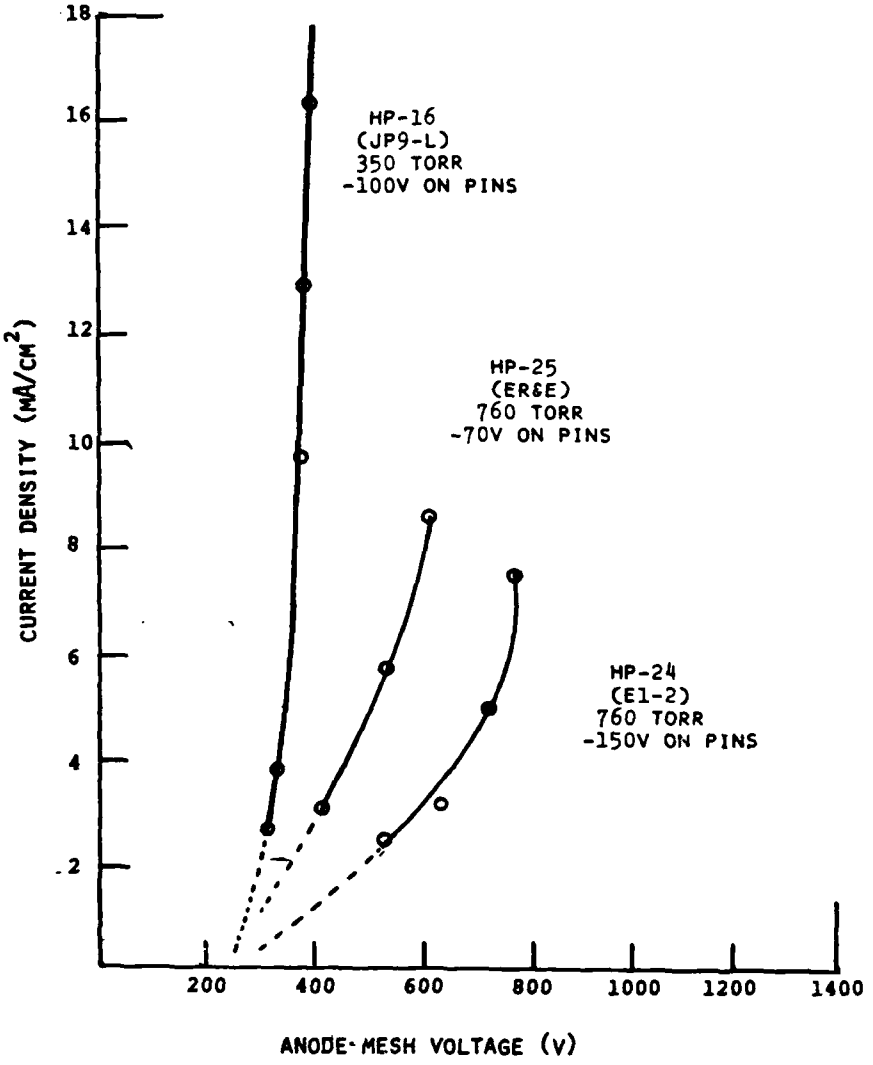

Figure 31. Discharge Current Density Versus Anode-Mesh Voltage at Constant Pin Voltage for Selected Discharge Tests.

Tables B-20 and B-21. In both tests, the discharge current measurements were variable. In order to illuminate the trends shown by the average data, a simplistic linear fit was made of the form:

$$I_m = a_0 + a_1 V_A + a_2 V_p \qquad (23)$$

where: I_m = measured current

V_A = anode mesh voltage

V_p = negative pin voltage

a_0, a_1, a_2 = regression coefficients

The results of the linear regression are shown in Table 13. Although, the functional relationships are not linear and should be exponential, the sign of the regression coefficients indicate the expected and desired trend, i.e., the discharge current was increased by increasing the negative voltage to the pins, independent of the anode voltage. From an analysis similar to Jain, et al. [29], a more quantitative treatment of HP-25 data is possible. They considered the important characteristics of the laser discharge to be E/p in the positive column region of the discharge. The voltage across the positive column is calculated by subtracting the voltage drop across the cathode fall region and the voltage drop across the series resistor, R, from the total voltage applied across the discharge. This can be done graphically if a line of slope 1/R is drawn intercepting the axis at the cathode fall voltage. This voltage (regardless of the type

Table 13. Linear Regression Coefficients for Equation (23)[1].

	Test HP-24	Test HP-25
a_0	-13.14	-10.61
a_1	0.0135	0.0186
a_2	0.0509	0.0686

[1] $I = a_0 + a_1$ (anode-mesh voltage) + a_2 (-pin voltage).

of discharge) is the minimum which can sustain a discharge. The x intercept of the current vs anode voltage curves is an estimate of the cathode fall. For the HP-25 data, Figure 32, the intercept is taken as 280 V and a line of 1/R has been drawn through that voltage. (Note that the small currents make 1/R almost vertical.) The voltage drop across the positive column for each pin voltage is the voltage between that line and the discharge current vs anode-mesh voltage curve. Table 14 shows the range of E/p which can be achieved at a constant current density for three pin voltages. Although these are only approximate, they are certainly in the desired range for CO_2 laser operation. Furthermore, higher pin voltages would provide even lower E/p values.

Despite this independent control of current and field, the fact remains that the current densities of the 760 torr discharges were not sufficient to produce a glow discharge. In a He glow discharge, the current density divided by the pressure squared should be on the order of 2 $\mu A/cm^2\text{-}torr^2$ [8]. For the discharges HP-24 and HP-25, this value was two orders of magnitude less, indicating that the discharges were in the subnormal range. This also explains why the voltage drop at the cathode was higher than the normal cathode fall.

In all of the three electrode discharge tests, the discharge current pulses did not last any longer than the pulse to the field emitter, indicating an insufficient current flow to sustain a discharge. From Figure 32, the increase

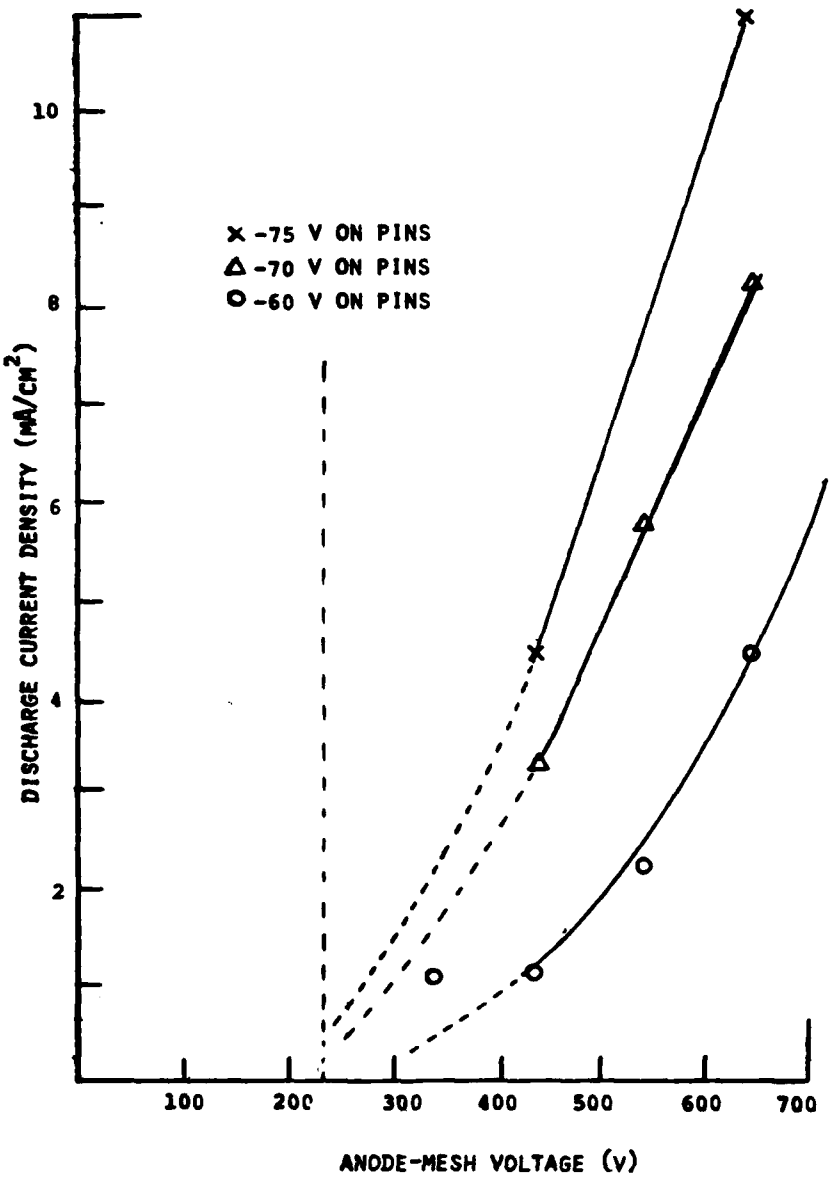

Figure 32. Discharge Current Density versus Anode-Mesh Voltage at Various Pin Voltages for Cathode ER+E, Test HP-25.

Table 14. E/p vs Pin Voltage for Test HP-25.

Pin Voltage (V)	Voltage Across Pos. Column (V)	(1) Field (E) (V/cm)	(2) E/P V (cm-torr)
60	440	4.4	5.8
70	380	3.8	5.0
75	300	3.0	3.9

(1) Field calculated as V/0.10 cm
(2) Pressure = 760 torr

in current due to field increase was exponetial in nature. This same response was seen in the two electrode configurations. Again, the increase in current seemed to be due to field intensified ionization. When there is no secondary emission (a good assumption at the low current levels) and again noting that the positive ion current produced between the mesh and the anode, $P_{i_{Am}}$, equals the negative of the electron current produced, $e_{i_{Am}}$, equation (20) becomes:

$$I_m = (1 - M)(e_{i_{Am}} - e_i), \tag{24}$$

and since $e_{i_{Am}} = Ae_e$, the current between the anode and the mesh should be:

$$I_m = (1 - M)(A - 1)e_i. \tag{25}$$

A Fowler-Nordheim plot of measured current at constant voltage should have the same relationship to 1/V as the emission current, this time with an intercept higher by log[(1-M)(A-1)]. Figure 33 shows the Fowler-Nordheim plot for test HP-25 at various anode voltages. It can be seen from that figure that the data does not fit extremely well, partially because of the scatter in the data. Within the scatter of the points, one could hypothesize that all the lines might have a similar slope. Certainly the intercepts increase, indicating the expected increase in amplication. As has been seen before, the currents at the higher voltages seem to be lower than

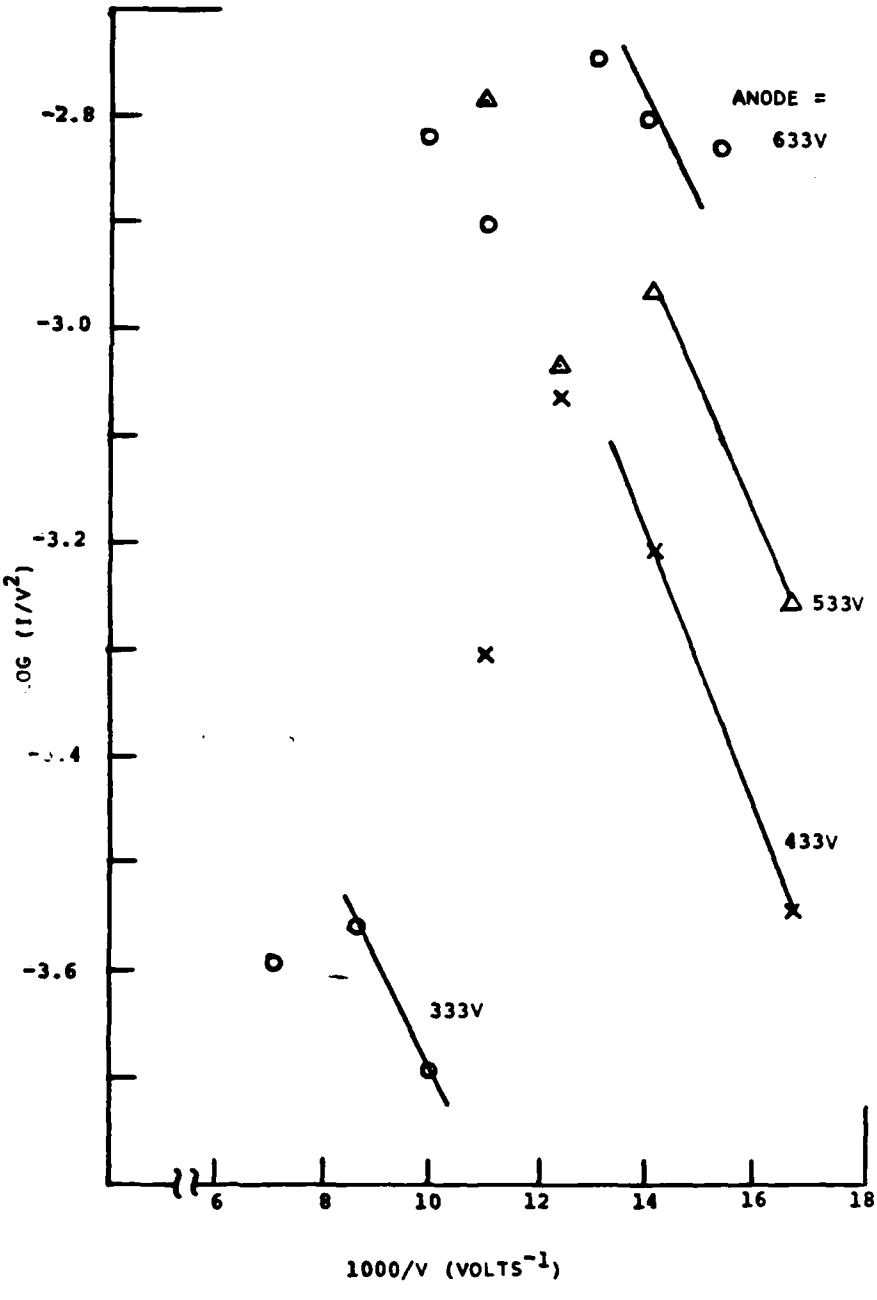

Figure 33. Fowler-Nordheim Plot of Discharge Current at Various Anode-Mesh Voltages for Cathode ER+E, Test HP-25.

expected, an indication of a space charge limit. Whether this was occurring from field emission could not be determined since no low field emission data was available for this cathode.

Assessment of LVFE Cathodes for Preionization. Despite the lack of consistent data, it is clear that the source of current in the discharges observed was ionization due to the field emitted electrons, with very little if any secondary emission. Thus, it was possible to detect a discharge only during the field emission pulse. Occasionally, during the discharge tests, the current from the pins would initiate a very unstable discharge, which, were it not for the large series resistor, would probably have been an arc. This problem is also seen in the e-beam sustained discharges when the field is too high. Stability in the e-beam sustained cases can be achieved by pulsing the field [3]. This was not attempted here.

Based on the fact that test HP-25 provided an amplification of over 50 (0.30 mA/cm^2 to 16.5 mA/cm^2) and that current densities as high as 10 mA/cm^2 have been produced, it is conceivable that currents in the neighborhood of the glow discharge range could be achieved between the anode and the mesh. In that situation, the LVFE could be used directly as a current source if the emitter pulse length were matched to the pulse length required for the laser. This would make the LVFE act exactly like an e-beam but at lower energy require-

ments. However, the fields would have to be higher for the LVFE since the amplification mechanism is field intensified ionization and not ionization from the high energy electrons. At these higher values, the field would most likely have to be pulsed to be stable.

At the low currents produced by the field emitters of tests HP-24 and HP-25, it is doubtful whether a discharge pulse length could have been sustained beyond the field emission pulse. The question remains whether higher current levels could have produced stable discharges in a true preionization mode. In the tests done by Jain, et al. [29], it was only at the higher field strengths from the long pulses that the discharge lasted for the entire pulse length. Furthermore, it was the reversal of polarity after the high voltage arc which probably led to the stable glow discharge [8, 29]. With higher currents, it might be possible to synchronize the discharge pulse with the field emission pulse so that the residual ions can be used to preionize. But, the most likely technique for stability would be to use a two electrode configuration and reverse the polarity after a short burst of field emission. Reversing the polarity should protect the cathode from the detrimental effects of the discharge.

From the three electrode tests, the ability to control the magnitude of the current independent of E/p using the LVFE cathodes has been demonstrated. In addition, control of

the emission would require only several hundred volts. This is in contrast to the several thousand required for preionization or the 150 kV electron beam sustained discharges which required separation laser gas from a vacuum. This leads to simpler circuitry and lower power requirements, a true incentive for development of LVFE controlled lasers. It should be mentioned that no work has actually been done with lasing or even laser gas. However, the phenomena described above are all similar in high pressure gases and the lasing is only a function of the current flow and uniformity. Therefore, there is no reason why the results shown here should not apply to a true laser system. However, it still must be demonstrated that the emitters, once operating, can survive the high pressure environment.

Survivability of LVFE Cathodes at Laser Gas Pressures

Ironically, the most serious threat to the LVFE in the high pressure environment is the very process by which discharges are sustained, positive ions bombarding the negative cathodes. These positive ions will sputter the cathodes, which in the case of LVFE cathodes results in the rounding and wearing away of the tungsten pins. Naturally, this reduces the field emission drastically and, had this occurred in all the LVFE tests, the use of the cathodes would have proven to be severely limited. Fortunately, it did not. The cathode damage observed in the SEM after testing was divided into three categories: major damage - the pins were

completely worn down and/or blunted, minor damage - the pins were slightly rounded, but usually not shortened significantly, and no damage - no discernible change in pin tip or length.

To determine the conditions under which each type of damage occurs, it is necessary to examine the factors involved in the sputtering of the cathodes. The amount of sputtering of cathodes by positive ions depends on a number of variables: the number of ions produced, the energy with which they are accelerated back to the surface and the mass of the ions. The first variable is actually made up of two factors since it depends on the number of electrons leaving the cathode and the number of electrons produced by each of those electrons. The latter value can be estimated by using the field intensified ionization equation (3), at least in the region where all electrons are produced by the field emitter (i.e., no secondary emission). Table 15 shows a summary of those tests for which post test evaluation of pin condition was made. Also included are the conditions (pressure, voltage) that would be expected to be the most detrimental, the calculated field intensified ionization for that condition, and the approximate duration of the run. As will be seen, the number of positive ions returning to the cathode explains almost all the observations.

At pressures between 5 and 100 torr, the amount of ionization was very large. Consequently, every test that was run at these pressures (HP-13, HP-17, HP-18-, HP-21) showed

Table 15. Summary of Post-Test Pin Condition.

Test #	Cathode	Approx. Duration (min)	Pressure (torr)	Net Accelerating Voltage[1] (V)	Current Density (mA/cm^2)	Spacing[2] (cm)	Empirical[3] Ionization	Damage[4]
HP-1	S-11C	15	500	360	5.6	0.1	3.5	(5)
HP-4	E17-2	15	500	400	100	0.1	7.4	Min
HP-7	E20-1	19	500	167	12.7	0.1	1.005	ND
HP-9	E20-1	20	500	400	700-800	0.1	7.4	Maj
HP-13	L19D-A	30	7.7	380	187	0.1	7.48	Maj
HP-14	E13-2	10	500	127	1.6	0.16	1.000	ND
HP-(15-17)	JP9-1	>30	31	242	6-225	0.32	985	Maj
HP-18	L19E	20	34	247	0.63	0.32	909	Maj
HP-19	JP9-3	45	500	317	1-4	0.32	1.000	Maj
HP-21	L19D-B	10	13	217	1-2	0.15	16.2	Maj
HP-23	JP-2	5	0.030	217	723	0.32	1.027	Min
HP-24	E1-2	30	760	217	None Measured	0.32	1.000	ND
HP-25	ER+E	45	760	217	<0.25	0.32	1.000	ND

(1) Sum of pin voltage and collector voltage
(2) Pin-collector spacing
(3) Calculated from equation (3)
(4) Maj - major damage, Figure 34 and Figure 36a
Min - minor damage, Figure 35
ND - No damage, Figure 36b
(5) Build up on pins, Figure 37

major damage to the pins, Figure 34. Since that is not the desired range of operation, these results present no problem. The tests at higher pressures are not as easily categorized. Tests HP-4 and HP-9 for example, were both run in the two electrode configuration, and both had high current density discharges. Test HP-4 resulted in minor damage, Figure 35, while test HP-9 resulted in very severe damage, Figure 36a. The current densities for HP-9 were on the order of glow discharge which means that the cathode was subject to the same type of sputtering which plagues the life of solid metal cathodes. Clearly, the small tungsten pins cannot take that kind of abuse.

Four tests showed no ion milling at all (HP-7, HP-14, HP-24, HP-25), Figure 36b. These tests were all run at conditions at which no amplification was expected. In addition, the current densities were all under 13 mA/cm^2. These tests indicate that, with moderate current and the right conditions, minimal pin damage occurs. An interesting comparison of damage can be made using cathode E20-1 which was run both with no ionization (HP-7) and with significant ionization (HP-9), Figure 36. Clearly, this demonstrates the effect of ionization on the cathodes.

The remaining tests were all somewhat unique. Test HP-23 was operated at 0.030 torr. At this pressure little ionization would be expected. However, the very large current densities would translate into very heavy positive

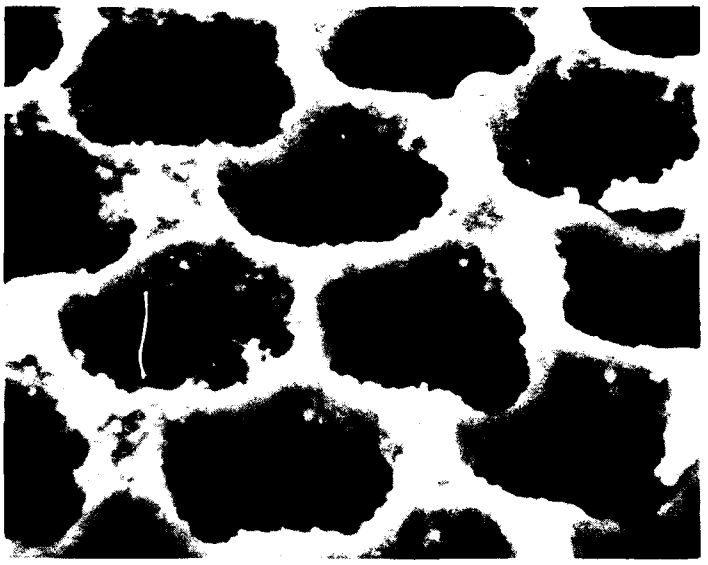

Figure 34. Example of Major Damage to LVFE Structure (Cathode L19D-B, Test HP-21) at 13 Torr, X7500, 45°.

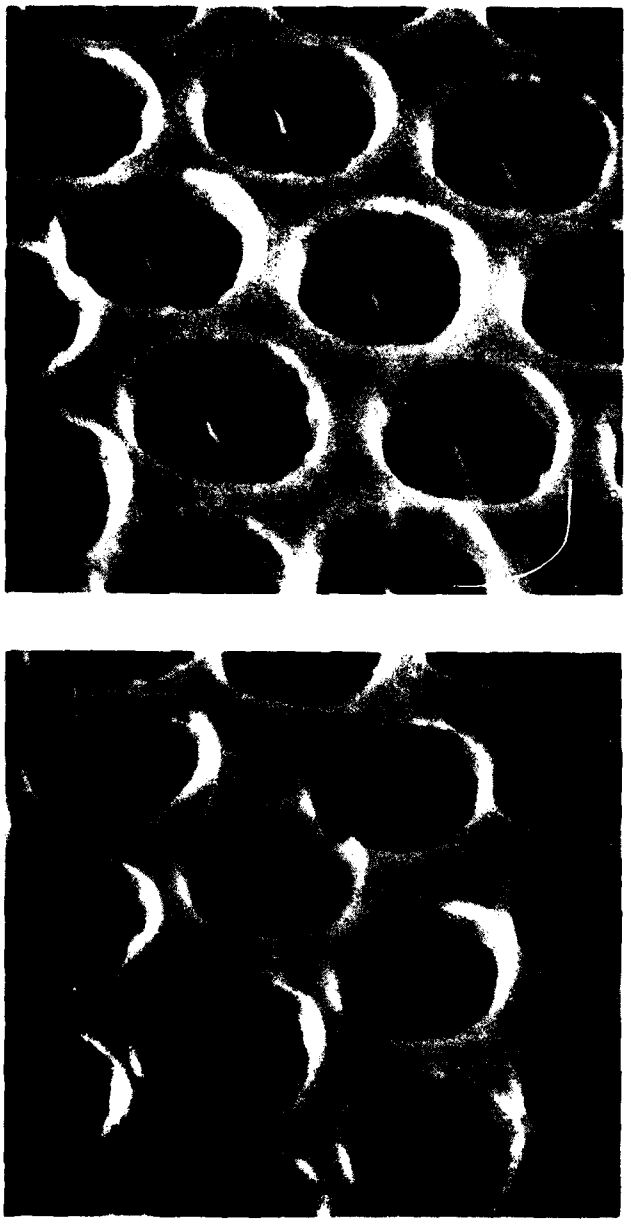

Figure 35. Example of Minor Damage to LVFE Structure (Cathode E17-2), (a) Pre-test and (b) Post-Test (HP-4), X7500, 45°.

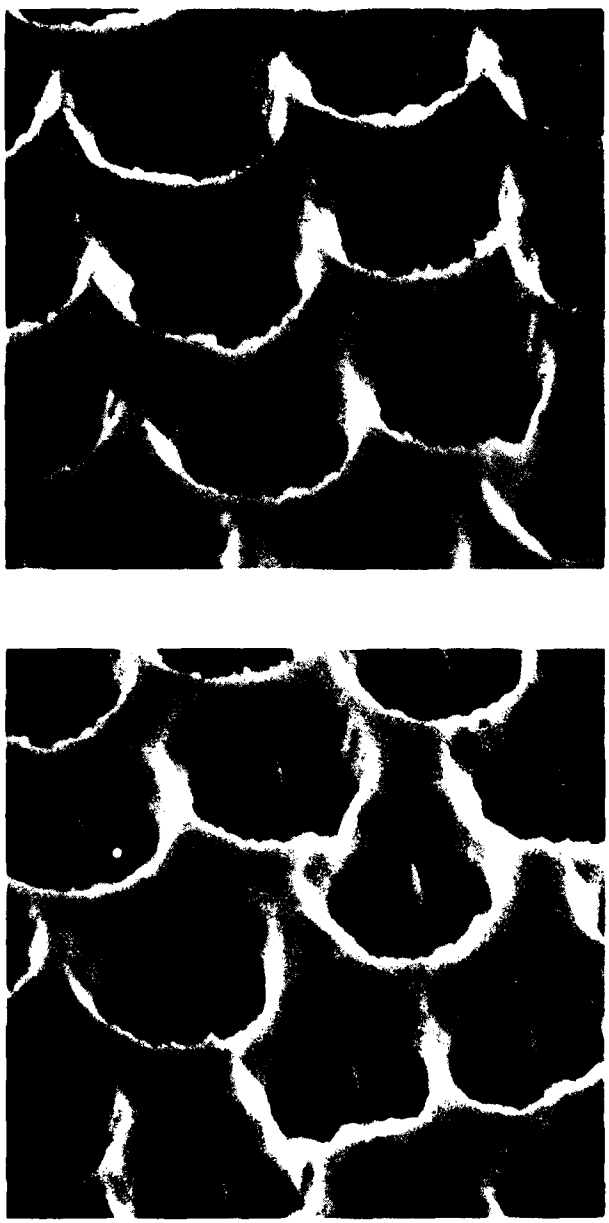

Figure 36. Comparison of Damage to LVFE Cathode E20-1 at (a) High Accelerating Field (Test HP-9) and (b) Low Accelerating Field (Test HP-7), X7500, 45°.

ion bombardment. Test HP-1 was run with laser gas, and under conditions which produced a significant amount of ionization. While no ion milling was observed, a build-up on the pins did occur, Figure 37. This was probably due to the ionizing of carbon, and could be avoided if conditions of lower ionization were used. Only test HP-19 lacked satisfactory explanation because milling was noticed even though little ionization would be expected. This test was run for a longer period of time than most, but most of the test was made at low current densities (see Table B-14). Test HP-7 was run for 1/3 the time of HP-9, but at over 10 times the current density with no effect on the pins. However, the voltage at which the cathode for test HP-19 was run was over 100 V higher than for the four tests where cathode damage was negligible. The effect of increased voltage can be understood if one considers the movement of positive ions in the direction of an electric field. These ions will achieve a drift velocity proportional to the field once they have made several collisions under that field's influence. Away from the cathode, the field on the ions was that between the collector and the pins while in the neighborhood of the pins, the field was enhanced by the pin geometry and depended on the pin voltage (since the extractor was always ground). In a vacuum, the mean free path of the ions is large and most collisions are made in the external field. At the high pressure conditions, however, the mean free path of the ions was very small ($\sim$0.3 μm at 760 torr for

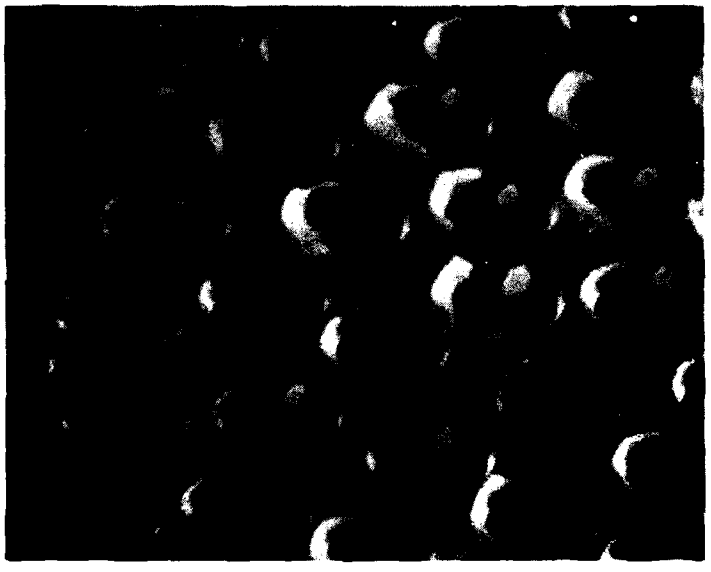

Figure 37. Deposit on Field Emission Tips Resulting From Discharge in Laser Gas, X5000, 45°.

He^+ [8]) and the ions probably were influenced by the enhanced field since they would make many collisions near the pins. Thus, the pin voltage controlled the drift velocity and thus the momentum of the ion. This extra energy imparted to the ion appears responsible for the damage seen in test HP-19 and was an indication that pin voltage should be kept low to avoid this damage.

From the above discussion, it is clear that the LVFE can survive if the pressure is kept high enough to avoid the deleterious range of intense field ionization. Pressures above 500 torr should accomplish this. Secondly, voltage on the pins should be kept as low as possible to avoid providing excess energy to the positive ions. Finally, discharges with the LVFE as the cathode should be avoided.

Composite Electrode Tests

The purpose of the electrode discharge tests was to evaluate the unidirectionally grown composites for use as electrodes in CO_2 laser discharges. As has been previously described, there are several reasons why these composites might offer advantages over conventional electrodes. If these advantages are realized, they would be observed in the uniformity of the discharge and a favorable improvement in the discharge voltage-current characteristics. In this section, the results of the discharge tests are discussed in light of those potential advantages.

Initially, cathode fall of the electrodes listed in

Table 6 was measured using a CW discharge. For each of the electrodes, a great deal of data was taken. However, only those tests for which conditions appeared to meet the criteria for a "normal" glow are reported. Appendix D contains the raw data and conditions for each test.

The discharge voltage drop, V_D, versus pressures times distance, pd, for each composite electrode is plotted in Figure 38. For each set of data, a least square fit of supply voltage, V_s, versus current, I, was calculated, Table 16. The intercept of this fit is an estimate of the cathode fall. The lines drawn in Figure 38 show that the calculated values are reasonable extrapolations of the pd vs V_D data which should level off to the cathode fall value. However, the data in most cases seems to level at a value higher than the calculated intercept. In fact, one expects the discharge voltage drop, V_D, to level off near the minimum and not take the dip the calculated values indicate. This dip may in fact be because data at pd less than 2 cm-torr could not be taken and thus the extrapolation could not predict the leveling off. Perhaps, a better estimate could be made by using the actual value that V_D appeared to be approaching. This technique results in the values which are also shown in Table 16 (no estimate was made for U-2E since this data had not yet leveled off). The fact that there is a strong (.906) correlation between the two approaches indicates that either can be used for comparison among the elec-

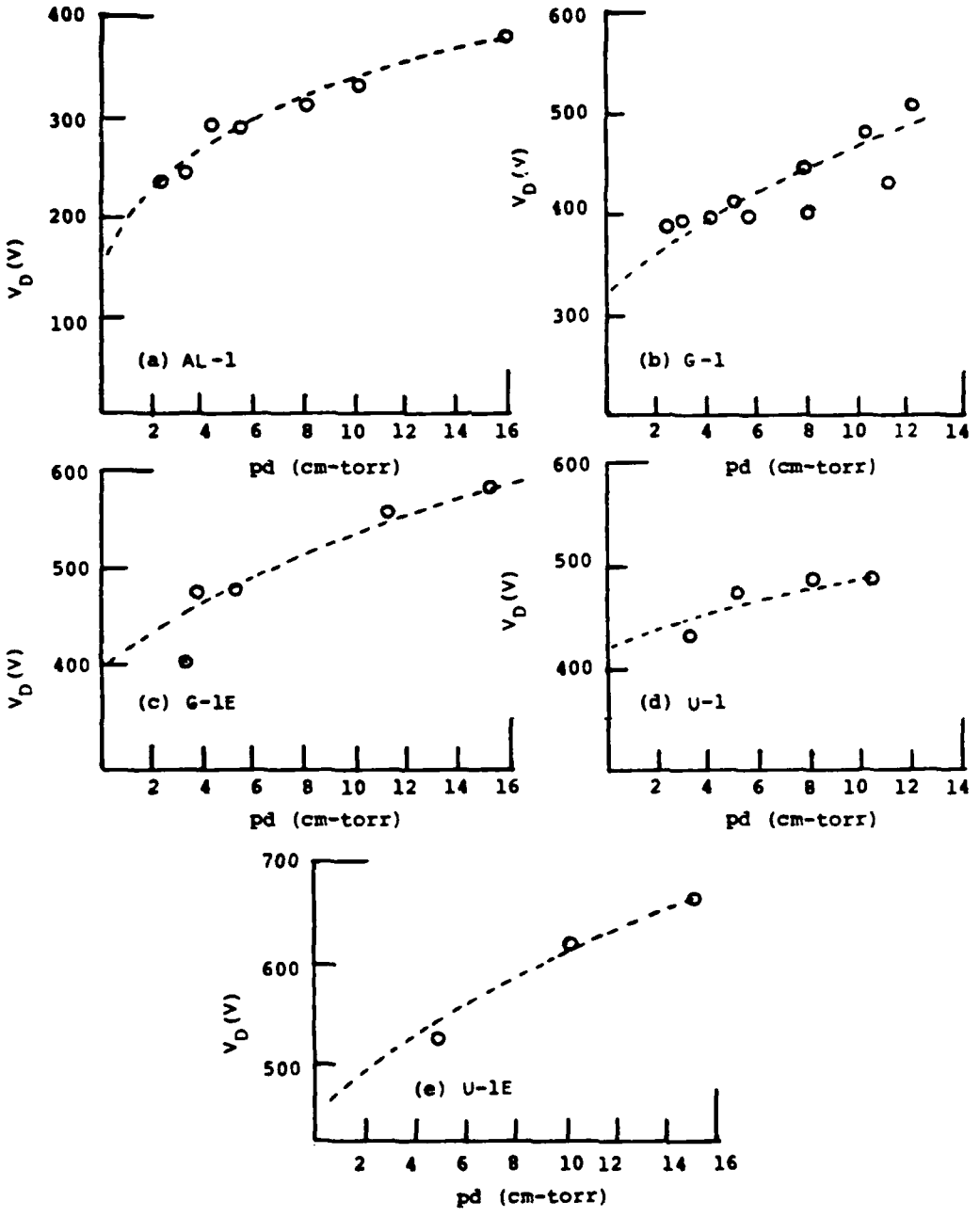

Figure 38. Discharge Voltage, V_D, Versus Pressure Times Distance pd, for CW Discharge Tests of Composite Electrodes (a) AL-1, (b) G-1, (c) G-1E, (d) U-1, (e) U-1E.

Table 16. Cathode Fall Summary for CW Discharge Tests.

Cathode	Cathode Fall (V)	r^2	Slope (KΩ)	Resistance (KΩ)	Cathode Fall Estimated
Aluminum (AL-1)	153	0.973	768	500	232
Gd_2O_3-Ce_2O_3-Mo(G-1)	331	0.867	769	500	380
Gd_2O_3-Ce_2O_3-Mo (Exposed pin) (G-1E)	417	0.959	729	500	400
UO_2-W (U-1)	425	0.973	90	68	425
UO_2-W (Exposed pin) (U-1E)	464	0.998	315	250	-

trodes tested.

A direct comparison between the cathode fall values measured here and published data was not possible since this value depends on both the cathode and the gas. Naturally, there is no data available for the composites. While there is much data for aluminum, it is not for the specific gas mixture used here. It has been estimated that the cathode fall for copper in the same gas mixture is about 350 V [16]. For a variety of gases, the ratio of the cathode fall for copper to that of aluminum is about 1.5, Table 2. Thus, 230 V is probably a reasonable estimate for the aluminum cathode fall. That this agrees with the value shown in Table 16, again indicates that the experimental values can be used for comparison.

In addition to the CW cathode fall data, cathode fall data was also taken using the pulsed configuration. The conditions and raw data for these tests are presented in Appendix D. As with the CW tests, either pd vs V_D, Figure 39, or a least square fit of V_s vs I, Table 17, can be used to estimate the cathode fall. Because the major purpose of these tests was observation of the discharge, many tests were performed with d = 0.3 cm, resulting in even larger pd values than for the CW tests. In addition, the lower series resistances resulted in higher currents which may have exceeded the normal glow range. Thus, using the cathode fall data quantitatively is difficult. However, once again the cathode

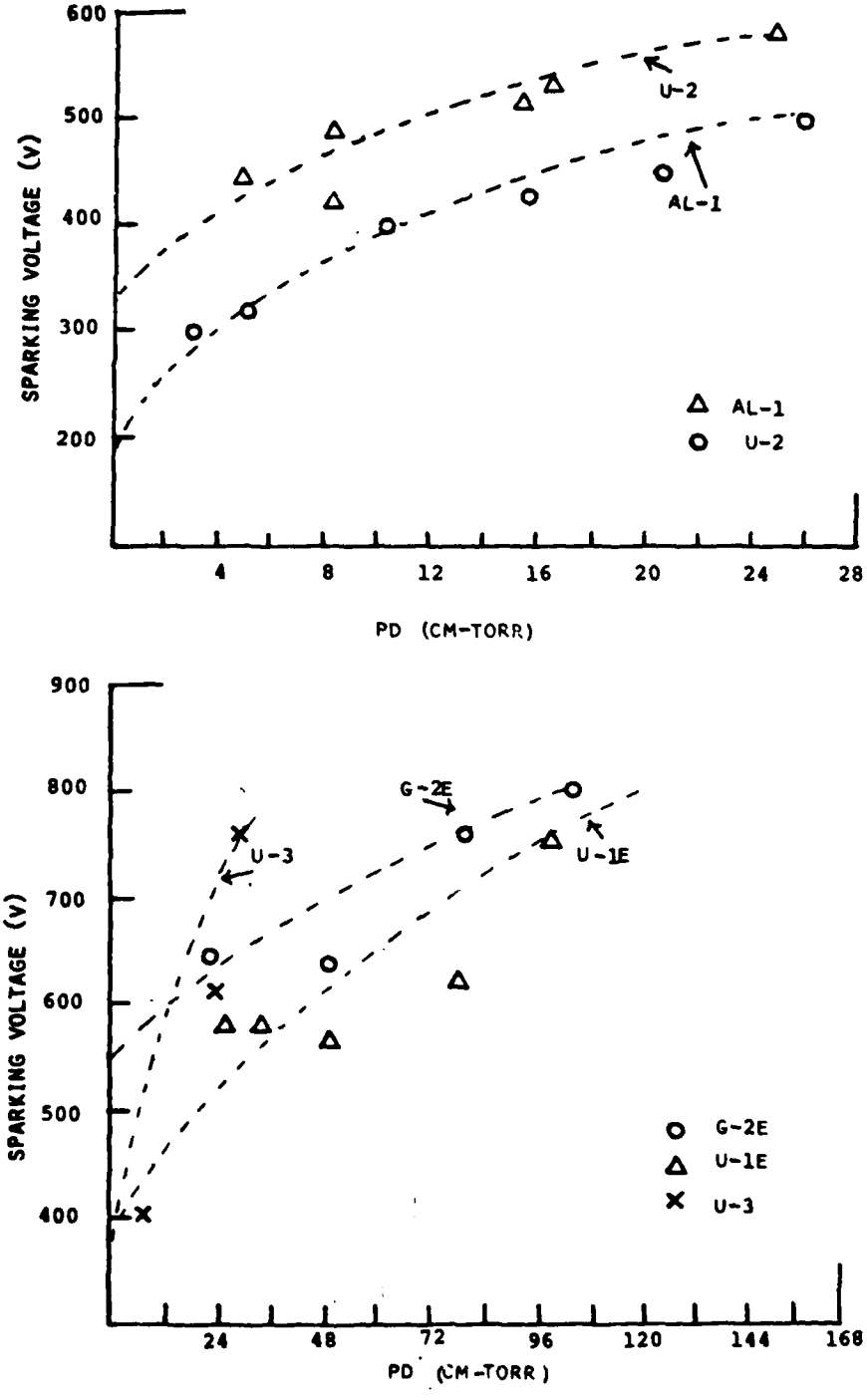

Figure 39. Discharge Voltage, V_D, Versus Pressure Times Distance, PD, for Pulsed Discharge Tests of Composite Electrodes (a) AL-1 and U-2, (b) G-2, U-1E and U-3.

Table 17. Cathode Fall Summary for Pulsed Discharge Tests.

Cathode	Cathode Fall (V)	r^2	Slope (KR)	Resistance (Kℓ)
Aluminum (AL-1)	187	0.995	90.9	68
UO_2-W (U-2)	329	0.954	99.5	68
UO_2-W (Exposed pin) (U-1E)	386	0.944	100.5	68
Gd_2O_3-Ce_2O_3-Mo (Exposed pin) (G-2E)	553	0.980	95.12	68
UO_2-W (U-3)	358	0.993	38.3	25

fall for the aluminum samples was well below that for the composite electrodes, qualitatively confirming the CW results.

That the cathode fall for an aluminum sample was less than that for the composites, especially the exposed pin samples, was disappointing. A low cathode fall is an indication of the secondary emission characteristics of the electrode. It had been hoped that the composite electrodes, especially those with exposed pins, Figure 40, would have a lower cathode fall than solid metal electrodes. The higher cathode fall from the composites indicated that field emission was not taking place.

In the cathode fall region, a voltage drop of about 300 V is expected across a distance of about 0.013 cm (at 100 torr) [8] or a field strength of 2.3×10^4 V/cm. In order to provide fields sufficient for field emission (3×10^7 V/cm), an enhancement on the order 1000 in the cathode fall region would be necessary. Even at higher pressure where the field across the cathode region is greater, enhancements of over 100 would be necessary. In the exposed pin field emission work, dimensionless field enhancement factors of only between 6 and 17 were observed [39, 41]. Thus, it is apparent that field emission from the composites would not be expected and the present results confirm this.

Despite the lack of any cathode fall advantage, it is still possible that the composites could offer advantages in the stability and uniformity of the discharge at high pres-

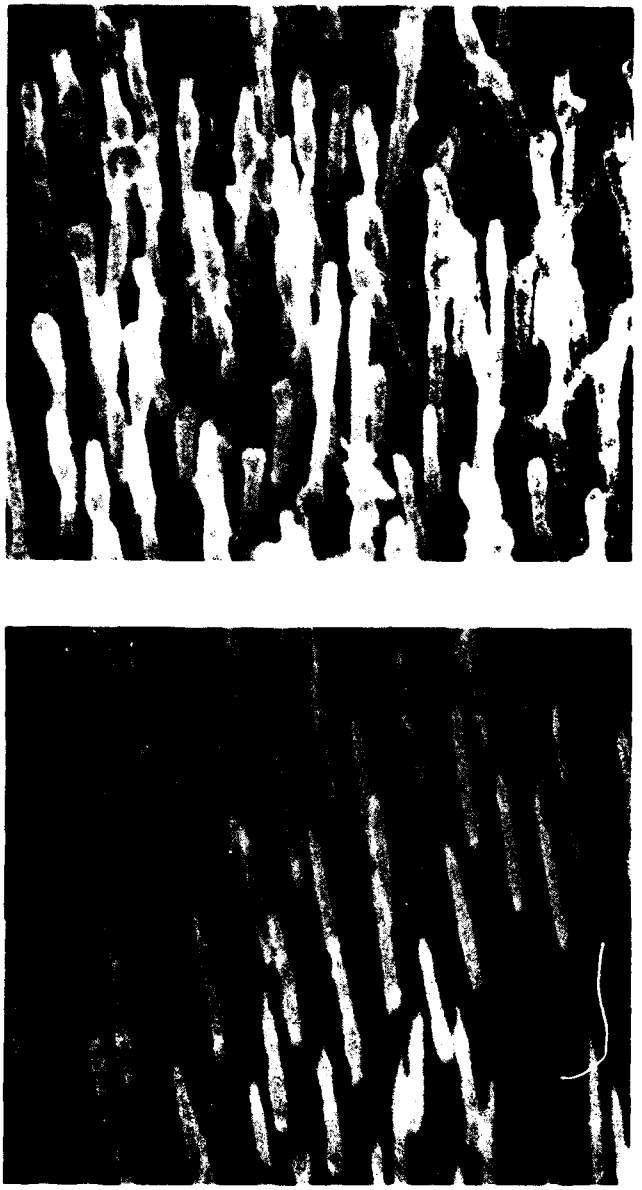

Figure 40. Examples of Pre-test Exposed Pin Composite Electrodes, (a) Gd_2O_3-Ce_2O_3-Mo, (b) UO_2-W, X5000, 45°.

sures. The high pressures pulse discharge tests were designed to examine those aspects of the discharge. An important observation made during the low pressure pulse tests was that discharge stability was improved with finer polishing. Consequently, the electrodes used in the high pressure tests were all polished to a 0.3 μm finish.

A description and the raw data for these tests are presented in Appendix D. It can be seen, Figure 41, that the minimum sparking voltage as a function of pressure is not significantly different for the three electrodes tested. This was expected since at higher pressures the sparking voltage is independent of the cathode material. Howeve , there was a difference observed in discharge uniformity. The polished UO_2-W sample provided a stable discharge up to 250 torr, while the aluminum cathode only up to 180 torr. When the aluminum cathode arced (about 200 torr), the arcs were confined to two spots in the neighborhood of the wall. However, when the polished UO_2 began to arc (at about 350 torr), the arcs were all across the area of the cathode with a glow still spread across the surface at 380 torr. The arcs observed on the surface of the UO_2-W electrode were probably similar to those from the aluminum electrode. However, because of the uniformly dispersed metal in the composite, the discharge remained somewhat uniform. This shows that the UO_2-W electrodes behave like the pin-type electrodes. Apparently, when the current got very high in any pin, that

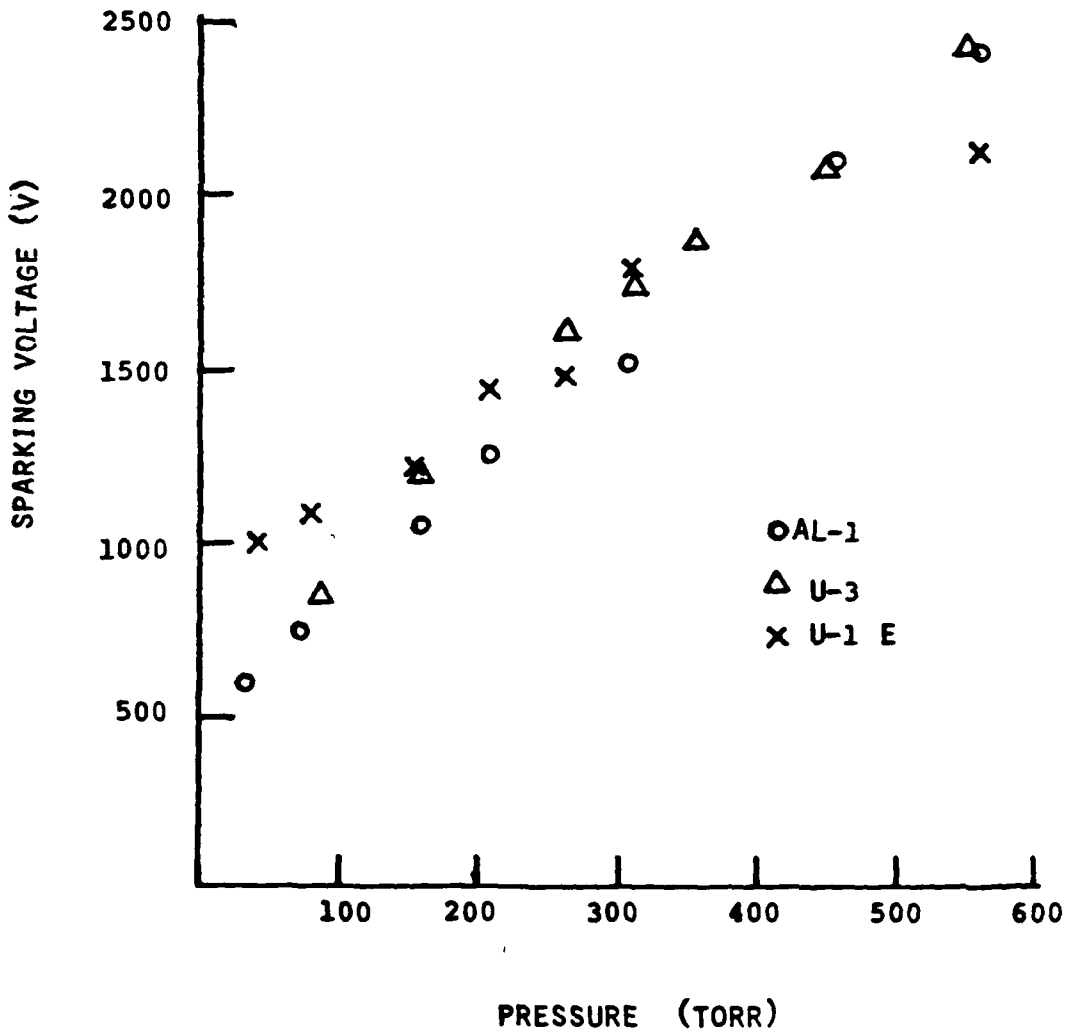

Figure 41. Minimum Sparking Voltage versus Pressure for Composite Electrodes AL-1, U-3, U-1E.

pin burned out and a localized arc could not be maintained. This is confirmed by the post test analyses which showed several pins completely removed, Figure 42a. The role the oxide played in the improved stability is not clear since it was impossible to tell if the secondary emission was from the metal pins or the oxide matrix. The etched UO_2-W composite, like the polished cc osite, spread the arcs uniformly across the surface. However, there was a great deal of flickering across the surface at pressures as low at 200 torr. Post-test examination revealed mass destruction of several areas of the cathode, Figure 42b. This damage is very typical of vacuum arc pin destruction observed from exposed pins [39]. Whether field emission was important at the higher pressures could not be determined. If the field emission process were active, it probably only served to increase current density over a localized area and was then a very likely cause of the arcs. Stability over a period of time, after the very high field emitting pins burned out, is a possibility that was not examined, nor was the operation of the electrodes at higher pressure with lower current. The limited testing discussed here did indicate that there is conceivably an advantage to the polished UO_2-W cathodes in terms of stability, at least over the aluminum cathode tested. The exposed pin UO_2-W cathode appeared to offer no advantage over the other electrodes.

It must be remembered that very little was done to

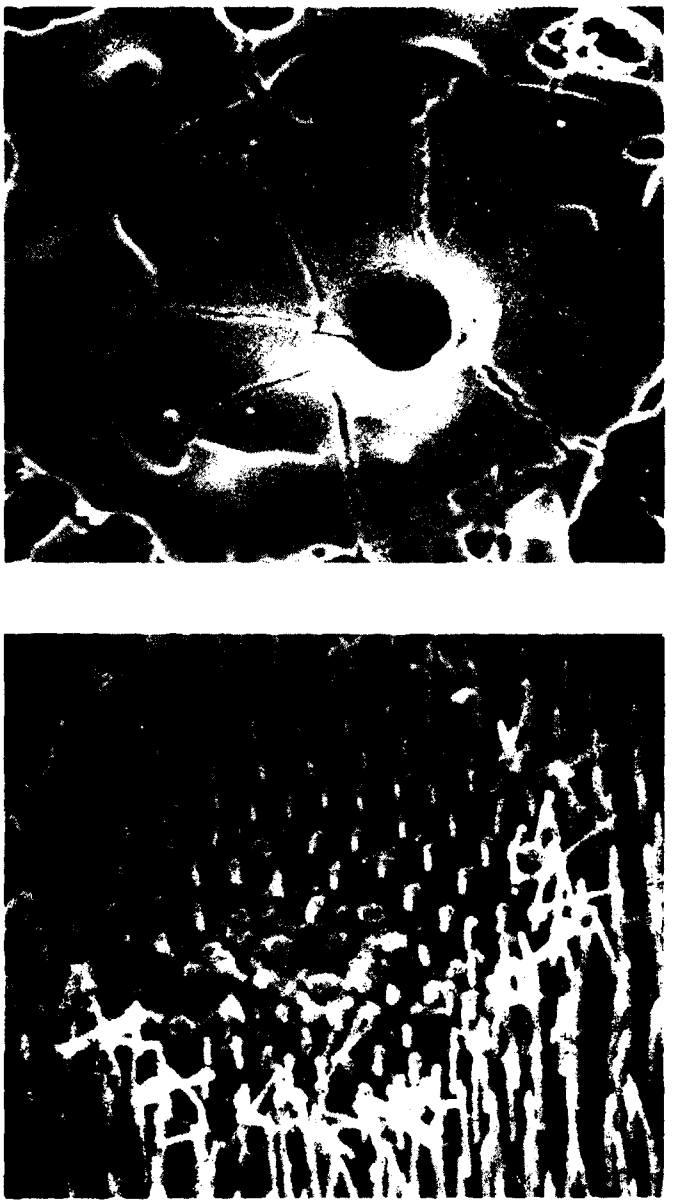

Figure 42. Examples of Damage at High Pressure to Composite Electrodes (a) Polished UO_2-W (b) Exposed Pin UO_2-W, X2500, 20^{o}.

optimize the performance of the electrodes tested and that the composite testing at high pressure was limited to only UO_2-W samples. No Gd_2O_3-Ce_2O_3-Mo composite electrodes were assessed at high pressure.

CHAPTER V

CONCLUSIONS AND RECOMMENDATIONS

Conclusions

High pressure (up to 760 torr) field emission in helium from Low Voltage Field Emitter (LVFE) arrays has been demonstrated under conditions which pose minimal damage to the LVFE pins. Control of the magnitude of discharge currents at constant field has been accomplished by varying the emission from the LVFE structure. Although true preionization was not achieved for the conditions tested, the LVFE structure has been shown to be a potentially viable technique for independent control of field (and E/p) and current for atmospheric pressure gas lasers.

Oxide-metal composites of compositions UO_2-W and Gd_2O_3-Ce_2O_3-Mo used as electrodes have been shown to offer no advantage over a standard aluminum electrode in the control of gas discharge characteristics. Cathode falls for both the polished and exposed-pin composites were significantly higher than for the aluminum electrode. An exposed pin UO_2-W composite was less stable than an aluminum electrode at high pressure, while a polished UO_2-W electrode provided only marginally improved stability.

Recommendations

The performance of the composites as discharge electrodes indicated that the probability of obtaining lasing advantages is small. Consequently, no additional work in that area will be recommended. Conversely, the LVFE structures were shown to be very promising and the remainder of this section is devoted to recommendations for continued research in the area of preionization.

Undoubtedly, one of the most important general considerations for successful use of the LVFE cathode is the magnitude of emission at high pressure. Higher emission should result in more stable discharges and more flexibility in the control of discharge current by the LVFE. The effects of space charge and contamination should be examined as well as the use of general improvements in LVFE structure that are presently being developed. In all high pressure emission work, the long term effects of the environment on emission levels should be evaluated.

In addition to the improvement of emission, several specific programs could be developed which would lead directly to the use of the LVFE structure in lasers. The most direct approach is with the two electrode configuration, using a short (0.1-1.0 μsec) emission pulse from the LVFE followed by a longer (10-100 μsec) pulse reversing the polarity and using the collector as the cathode. This would serve to simulate the conditions used in many of the double discharge techniques

but with the first pulse at a significantly lower voltage. The two electrode configuration has an advantage in that it may not be necessary for the electrons to travel far from the cathode, reducing the effect of space charge. In addition, reversal of polarity should provide protection for the pins from the positive ions. This is probably the only configuration in which true preionization could be achieved and that would depend on the emission current density obtainable from the LVFE.

An alternative to two electrode preionization would be to sustain a discharge in the three electrode configuration. Here the magnitude of current arriving at the mesh is critical and space charge would be important. An attempt should be made to sustain the discharge duration beyond the emission pulse using discharge pulses synchronized to follow the emission pulse. Also, the use of LVFE emission pulses to sustain a discharge could be considered.

APPENDIX A

GROWTH OF UNIDIRECTIONAL OXIDE-METAL COMPOSITES

This appendix describes briefly the basic techniques involved in the growth of the two unidirectionally oxide-metal composites used in this research, UO_2-W and Gd_2O_3-Ce_2O_3-Mo.

UO_2-W

The UO_2-W composites were grown using a modified floating zone technique in which pressed rods of a 94% UO_2, 6% W oxide-metal mixture were sintered with rf-heated molybdenum tubes in an inert atmosphere. After this initial heating, which served to densify and preheat the material as well as to increase the electrical conductivity of the oxide, the molybdenum tube heaters were separated to expose the sample to an rf field (normally between 3 and 5 MHz). The heating continued until the interior of the rod melted at temperatures up to 3000°C. The solid skin of the rod was well below the eutectic temperature of the mixture and acted as a crucible to contain the molten zone. Composite growth was obtained by moving the molten zone up through the rod. The rate of movement of the molten zone, oxide stoichiometry, and other parameters play an important role in the final structure of the composite. Additional details on the growth

as well as optimization of the growth parameters can be found in reference [41].

$\underline{Gd_2O_3\text{-}Ce_2O_3\text{-}Mo}$

The technique used for growing this composite was similar to that for UO_2-W described above, i.e., a modified floating zone technique. The oxide-metal mixture used was 68% Gd_2O_3, 20% Ce_2O_3, and 12% Mo. Only limited effort has been done at the Georgia Institute of Technology with the growth of this and other rare-earth oxides. This information is included in reference [45].

APPENDIX B

LVFE PREIONIZATION SOURCE TESTS

This appendix describes each of the tests (HP-1 through HP-25) in the LVFE preionization source phase of this study. A summary of the test conditions is provided in Table B-1, while a description of the LVFE cathodes is provided in Table B-2. A detailed description of the test configurations has been presented in the text, Table 7, and this information will not be repeated unless it is of specific interest to the particular test.

Test HP-1

Cathode S-11C had previously been used in vacuum LVFE investigation and was run in Test HP-1 using the mixture of laser gas used in the discharge tests. At 500 torr, erratic emission current of 2-3 μA was measured with +67 V on the collector and -100 V on the pins (voltage between the tungsten pins and the molybdenum extractor). The voltage on the collector was increased to +300 V, and the emission current rose to between 10 and 20 μA.

Throughout the 15 minutes of the 0.5% duty cycle operation (100 μsec/50 Hz), the emission current declined. Examination in the SEM indicated a thickening at the tips of the pins, Figure 37.

Table B-1. Preionization Source Test Summary.

Test #	Cathode	Pressure Range (torr)	Test Description
HP-1	S-11C	500	Emission test - laser gas
HP-2	S-11C	500	Emission test - argon
HP-3	L-44C	500	Emission test
HP-4	E17-1	500	Emission test/two electrode discharge
HP-5	E17-1	500	Emission test
HP-6	L19B	500	Emission test
HP-7	E20-1	500	Emission test
HP-8		(No Test)	
HP-9	E20-1	500	Two electrode discharge
HP-10	E17-1	500	Emission test
HP-11	E20-1	500	Three electrode discharge/ emission test
HP-12		(No Test)	
HP-13	L19D-A	7.7	Three electrode discharge/ emission test
HP-14	E13-2	500	Emission test/three electrode discharge
HP-15	JP9-1	39-500	Variable pressure emission
HP-16	JP9-1	350	Emission test/three electrode discharge
HP-17	JP9-1	31	Emission test/three electrode discharge
HP-18	L19E	34	Emission test
HP-19	JP9-3	500	Emission test
HP-20	L19D-B	8-220	Emission test
HP-21	L19D-B	13	Emission test/discharge test
HP-22	JP9-2	10^{-6}	Emission test
HP-23	JP9-2	10^{-6}/760/.030	Emission test
HP-24	E1-2	10^{-6}/760	Emission test/three electrode discharge
HP-25	ER+E	10^{-6}/760	Emission test/three electrode discharge

Table B-2. LVFE Cathode Summary.

Cathode	Area x 10^4 (1) (cm^2)	Pin Height (2) (μm)	Hole Diameter (μm)	Factor (3) (cm^{-2})
S-11C	5.4	2.3	2.1	1852
L-44C	6.1	2.5	2.4	1639
E17-1	6.5	2.6	3.3	1529
L19B	9.6	2.8	3.1	1039
E20-1	4.7	2.6	3.7	2130
L19D-A	7.8	4.0	1.3 x 2.7 (4)	1283
E13-2	8.0	4.2	2.4	1243
JP9-1	7.0	3.8	4.0	1415
L19E	14.0	3.4	3.4	699
JP9-3	8.3	4.7	2.6 x 6.6 (4)	1205
L19D-B	8.3	6.4	4.0	1201
JP9-2	20.3	3.3	4.0	493
E1-2	13.3	2.3	3.0	747
ER+E	9.0	4.2	2.4	1101

(1) Area of active area
(2) All pins pointed except L44C - cylindrical
(3) Factor times current = current density
(4) Elliptical hole - minor x major axis

Test HP-2

The identified accumulation from HP-1 rinsed off cathode S-11C with HF and that cathode was rerun in argon at 500 torr. Once more erratic emission in the 10 μA range was observed and emission died more rapidly than in Test HP-1. After 15 minutes of operation, emission was only 2 μA. SEM post-test examination showed that the pin tips had been severely ion-milled.

Test HP-3

No 500 torr emission was detectable with cathode L44C. This cathode had cylindrical pins.

Test HP-4

In order to avoid the ion milling properties of argon and to prevent the coating which seemed to result from the laser gas, it was decided to use helium in all subsequent tests. This test (E17-1) was the first to demonstrate stable high pressure field emission. Table B-3 summarizes the emission data. During -80 V emission, the current was seen to drop and consequently, the -100 V emission was not as high. When the pulse length was raised to 100 μsec, the emission increased. This was probably due to the charging time of the 100 kΩ resistor being so long that much of the current of the shorter pulses was masked. At the high emission value (24.5 mA/cm^2) with +67 V was on the collector, a glow on the cathode was observed. At + 300 V on the collector, a column

Table B-3. Field Emission from Cathode E17-1, Test HP-4 (500 torr).

Pulse Length (μsec)	Applied Voltage (V)	Emission Current[1] (μA)	Emission Current Density (mA/cm^2)	Leakage Current (mA)
50	-60	1.6	2.4	0.1
50	-80	16.0[2]	24.5	0.2
50	-100	10.0	15.3	0.4
100	-100	16.0	24.5	0.3

(1) +67 V on collector.
(2) Decreased with time to below 10 μA.

of ionization became visible and a current of 200 μA (0.1 A/cm^2) was measured with only -60 V on the pins. Operation at the 0.5% duty cycle with + 67 V on the collector and -100 V on the pins was continued for 15 minutes with no loss of emission (15 μA). SEM examination revealed some minor melting of the tips and some pins missing, but there was no mass destruction of the surface and no major arcs.

Test HP-5

Cathode E17-1 was remounted and tested. Now, emission much more sluggish than in the previous test. Emission was not detected until -100 V was on the pins, and then only 2 μA (3 mA/cm^2) emission was measured. Even up to -170 V only 4 μA (6.1 mA/cm^2) was measured. During this test, the cathode inadvertantly shorted. Despite the low emission, no additional destruction due to this test was observed.

Test HP-6

This test, like HP-5, was short lived. Emission from cathode L19B was measured at 3.0 μA (3.1 mA/cm^2) at -80 V, but the sample shorted when the pin voltage was raised to -100 V.

Test HP-7

This test was the second which demonstrated significant high pressure emission. The cathode used in this test, E20-1, had a very non-uniform active area. In addition, the

silica and molybdenum films did not adhere well in the deposition. Nevertheless, with -110 V on the pins, emission of 6.2 μm at 500 torr was measured, Table B-4. The test was run for 15 minutes with no change in the emission. Examination of the active area showed no major arcs or ion-milled pins. There was a slight increase in the lifting of the films.

Test HP-9

Cathode E20-1 was remounted and retested, again at 500 torr. This time the + 67 V that had been on the collector was increased to + 300 V. When emission started, a glow between the collector and the cathode was observed similar to that in Test HP-4. Table B-5 shows the emission measured as a function of applied voltage on the pins. When the voltage was removed from the pins, and +350 V placed on the collector, a discharge was observed. This discharge was erratic and random in position going from the collector to the shortest path, not to the center of the cathode as when emission was present. At -90 V on the pins, emission became less stable and began to resemble the dc discharge.

With +300 V still on the collector, the emission current was observed at a range of pressures between 300 and 500 torr. Gradually during this test the voltage at which the emission became less stable increased from -90 to -100 V. Since the pressure was not varied unidirectionally, the increase was not directly associable to any particular

Table B-4. Field Emission from Cathode E20-1, Test HP-7 (500 torr).

Applied Voltage (V)	Emission Current[1] (μA)	Emission Current Density (mA/cm^2)
-90	2.0	4.3
-96	3.5	7.5
-100	4.2	8.9
-110	6.2	13.2

[1] +67 V on collector.

Table B-5. Emission from Cathode E20-1, Test HP-9 (500 torr)

Applied Voltage (V)	Emission Current[1] (μA)	Current Density (mA/cm^2)	Description of Column of Ionization
-76	30	64	Slight Glow
-80	150	319	Stable Glow
-84	300	639	Stable Glow
-90	350-400	746-852	Tendency to Arc

[1] +300 V on colltector.

pressure range. In fact, if this slight degradation in cathode performance is ignored, no effect of pressure change was seen.

The cathode-collector separation was changed from one mm to two mm and, leaving the cathode untouched, emission data was recorded with +300 V on the collector, Table B-6. No current (no discharge) was measured with 450 V DC across the anode and no voltage on the LVFE.

SEM analysis of cathode E20-1 after the above testing indicated that the pins had been shortened considerably. An examination of the active area also showed that extensive damage had been done to the extractor film. For this reason it was decided that in future tests the cathode should be protected from the main discharge. To accomplish this, a wire mesh electrode was placed between the cathode and what had previously been the collector. The previous collector was now the anode for the main discharge, while the wire mesh served the dual purpose as collector for emission and cathode for the main discharge. In this way, it was hoped that the high current discharges and associated positive ions would be kept away from the LVFE cathode. Most subsequent tests used this three electrode configuration. The circuit and design of this set up have previously been discussed, Chapter III.

Test HP-10

The short in cathode E17-2 was burned out and emission

Table B-6. Field Emission from Cathode E20-1 at Two Collector Spacings, Test HP-9 (500 torr).

Voltage Applied (V)	Emission Current[1] at 1 mm spacing (μA)	Emission Current[1] at 2 mm Spacing (μA)
-80	2.0	{Not Detected
-90	6.0	
-100	60.0	12.0
-104	{Not Measured	15.0
-114		30.0

[1] +67 V on collector.

as high as 6 μA (9.1 mA/cm^2) was measured at -100 V on the pins. Again a glow on the surface was observed before this cathode shorted for good.

Test HP-11

This was the first test to use the three electrode configuration and used cathode E20-1. The wire mesh was placed at a potential of +67 V. When +600 V was placed on the anode, a discharge of about 5 μA was measured at the collector. It should be remembered that a discharge differs from emission in the polarity of the current; in the latter, electrons flow from the collector to ground, while in the former they flow from the collecto· to the anode. With +375 V on the anode a slight, unmeasurable discharge was observed. With only +300 V on the anode, no discharge was observed. All the discharges discussed above occurred when the pin voltage was a -220 V. When the positive voltage was removed from the anode, emission of 1 μA (2.1 mA/cm^2) was observed in the same voltage range (-200 to -220 V). Unfortunately, this cathode shorted before further tests could be made. The active area of this cathode had been in such terrible shape before test HP-11, that the post-test SEM examination proved inconclusive.

Test HP-13

Cathode L19D-A did not emit at 500 torr even with +300 V on the wire mesh. At -150 V on the pins, the leakage became unstable and this voltage was raised no higher.

Instead of discarding the cathode, the pressure was dropped to 7.7 torr and emission tested. Now extremely high emission was observed as indicated in Table B-7. Emission could not be detected at any pressure greater than 40 torr. At 7.7 torr, a discharge was observed when +300 V was placed on the anode and the pin voltage was raised to -80 V. (Discharge current was not measured.) When the anode voltage was removed, the emission became much more sluggish. No emission was measurable until -110 V was applied to the pins and only 68 μA (84 mA/cm^2) could be detected with as much as -140 V on the pins. Now with +300 V on the anode, no discharge could be observed until -125 V was on the pins. This corresponded to the voltage at which emission began, and indicated that the discharge coincided with emission from the cathode. With no voltage on the pins, a discharge was found to occur at +400 V on the anode. Unfortunately, this discharge arced through the mesh to the cathode. After this major arc, the sample no longer emitted.

The SEM post-test examination of this cathode showed severe damage. There was almost no grid structure left to the extractor. Unfortunately, the large arc and the low pressure operation clouded the results.

Test HP-14

Cathode E13-2 emitted at a low level at 500 torr, Table B-8. After about 5 minutes, the current at -50 V had

Table B-7. Field Emission from Cathode L19D-A, Test HP-13 (7.7 torr).

Voltage Applied (V)	Emission Current[1] (μA)	Current Density (mA/cm^2)	Leakage Current (mA)
-70	45	58	1.8
-80	68	87	2.0
-90	113	145	2.5
-100	136	174	3.0

[1] +67 V on collector.

Table B-8. Field Emission from Cathode E13-2, Test HP-14 (500 torr).

Voltage Applied (V)	Emission Current[1] (μA)	Current Density (mA/cm^2)
-30	0.4	0.5
-35	0.8	1.0
-40	1.1	1.4
-50	1.8	2.2

[1] +67 V on collector.

dropped over 50% to 0.68 μA (0.8 mA/cm^2). At this point, a positive voltage was applied to the anode and emission was observed. Then, the polarity of the oscilloscope was changed and the discharge was meausred. Table B-9 presents a summary of these results. Note that the order in which the data was taken is indicated on this table, making apparent the hysteresis involved in the data. At first, these was sufficient emission at -45 V to cause a discharge with +500 V on the anode. However, when the 10^{th} piece of data was taken, no discharge with +500 V on the anode could be observed with even as much as -60 V on the pins. This hysteresis was further displayed with the emission at -50 V at the start of the discharge test which was done 75% from the original value. After the sample had been shut off for 15 minutes to prepare for an additional test, it no longer emitted at all. It is important to note that the current from the discharges which were observed coincided with the voltage pulse despite the fact that the voltage across the anode-mesh configuration was a DC voltage.

SEM analysis of cathode E13-2 indicated that many of the tungsten pins had been melted and that many arcs had occurred. This was especially noticeable when the silica film was dissolved away and the complete pins examined. However, there is no indication that any of the pins were ion-milled.

Table B-9. Discharge Current from Cathode E13-2, Test HP-14 (500 torr).

Anode Voltage (V)	Applied Voltage (V)		Emission Current (μA)	Applied Voltage (V)	Discharge Current (μA)
450	(2)*	-50	0.45		
	(4)	-60	0.91		
480	(3)	-55	Discharge		
500	(1)	-45	Discharge	(10)	No Discharge up to -60 V
600	(5)	-45	Discharge	(9)	-45 0.91
650				(19)	-55 14.0
700	(6)	-40	Discharge	(12)	-50 18.0
750	(7)	-40	Spark		
760	(8)		DC Discharge		

*Indicates order of the test.

Test HP-15

Cathode JP9-1 used in this test was peculiar in that the pins were tapered but still flat at the tip. Apparently, the pins were too large in diameter and the length of time in the pointing etch was not sufficient. In spite of this, this sample emitted at high pressure. Due to the damage done to cathode E13-2, the mesh-cathode distance was raised from 0.16 cm to 0.32 cm for this and subsequent tests. In this test, emission measurements were made at a series of pressures, Table B-10. Emission at 39 torr was then measured as a function of pin voltage, Table B-11.

Test HP-16

This test used the same cathode, JP9-1, as test HP-15. Emission at 39 torr was found to be identical to that shown in Table B-11, but still down from the original emission, Table B-10. This drop was discernible at all pressures. In fact, emission could not be measured above 350 torr. With -100 V on the pins, emission at that pressure was between 0.5 and 0.7 μA (0.7-1.0 mA/cm^2). Emission and discharge measurements were made with -100 V on the pins at 350 torr, Table B-12. Again all of the current measurements coincided in time with the voltage pulse, extinguishing when the pulse ended. The DC discharge at +520 V on the anode remained even when the voltage was removed from the pins.

Table B-10. Field Emission Current vs Pressure for Cathode JP9-1, Test HP-15.

Pressure (torr)	Emission Current (μA)[1]	Pressure (torr)	Emission Current (μA)[1]
36	22.7	52	9.1
54	4.5	57	6.8
59	2.7	62	2.7
72	4.5	207	1.8
259	0.9	362	0.7
465	0.7		

[1] -90 Volts on pin, + 67 V on collector.

Table B-11. Field Emission from Cathode JP9-1, Test HP-15 (39 torr).

Applied Voltage (V)	Emission Current[1] (μA)	Current Density (mA/cm^2)
-50	No emission	--
-64	0.5	0.7
-70	0.7	1.0
-75	1.4	2.0
-80	6.8	9.6
-90	13.6	19.2

Table B-12. Emission/Discharge Current vs Anode Voltage for Cathode JP9-1, Test HP-16 (350 torr).

Voltage on Anode (V)	Emission/Discharge[1] Current (μA)	Voltage on Anode (V)	Emission/Discharge[1] Current (μA)
0-200	-0.5	300	-0.3
320	-0.2	330	-0.1
340	-0.0	400	+1.8
420	+2.7	430	+4.5
440	+4.5	450	+6.8
460	+9.1	470	+11.4
480	+13.6	-	-
DC Discharge at 520 volts on anode: 0.5-0.9 μA			

[1] -100 V on pins, +67 V on collector mesh.

Test HP-17

Two days later, JP9-1 was again tested for emission. Although no testing had been done in the interim, it now required -175 V to obtain emission even at only 31 torr. In fact, no emission could be observed at any pressure higher than this value. The emission at those conditions was 1.8 μA (2.5 mA/cm^2). The results of a discharge test at this low pressure are presented in Table B-13. All discharge currents are measured with -175 V on the pins. Both 50 μsec and 100 μsec pulses were used in this test. From Table B-13, it can seen that the effect of pulse length on discharge current was negligible. Also, the voltages at which a DC discharge was initiated for each pulse length are shown. Although the values differ by 80 V, this discrepancy was most likely due to the difficulty in obtaining reproducible discharge measurements, and not a result of the pulse length differences. As in the previous test, the discharges lasted only for the duration of the voltage pulse and were confined to a column between the anode and the wire mesh directly above the cathode. The DC discharge were once again random and took place at the edges of the anode.

Test HP-18

Because it was felt that preionization or at least control of a discharge current by the LVFE cathodes had been demonstrated, the next few tests were designed to determine

Table B-13. Discharge Current vs Anode Voltage for Cathode JP9-1, Test HP-17 (31 torr).

Anode Voltage (V)	Discharge Current[1] 100 μsec Pulse (μA)	Discharge Current[1] 50 μsec Pulse (μA)
390	--	4.5
400	--	11.4
410	18.2	18.2
420	22.7	18.2
430	--	27.3
440	27.3	--
450	--	36.4
460	34.1	--
470	--	54.5
480	34.1	45.5
500	45.5	56.8
510	45.5	--
540	--	68.2
560	--	90.9
600	90.0	
660	--	159.1
DC Discharge:	620 V on Anode 15 μA	700 V on Anode 120 μA

[1] -175 V on pins, + 67 V on collector mesh.

the conditions under which the pins would last in a high pressure environment. Cathode L19E was not very useful toward that goal. No emission from that cathode was measurable above 34 torr. The cathode was run for 20 minutes at that pressure. The peak voltage used on the pins was -180 V which resulted in emission of 0.9 μA (0.63 mA/cm^2); the minimum voltage used during the run was -140 V. Throughout the run, the emission current steadily decreased. SEM examination showed that the tips of the pins were severely rounded. Upon re-assembly, no further emission could be measured from this cathode.

Test HP-19

Since the purpose of this test was to measure the effects of emission, this test was run in the original two electrode configuration. In this test, cathode JP9-3 had measureable emission at 350 torr when -225 V was placed on the pins. Raising the pressure to 500 torr resulted in no change of emission current, Table B-14. It can be seen that after about 16 minutes of operation, a dramatic step change in current occurred. Pin voltage had to be raised to -250 V to maintain measureable emission. When the test was completed, after 45 minutes of operation, the cathode was still emitting at low levels in the 500 torr atmosphere. The post-test, SEM analysis showed many arcs and a large variation in pin heights varying from unchanged to too short to be seen.

Table B-14. Field Emission vs Time for Cathode JP9-3, Test *HP-19 (500 torr)*.

Elapsed Time (min)	Voltage Applied (V)	Emission Current[1] (μA)	Current Density (mA/cm^2)
0	-225	3.6	4.3
3	-225	4.5	5.4
4	-175	3.6	4.3
16	Emission Reduced Significantly		
19	-250	0.5	0.6
45	-250	0.9	1.1

[1] +67 V on the collector.

Test HP-20

Cathode L19D, like JP-3, was also run in the two electrode configuration. When no emission could be measured at high pressure, the collector cathode spacing was reduced from 0.32 to 0.15 cm. There was still no measureable emission at any pressure greater than 8 torr. At this pressure, emission was observed at -120 V on the pins. At -150 V, emission was between 0.9 and 1.3 μA (1.1-1.6 mA/cm^2). Pressure was raised and emission was measureable up to 220 torr. At this pressure, -170 V on the pins extracted an emission current at 2.7 μA (3.2 mA/cm^2). SEM examination of this cathode provided the same results as HP-19. The surface of the extractor grid looked excellent, but the pins were of various heights all along the active area.

Test HP-21

Cathode L19D-B was put back into the three electrode configuration. Now emission was very sluggish. It required -225 V to obtain emission at 13 torr. Emission could not be achieved at higher pressures. A discharge test was attempted with this cathode, Table B-15. However, the discharges in this test were not very stable and consequently, the actual current values may be suspect. Of greater importance was the drop in emission current which occurred as a result of the test. Before this discharge test, the current at -225 V was 12.0 μA (14.4 mA/cm^2) while after the test it was 0.9 μA (1.1

Table B-15. Discharge Current vs Anode Voltage for Cathode L19D-B, Test HP-21 (13 torr).

Anode Voltage (V)	Discharge Current (μA)[1]	Anode Voltage (V)	Discharge Current (μA)[1]
100	Emission[2]	200	Emission[2]
300	Emission[2]	400	Minor Discharge[2]
420	Discharge[3]	440	2.3
460	4.5	500	6.8
540	9.1	570	18.2
620	36.4	640	36.4
650	DC Discharge		

(1) -225 V on pins, +67 V on collector mesh
(2) Approximately 0.9 μA
(3) Not measurable

mA/cm^2). Once again the SEM examination showed the same large variation in pin heights.

Test HP-22

Test HP-22, despite the erratic emission results, did provide an interesting concept for improvement of high pressure emission. In the vacuum LVFE work, it has been well established that the pins would "clean-up" with emission [40]. That is, the current at a particular applied voltage increases and the voltage at which emission initiates decreases as emission time increases. In Test HP-20, the cathode emitted at higher pressure only after emitting at lower pressure. The next tests were designed to capitalize on this concept.

Cathode JP9-2 was assembled in the three electrode configuration and placed in the LVFE vacuum test assembly. This assembly and the details of the vacuum testing have already been described. During the field emission testing, the anode and mesh were connected together and both held at +67 V. Pressure during the entire vacuum was mid 10^{-6} torr. It can be seen, Table B-16, that in the first 270 minutes, significant improvement in the vacuum emission was made with time. However, between 270 minutes and 444 minutes, a degradation in emission was observed. And, when the emitter was left over night, the emission dropped dramatically.

Despite the low emission, the diffusion pump and baffle

Table B-16. Field Emission Current vs Time for Cathode JP9-2, Test HP-22 (10^{-6} torr).

Voltage Applied (V)	Current (μA) at Elapsed Time (min)[1] 0	82	177	270	444	1402
-60	ND[2]	7.5	5.5	9.0	ND	ND
-70	ND	12.5	-	-	ND	ND
-80	6.8	15.0	28	40	12.5	ND
-90	11.3	20	40	-	-	ND
-95	(3)	-	-	80	-	ND
-100	-	28	50	100	18	ND
-110	-	-	-	-	-	ND
-115	-	-	-	140	-	ND
-120	-	-	76	150	52	ND
-150	-	-	-	235	100	5
-200	-	-	-	-	-	10

(1) +67 V on the collector
(2) ND = No emission detected
(3) - = No emission measurement made

were shut off and the system pressure was allowed to rise. No change in emission was noticed at either 10^{-4} torr or 10^{-3} torr. At 15 μm, the emission actually rose from about 5 μA at -150 V applied to about 6 μA. When helium was allowed to fill the chamber to 760 torr, emission died. The pressure was reduced again to mid 10^{-6} torr and emission remeasured.

The sample now showed an increase in emission above that observed before the high pressure test. In an attempt to clean up the pins, -300 V was applied resulting in an emission current of 110 μA (54.2 mA/cm^2). At -200 V, the current was now 70 μA (34.5 mA/cm^2), a large increase from the 10 μA (4.9 mA/cm^2) shown in Table B-15. Once again the pressure was raised to atmospheric pressure with He and once again the cathode did not emit. At this point, the cathode was examined in the SEM. Very minor destruction was observed with the pins remaining unaffected.

Test HP-23

Cathode JP9-2 was once again put into the vacuum chamber and retested. Prior to evacuating the chamber, 760 torr emission was tested. When the test began, the cathode was shorted. In an attempt to burn out the short, the voltage was raised and the pulse length increased. When the short burned out there was a rapid increase in emission. In order to avoid a new short, the voltage was dropped to -100 V and the emission measured. This voltage yielded an emission

current at 4.5 μA (2.2 mA/cm^2). Now the chamber was evacuated and vacuum (10^{-6} torr) V-I data was recorded, Table B-17. It can clearly be seen that the cathode after 1124 minutes of operation was emitting much better than before.

After the 1124 minute reading, the diffusion pump and baffle were shut off and the pressure allowed to come up to 760 torr. Once again emission was detected at -100 V on the pins, but this time only 1.6 μA (0.8 mA/cm^2). At -120 V, the emission increased to 2.6 μA (1.3 mA/cm^2) but decreased with time. Pressure was reduced to less than .030 torr and emission retested. Emission as high as 600 μA (295.8 mA/cm^2) at -150 V was detected, but this emission also decreased with time. Pressure was raised to 760 torr and emission of 2.7 μA (1.3 mA/cm^2) was recorded with -100 V on the pins and 9.0 μA (4.4 mA/cm^2) with -150 V on the pins. Pressure was then alternated between .030 torr and atmosphere, Table B-18. As can be seen by comparing the 30 x 10^{-3} torr emission results, this cathode's emission was gradually deteriorating. The chamber pressure was not reduced to 10^{-6} torr and the field emission was remeasured. After raising the voltage to -230 V, the current at -150 V was 70 μA (34.5 mA/cm^2). When this value is compared to the final entry in Table B-17, the degradation of this cathode is clearly illustrated. The post-test SEM examination indicated that there has been a significant shortening of the pins.

Table B-17. Field Emission Current vs Time for Cathode JP9-2, Test HP-23 (10^{-6} torr).

Voltage Applied (V)	Time:	Current[1] (μA) at Elapsed Time (min) 0	39	61	1092	1124
-40		ND[2]	ND	ND	4	-[3]
-50		ND	ND	ND	24	-
-60		25	-	22	55	-
-80		64	-	90	175	-
-100		150	-	150	340	400
-110		190	170	-	-	-
-130		-	-	-	-	600

(1) +67 V on collector
(2) ND = No emission current detected
(3) - = No emission measurement made

AD-A091 407 AIR FORCE INST OF TECH WRIGHT-PATTERSON AFB OH F/G 20/5
UNIDIRECTIONAL COMPOSITES AS ELECTRODES/PREIONIZATION SOURCES F--ETC(U)
DEC 79 S G WAX
UNCLASSIFIED AFIT-CI-79-249D NL

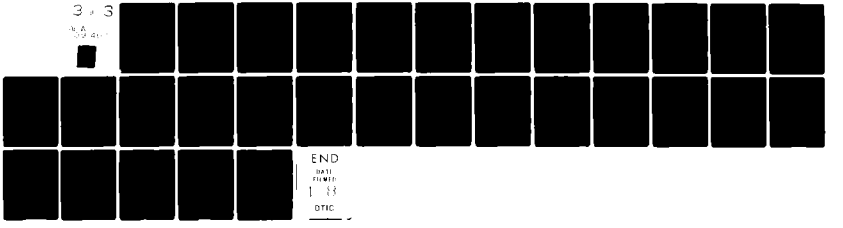

Table B-18. Comparison of 760 torr and .030 torr Field Emission from Cathode JP9-2, Test HP-23

Applied Voltage (V)	Emission Current (μA)[1] at Pressure (torr)						
	Pressure						
	760	.030	760	.030	760	.036	760
100	1.6	-[3]	2.7	10	ND	-	ND
120	2.6	-	-	70	ND	-	ND
130	-	125	-	-	ND	-	ND
150	-	600[4]	9.0[4]	400[4]	ND	181[5]	ND
160	-	-	-	-	9[6]	-	ND

(1) +67 V on the collector
(2) Time increased from left to right
(3) No emission measurement made
(4) Decreased with time
(5) Down to 90 μA after 10 minutes
(6) Down to 6.3 μA after 10 minutes

Test HP-24

Cathode El-2 was also tested at both 10^{-6} torr and 760 torr. Although the 10^{-6} emission appeared to have little effect on the 760 torr emission, this test was retained to provide a means for comparison of the cathodes. The leakage current from this cathode was very high, over 16 mA at -100 volts. To minimize the chance of shorting the cathode, the pulses were reduced to 50 μsec. At -200 V the emission from this cathode was 75 μA (56.0 A/cm^2). Unfortunately, after the cathode was shut off for a night, emission at -200 V was only 15 μA (11.2 mA/cm^2). At this point, the pressure was raised and a fruitless attempt was made to measure emission. Assuming that this cathode would not emit at high pressure, it was decided to measure the effect on the discharge of the pin voltage without emission. This test proved to be a serendipity because a clear preionization effect was observed. Holding the anode at a constant DC voltage, the pin voltage was raised until a discharge current was measured. The discharge occurred at -510 V when 500 V was on the anode and at -100 V when 900 volts was on the anode, indicating that emission and not pin voltage per se caused the discharge. Table B-19 shows the effect of anode voltage at constant pin voltage (-150 V). More interesting is the effect of pin voltage on the discharge at constant anode voltage, Table B-20. Although not complete, there is a definite trend toward higher discharge current at higher

Table B-19. Discharge Current from Cathode E1-2, Test HP-24 (760 torr).

Anode Voltage (V)	Discharge[+] Current (μA)	Average Discharge Current (μA)
500	++	0
600	(2-5)[+++]	3.5
700	(5-6), 2	4.3
720	5	5
800	(5-7.5)	6.3
850	(5-15)	10

[+] -150 V on pins, +67 V on collector mesh.
[++] Flicker indicating beginning of discharge
[+++] ( ) = range for one data point

Table B-20. Discharge Current for Cathode E1-2, Test HP-24 (760 torr).

Anode Voltage (V)	Applied Voltage (V)	Discharge[+] Current (μA)	Average Discharge Current (μA)
500	-150	0	0
	-160	2	2
	-170	2	2
	-190	2	2
	-200	(2-5)[++]	3.5
600	-100	1	1
	-110	0	0
	-120	(2-5)	3.5
	-150	(2-5),5,(2-5),2	3.5
	-170	(4-5)	4.5
650	-140	(2-5)	3.5
700	-110	0	0
	-120	1,(.5-5)	1.8
	-130	2	2
	-140	1,2	1.5
	-150	(5-6),2	3.7
710	-120	5	5
	-140	5	5
720	-140	4	4
	-150	5	5
800	-150	(5-7.5)	6.3
	-120	1	1
	-150	(5-15)	10

[+]67 V on the collector
[++]( ) = range of current for single test

pin voltage. This was the first evidence of the LVFE pre-ionization source controlling the discharge current. After completing the discharge tests, emission from the cathode was once again measured at 10^{-6} torr. Now only 10 μA (7.4 mA/cm^2) was measurable at -200 V. SEM analysis of the sample indicated that none of the pins had been ion-milled.

Test HP-25

This was made in the same manner as Test HP-24. Low pressure emission (10^{-6} torr) with the cathode (ER+E) was measured as 130 μA (143 mA/cm^2) at -150 V after about two hours of conditioning. When the pressure was raised to 760 torr, trace emission was observed at -120 V. Discharge tests were then performed as before. These are summarized in Table B-21. Occasionally as the pin voltage was raised, a DC discharge would be initiated. This did not happen consistently and those data points were not recorded. Once again the trend toward control of the discharge current with the LVFE was evident, in fact more so than with the previous test.

Throughout this test, there was an observed tendency for the discharges to become more sluggish. After a while, it was found that the voltage had to be raised to -120 V before discharges would occur at the lower voltages. SEM examination of this sample, however, did not reveal any blunting of the pins.

Table B-21. Discharge Current for Cathode ER+E, Test HP-25 (760 torr)

Anode Voltage (V)	Applied Voltage (V)	Discharge Current (μA)	Average Discharge Current (μA)
400	-60	1	1
	-100	2	2
	-120	4	4
	-140	5	5
500	-60	1,1	1
	-70	4,2,3	3
	-80	4,4,8,4,8	5.6
	-90	4	4
600	-60	2,2,2	2
	-70	2,12,3,4	5.25
	-80	14,1,3,5	5.75
	-100	18,15	16.5
700	-60	4	4
	-65	6	6
	-70	8,5	7.5
	-75	10	10
	-90	10	10
	-100	15	15

APPENDIX C

SPACE CHARGE AT HIGH PRESSURE

In a high pressure discharge, if the current density is large enough to distort the field, space charge must be considered. The current-voltage relationship of ions travelling between parallel plane electrodes under space charge conditions is given by [8, 46].

$$J = 9.95 \times 10^{-14} \frac{V^2}{d^3} K \qquad \text{(C-1)}$$

where: V = the voltage between the electrodes

d = the distance between the electrodes

K = the mobility of the ions.

Usually this equation is used when positive ions from the cathode are considered [46]. However, in the case where the only charge carriers are electrons, this equation can be used. Field emitters under conditions of no ionization meet this criterion.

In order to apply equation (C-1) to high pressure electron space charge, the mobility of the electrons must be known. The mobility, K_e, is related to the average distance travelled by the electron in one second in the direction of a field, E, as:

$$K_e = Vd/E \qquad (C-2)$$

where Vd is the drift velocity. Naturally, the mobility will depend on the mean free path or the inverse of pressure as well as the gas. Consequently, Vd is a specific function of E/p for a particular gas. Reference [46] provides a graph of E/p vs Vd for electrons in helium. For each of the cathodes which emitted at high pressure, E/p, Vd, and K_e can be calculated using those values and equation (C-2). Then, from equation (C-1), the space charge limited current for each condition can be calculated. These results are presented in Table C-1, along with the maximum experimental current density for that condition. A correlation of 0.573 exists between these values. While this does not confirm the presence of space charge limited current, it provides an indication that space charge could be playing an important role.

Table C-1. Space Charge Current Limit.

Cathode	d (cm)	E (V/cm)	E/p (v/cm torr)	Vd x 10^{-6} (cm/sec)	K_e cm^{-1}	J_{Theo} mA/cm^2	J_{Exp} mA/cm^2
E17-1	0.1	1670	3.3	2.41	1443	4.0	24.5
L19-B	0.1	1570	3.2	2.33	1484	3.6	3.9
E20-1	0.1	1670	3.3	2.41	1493	4.0	12.7
E13-2	0.16	731	1.5	1.28	1751	0.6	2.2
JP9-1	0.32	521	0.6	0.58	1113	0.09	1.0
JP9-2	0.32	709	0.9	0.83	1170	0.18	4.4
ER+E	0.32	584	0.8	0.75	1284	0.14	0.3

APPENDIX D

RESULTS FOR COMPOSITE ELECTRODE TESTS

This appendix provides the test conditions, raw data and observations for the composite electrode testing.

CW Tests

Data for the CW cathode full tests for the five different electrodes, Table 6, is presented in Tables D-1 through D-5. A 500 kΩ series resistor provided a discharge which appeared to behave as a glow discharge for all but the two UO_2-W electrodes. For these, the current did not appear to be sufficient to sustain a stable glow and the resistor was reduced to 250 kΩ or to 68 kΩ.

Pulsed Discharge Tests

The first tests performed were a repeat of the CW cathode fall tests using 50 μsec, 500 Hz pulses. A 68 kΩ resistor was used as the series resistor. With the 0.1 cm separation, both a new UO_2-W electrode (U-2), Table D-6, and the original aluminum electrode (Al-1), Table D-7, were run in discharge tests. A major problem with using the 0.1 cm discharge gap was that it was difficult to observe the cathode during a discharge. Since the main purpose of the pulse tests was to observe discharge uniformity, the next tests were

Table D-1. CW Discharge Data for Cathode G-1 (500 kΩ).

P (torr)	V_S (V)	V_D (V)	I (mA)
23	503	385	0.23
32	522	392	0.26
41	552	398	0.30
51	571	406	0.33
78	660	448	0.43
103	739	481	0.51
121	808	511	0.60
155	907	542	0.73
23	513	408	0.20
55	591	396	0.37
80	661	400	0.51
112	759	422	0.66
155	883	570	0.54

Table D-2. CW Discharge Data for Cathode AL-1 (500 kΩ).

P (torr)	V_S (V)	V_D (V)	I (mA)
43	522	292	0.46
52	562	292	0.54
81	641	312	0.65
101	710	330	0.75
158	808	383	0.82
23	493	233	0.52
34	512	242	0.54

Table D-3. CW Discharge Data for Cathode U-1E (250 kΩ).

P (torr)	V_S (V)	V_D (V)	I (mA)
50	847	520	1.2
100	1210	616	2.4
150	1389	669	2.9
50	1044	522	2.3
	1438	528	3.6
	2320	515	7.3
100	1477	605	3.5
	1970	587	5.5
150	1477	657	3.3

Table D-4. CW Discharge Data for Cathode U-1 (68 kΩ).

P (torr)	V_s (V)	V_D (V)	I (mA)
31	522	432	1.32
52	591	475	1.62
79	660	480	2.54
101	729	485	3.40

Table D-5. CW Discharge Data for Cathode G-1E (500 kΩ).

P (torr)	V_s (V)	V_D (V)	I (mA)
36	522	484	0.09
34	532	409	0.24
54	641	480	0.32
112	792	557	0.47
152	985	586	0.78

Table D-6. Pulsed Discha ge Data for Cathode U-2.

P (torr)	V_S (V)	V_D (V)	I (mA)
85	739	430	4.5
155	1015	520	7.3
247	1043	580	6.8
85	833	500	4.9
47	697	450	3.6
163	982	550	6.4

R = 68 kΩ
d = 0.1 cm
dc = 50 μsec/500 Hz

Table D-7. Pulsed Discharge Data for Cathode AL-1.

P (torr)	V_s (V)	V_D (V)	I (mA)
28	620	280	5.0
52	753	320	6.4
	691	320	5.5
101	913	400	7.5
155	1100	420	10.0
207	1285	450	12.3
259	1427	500	13.6

R = 68 kΩ
d = 0.1 cm
dc = 50 μsec/500 Hz

performed using the 0.3 cm separation. The data for an exposed pin Gd_2O_3-Ce_2O_3-Mo electrode (G-2E) and an exposed pin UO_2-W composite electrode (U-1E) is shown in Table D-8 and D-9, respectively. In these tests, electrode G-2E was very unstable with arcs appearing on the surface at pressures as low as 25 torr. The discharge from the exposed pin UO_2-W composite, on the other hand, looked quite uniform up to the highest pressure tested, 100 torr.

To examine the uniformity of the discharge at higher currents, the 68 kΩ resistor was replaced with a 25 kΩ resistor. A UO_2-W electrode (U-3), Table D-10, was tested using this lower resistance. In this test, small arcs were observed on the surface at 28 torr and continued throughout the higher pressures. The 25 kΩ resistor was also used with a test of Al-1, but the discharge was very erratic and no data was taken.

In an attempt to stabilize the discharge, electrode U3 was polished to a 0.3 μm finish and retested using a 8.4 kΩ resistor. Now the discharge was much more stable. Repolishing the aluminum cathode Al-1 also stabilized the discharge from this cathode. Therefore, before testing the electrodes at high pressure, the UO_2-W and aluminum electrode were both polished to 0.3 μm. For the high pressure tests, the 0.1 cm separation was used in order to lower the voltage required for the high pressure discharge. This made examination of the glow on the cathode surface more difficult, but it was still

Table D-8. Pulsed Discharge Data for Cathode G-2E.

P (torr)	V_s (V)	V_D (V)	I (mA)
78	800	640	2.4
164	971	640	4.7
267	1230	760	6.9
349	1418	800	9.1

R = 68 kΩ
d = 0.3 cm
dc = 50 μsec/500 Hz

Table D-9. Pulsed Discharge Data for Cathode U-1E.

P (torr)	V_s (V)	V_D (V)	I (mA)
85	951	580	5.5
110	976	580	5.8
160	962	560	5.9
260	1238	620	9.1
330	1374	750	9.2

R = 68 kΩ
d = 0.3 cm
dc = 50 μsec/50 Hz

possible to observe the uniformity of the discharge. For these tests pulse characteristics more typical of laser operation, (4 μsec, 500 Hz pulses) were used. Because of the short pulses, the resistance had to be lowered to 4.2 kΩ. The data taken for these runs is presented in Table D-10 through Table D-14.

With the aluminum cathode, flickering in the discharge was observed as low as 150 torr. At 200 torr, many arcs were noticeable in the discharge. It was not possible to get any kind of uniform discharge from the aluminum cathode at pressures above 180 torr. The UO_2-W cathode, on the other hand, produced a discharge which was uniform and stable up to 250 torr. The glow at that pressure was not confined to the walls. At 380 torr, arcs occurred in the discharge, but a glow could still be spread on the surface. At 350 torr, a stable discharge could be achieved. The etched UO_2-W cathode, produced a uniform glow at 200 torr with the exception of occasional bright flickering at the surface. At 300 torr, an arc was present and the discharge could not be spread along the cathode surface.

Post test evaluation of the aluminum cathode showed oxidation at each of the four corners of the discharge indicating the extent to which arcing occurred on the aluminum cathode. The UO_2-W cathode was remarkably undamaged with the exception of a few missing pins. The etched UO_2-W cathode showed the most visible destruction. Many arcs were evident

Table D-10. Pulsed Discharge Data for Cathode U-3.

P (torr)	V_s (V)	V_D (V)	I (mA)
28	807	406	13.2
80	1250	616	21.8
103	1575	762	30.9
148	2250	935	50.0

R = 25 kΩ
d = 0.3 cm
dc = 50 μsec/50 Hz

Table D-11. High Pressure Pulsed Data for Cathode AL-1.

P (torr)	V_s (V)	V_D (V)	I (mA)
32	600	420	43
78	750	460	78
155	1050	520	118
55	1100	560	126

R = 4.1 kΩ
d = 0.1 cm
dc = 4 μsec/500 Hz

Table D-12. High Pressure Pulsed Data for Cathode U-2.

P (torr)	V_s (V)	V_D (V)	I (mA)
85	739	430	45
155	1015	520	73
247	1043	580	68
85	833	500	49
47	697	450	36
163	982	550	64

R = 4.1 kΩ
d = 0.1 cm
dc = 4 μsec/500 Hz

Table D-13. High Pressure Pulsed Data for Cathode U-1E.

P (torr)	V_s (V)	V_D(V)*	I (mA)*
80	1100	580	132
155	1200	560	144
207	1450	640	178
259	1550	750	216

*Data erratic

R = 4.1 kΩ
d = 0.1 cm
dc = 4 μsec/500 Hz

Table D-14. Minimum Sparking Voltage for Cathodes AL-1, U-2, U-1E.

Pressure (torr)	Pressure (psia)	Minimum Voltage (V) AL-1	U-3	U-1E
31	0.6	600	-	1000
78	1.5	750	-	1000
83	1.6	-	850	-
155	3.0	1050	1200	1200
207	4.0	1250	1400	1450
259	5.0	-	1500	1550
310	6.0	1500	1700	1750
362	7.0	-	1750	-
465	9.0	2100	2100	-
569	11.0	2400	2480	2100

along the surface, while several of the pins were either melted or destroyed by the arcs.

BIBLIOGRAPHY

1. D. C. O'Shea, W. P. Callen, and W. T. Rhodes, Introduction to Lasers and Their Applications, Addison-Wesley Pub. Co., Reading, Mass. (1977).

2. W. W. Duley, CO_2 Lasers, Effect and Applications, Academic Press, New York, NY (1976).

3. O. R. Wood II, "High-Pressure Pulsed Molecular Lasers," Proceedings of the IEEE, 62, 355 (1974).

4. O. R. Wood II, P. W. Smith, C. R. Adams, and P. J. Maloney, "Excitation of Transversely Excited CO_2 Waveguide Lasers," Appl. Phys. Letters, 27, 539 (1975).

5. H. G. Ahlotrom, et al., "Cold Cathode Electron Beam Controlled CO_2 Laser Amplification," Appl. Phys. Letters, 21, 492 (1972).

6. P. W. Smith, P. J. Maloney, O. R. Wood II, "Waveguide TEA Laser," Appl. Phys. Letters, 23, 524 (1973).

7. Encyclopedia of Physics, Vol. XXII, S. Flugge ed., Springer-Verlag, Berlin (1956).

8. J. D. Cobine, Gaseous Conductors Theory and Engineering Applications, Dover Publications, Inc., New York, NY (1958).

9. A. M. Howatson, An Introduction to Gas Discharges, Pergamon Press (1955).

10. F. Llewellyn-Jones and C. G. Morgan, "Failure of Paschen's Law and Spark Mechanism at High Pressure," Phys. Rev., 82, 950 (1951).

11. F. A. Maxfield and R. R. Benedict, Theory of Gaseous Conduction and Electronics, McGraw Hill Book Co. Inc., York, PA (1941).

12. F. Llewellyn-Jones, The Glow Discharge, An Introduction to Plasma Physics, Methuen and Co. LTD., London (1966).

13. P. K. Pearson and H. M. Lamberton, "Atmospheric Pressure CO_2 Lasers Giving High Energy Per Unit Volume," IEEE J of Quantum Electronics QE-8, 145 (1972).

14. D. C. Johnson, "Excitation of an Atmospheric Pressure CO_2-N_2-He Laser by Capacitor Discharges," IEEE J of Quantum Electronics QE-8, 185 (1971).

15. P. W. Smith, C. R. Adams, P. J. Maloney, and O. R. Wood II, "High Repetition Rate and Quasi CW Operation of a Waveguide CO_2 TE Laser," Optical Communications, 16, 50 (1976).

16. A. Papayoanou, Cathode Limited Operation of Transversely Excited Carbon Dioxide Channel Waveguide Laser, Combat and Target Acquisition Lab., U.S. Army Electronics Command, Fort Manmouth, NJ, ECOM-4510, July 1977.

17. A. Papayoanou, "Discharge Related Limitation of CO_2 Optical Gain in TE Channel Waveguides," Appl. Phys. Letters, 31, 736 (1977).

18. H. W. Mocker, G. R. Willenbring and R. Manning, FLIR Rangefinder Research, Honeywell Systems and Research Center, February 1977.

19. N. Karasiko and J. Shamir, "Operation of TEA CO_2 Laser with Rough Surface Electrode," IEEE J of Quantum Electronics QE-12, 257 (1976).

20. H. J. White, "The Variation of Sparking Potential with Intense Ultraviolet Illumination," The Physical Review, 48, 113 (1935).

21. A. K. Laflamme, "Double Discharge Excitation for Atmospheric Pressure CO_2 Lasers," Rev. of Sci. Inst., 41, 1578 (1970).

22. D. J. Baink and T. I. Salamon, "A Simple Photoionization Stabilized Waveguide Carbon Dioxide Laser," J. Appl. Phys. D, 10, 2117 (1977).

23. V. Hasson and H. M. Bergmann, "High Pressure Glow Discharge for Nanosecond Excitation of Gas Lasers and Low Inductance Switching Applications," J. Phys. E Sci. Inst. 1, 73 (1976).

24. O. P. Judd, "An Efficient Electrical CO_2 Laser Using Preionization by Ultraviolet Radiation," Appl. Phys. Letters, 23, 95 (1973).

25. Z. Bauman, F. Dothan, and S. Yatsev, "Glow Discharge Stabilization in a Transverse Flow CW CO_2 Laser," J. Phys. E-11, 189 (1978).

14. D. C. Johnson, "Excitation of an Atmospheric Pressure CO_2-N_2-He Laser by Capacitor Discharges," IEEE J of Quantum Electronics QE-8, 185 (1971).

15. P. W. Smith, C. R. Adams, P. J. Maloney, and O. R. Wood II, "High Repetition Rate and Quasi CW Operation of a Waveguide CO_2 TE Laser," Optical Communications, 16, 50 (1976).

16. A. Papayoanou, Cathode Limited Operation of Transversely Excited Carbon Dioxide Channel Waveguide Laser, Combat and Target Acquisition Lab., U.S. Army Electronics Command, Fort Manmouth, NJ, ECOM-4510, July 1977.

17. A. Papayoanou, "Discharge Related Limitation of CO_2 Optical Gain in TE Channel Waveguides," Appl. Phys. Letters, 31, 736 (1977).

18. H. W. Mocker, G. R. Willenbring and R. Manning, FLIR Rangefinder Research, Honeywell Systems and Research Center, February 1977.

19. N. Karasiko and J. Shamir, "Operation of TEA CO_2 Laser with Rough Surface Electrode," IEEE J of Quantum Electronics QE-12, 257 (1976).

20. H. J. White, "The Variation of Sparking Potential with Intense Ultraviolet Illumination," The Physical Review, 48, 113 (1935).

21. A. K. Laflamme, "Double Discharge Excitation for Atmospheric Pressure CO_2 Lasers," Rev. of Sci. Inst., 41, 1578 (1970).

22. D. J. Baink and T. I. Salamon, "A Simple Photoionization Stabilized Waveguide Carbon Dioxide Laser," J. Appl. Phys. D, 10, 2117 (1977).

23. V. Hasson and H. M. Bergmann, "High Pressure Glow Discharge for Nanosecond Excitation of Gas Lasers and Low Inductance Switching Applications," J. Phys. E Sci. Inst. 1, 73 (1976).

24. O. P. Judd, "An Efficient Electrical CO_2 Laser Using Preionization by Ultraviolet Radiation," Appl. Phys. Letters, 23, 95 (1973).

25. Z. Bauman, F. Dothan, and S. Yatsev, "Glow Discharge Stabilization in a Transverse Flow CW CO_2 Laser," J. Phys. E-11, 189 (1978).

26. H. M. Lamberton and P. R. Pearson, "Improved Excitation Techniques for Atmospheric Pressure CO_2 Lasers," Electronics Letters, 7, 141 (1971).

27. R. McLeary, P. J. Beckwith, and W. E. Gibbs, "Uniform Continuous Discharges and CO_2 Laser Action at Atmospheric Pressure by Plasma Injection," IEEE J. of Quantum Electronics QE-10, 649 (1974).

28. W. T. Leland, "Relaxation of Electrical Discharge Parameters to Short-Pulse CO_2 Laser Efficiency, Sov. J. Quantum Electronics, 6, 466 (1976).

29. R. K. Jain, O. R. Wood II, P. J. Maloney, and P. W. Smith, "Characteristics of High-Field Preionized Discharges for Transversely Excited Waveguide Lasers," Appl. Phys. Letters, 31, 260 (1977).

30. P. W. Smith, P. J. Maloney, and O. R. Wood II, "The Role of E/p in Waveguide TE Lasers," Appl. Phys. Letters, 31, 738 (1977).

31. P. E. Dyer and D. J. James, "Electrical Characteristics of Double-Discharge TEA CO_2 Lasers," J. of Appl. Phys., 46, 1679 (1975).

32. C. A. Fensternmachen, et al., "Electron Beam Controlled Electrical Discharges as a Method of Pumping Large Volumes of CO_2 Laser Medium at High Pressure," Appl. Phys. Letters, 26, 56 (1972).

33. T. F. Stratton, C. F. Erickson, C. A. Fensternmacher, and E. O. Swickard, "WA7-Electron Beam Controlled CO_2 Laser Amplifiers," IEEE J. of Quantum Electronics, QE-9, 157 (1973).

34. D. Dobschek, H. Jacobs and J. Freely, "The Mechanism of Self-Sustained Electron Emission from MgO," Phys. Rev., 91, 804 (1953).

35. R. R. Mitchell, L. J. Denes, and L. E. Kline, "Electrode Surface Field and Preionization Effects in the Spatial Distribution of Arcs in CO_2 Laser Discharge," J. Appl. Phys., 49, 2376 (1978).

36. H. Mocker, Private Communication, Feb. 27, 1979.

37. A. M. Robinson, "Effect of Inductance on Small Signal Gain of Transverse Excitation Atmospheric Pressure Discharge in Carbon Dioxide," IEEE J of Quantum Electronics, QE-7, 199 (1971).

38. T. W. Johns and J. A. Nation, "A Resistive Electrode, High Energy Transverse Laser Discharge," Rev. of Sci. Inst., 44, 169 (1973).

39. W. L. Ohlinger, "The Effect of Diode and Array Geometrical Parameters on Performance of High Field Electron Emitters Formed from Unidirectionally Solidified Uranium Dioxide-Tungsten Composites," Ph.D. Dissertation, Georgia Institute of Technology, School of Ceramic Engineering (1977).

40. D. N. Hill, "The Effect of Cathode Geometry on the Emission Characteristics of Low Voltage Field Emitters Fabricated from Uranium Dioxide-Tungsten Composites," Ph.D. Dissertation, Georgia Institute of Technology, School of Ceramic Engineering (1979).

41. A. T. Chapman, et al., "Manufacturing Methods for the Production of Field Effect Electron Emitters from Oxide-Metal Composites," Georgia Institute of Technology, Schools of Ceramic and Electrical Engineering, Final Technical Report for Contract DAAH01-75-C-0852 (1977).

42. R. A. Rieger, "The Selective Chemical Etching of CeO_2 Doped Gd_2O_3-Mo Composites," Master's Thesis, Georgia Institute of Technology, School of Ceramic Engineering 1973).

43. S. L. Prosser II, "Chemical Etching and Ion-Milling of Uranium Dioxide-Tungsten Unidirectional Composites," Master's Thesis, Georgia Institute of Technology, School of Ceramic Engineering (1978).

44. J. D. Lee, " Low Voltage Field Emission Cathodes from Eutectic Compositions," Ph.D. Dissertation, Georgia Institute of Technology, School of Ceramic Engineering (1978).

45. J. W. Stendera, "Unidirectional Solidification of Rare Earth Oxide-Metal Composites," Master's Thesis, Georgia Institute of Technology, School of Ceramic Engineering (1974).

46. A. von Engel, Ionized Gases, Oxford at the Clarendon Press (1955).

VITA

STEVEN GARY WAX

March 11, 1950 - Born - Chicago, Ill.

June, 1967 - Graduated from Framingham North High School, Framingham, Mass.

1967-1971 - Attended University of Massachusetts, Amherst, Mass.

May 1971 - B.S., Chemical Engineering, University of Massachusetts, Amherst, Mass.

June 1971 - Commissioned as a Second Lieutenant, USAF

1971-1973 - Research Assistant, Department of Chemical Engineering, University of Illinois, Urbana, Ill.

February 1973 - M.S. Chemical Engineering, University of Illinois, Urbana, Ill.

1973-1977 - Project Engineer, USAF Rocket Propulsion Laboratory, Edwards AFB, Cal.

1977-1979 - Attended Georgia Institute of Technology, Atlanta, GA under USAF Sponsorship.

December 1979 - Ph.D. Ceramic Engineering, Georgia Institute of Technology, Atlanta, GA.

Publications and Presentations

"Contamination Prediction in a 0.1 lbf Hydrazine Thruster."

Paper published in Classified Reference, presented Dec. 1976 at JANNAF Propulsion Conference, Atlanta, Georgia (Co-author, L. P. Davis).

"Integration of Monopropellant Hydrazine Technology." Paper published in Classified Reference, presented Oct. 1975 at JANNAF Propulsion Conference, Anaheim, California (Co-author, P. Erikson).

"Sensitivity of Concentration Polarization in Ultrafiltration Cells to the Suction Distribution." I&EC Fundamentals, Vol. 13, May 1974 (Co-author, A. Kozinski).

"Separation with Protein Liquid Crystals." AIChE J., Vol. 20, No. 6, 1974 (Co-authors A. Kozinski and L. Kizior).

"Transfer Through Biological Boundary Layers." MS Thesis, University of Illinois, Dept. of Chemical Engineering, Feb. 1973 (Advisor, A. Kozinski).